A METHODOLOGY FOR REAL-TIME SENSOR-BASED BLOCKAGE ASSESSMENT OF BUILDING STRUCTURES DURING EARTHQUAKES

A THESIS SUBMITTED TO
THE GRADUATE SCHOOL OF NATURAL AND APPLIED SCIENCES
OF
MIDDLE EAST TECHNICAL UNIVERSITY

BY

TULÛHAN ERGİN

IN PARTIAL FULFILLMENT OF THE REQUIREMENTS
FOR
THE DEGREE OF MASTER OF SCIENCE
IN
CIVIL ENGINEERING

JANUARY 2013

Approval of the thesis:

A METHODOLOGY FOR REAL-TIME SENSOR-BASED BLOCKAGE ASSESSMENT OF BUILDING STRUCTURES DURING EARTHQUAKES

submitted by **TULÛHAN ERGİN** in partial fulfillment of the requirements for the degree of **Master of Science in Civil Engineering Department, Middle East Technical University** by,

Prof. Dr. Canan Özgen _____
Dean, Graduate School of **Natural and Applied Science**

Prof. Dr. Ahmet Cevdet Yalçıner _____
Head of Department, **Civil Engineering**

Assoc. Prof. Dr. Murat Altuğ Erberik _____
Supervisor, **Civil Engineering Dept., METU**

Assoc. Prof. Dr. Özgür Kurç _____
Co-Supervisor, **Civil Engineering Dept., METU**

Examining Committee Members:

Prof. Dr. Mustafa Talat Birgönül _____
Civil Eng. Dept., METU

Assoc. Prof. Dr. Murat Altuğ Erberik _____
Civil Eng. Dept., METU

Assoc. Prof. Dr. Özgür Kurç _____
Civil Eng. Dept., METU

Asst. Prof. Dr. Esin Ergen Pehlevan _____
Civil Eng. Dept., İTÜ

Dr. Onur Pekcan _____
Civil Eng. Dept., METU

Date: **___29/01/2013__**

I hereby declare that all information in this document has been obtained and presented in accordance with academic rules and ethical conduct. I also declare that, as required by these rules and conduct, I have fully cited and referenced all material and results that are not original to this work.

Name, Last name : Tulûhan ERGİN

Signature :

ABSTRACT

A METHODOLOGY FOR REAL-TIME SENSOR-BASED BLOCKAGE ASSESSMENT OF BUILDING STRUCTURES DURING EARTHQUAKES

Ergin, Tuluhan
M.Sc, Department of Civil Engineering
Supervisor: Assoc. Prof. Dr. M. Altuğ Erberik
Co-Supervisor: Assoc. Prof. Dr. Özgür Kurç
January 2013, 104 pages

During and after earthquakes, occupants inside a damaged building should be evacuated rapidly and safely whereas related units outside the buildings (e.g. first responders) should know the current condition of the building. Obviously, this information should be as accurate as possible and accessed timely in order to speed up the evacuation. Unfortunately, absence of such information during evacuation and emergency response operations results in increased number of casualties. Hence, there arises a need for an approach to make rapid damage and blockage assessment in buildings possible.

This study focuses on sensor-based, real-time blockage assessment of buildings during earthquakes and it is based on the idea that; the blocked units of a building (e.g. corridors) can be assessed with the help of different types of sensors. The number and locations of these sensors are arranged in such a way that it becomes possible to picture the current condition of the building. Sensors utilized in this study can be listed as accelerometer, ultrasonic range finder, gyro sensor, closed cable circuit and video camera. The research steps of this thesis include (1) examination of the damage indicators which can cause blockage, (2) assessment of the monitoring devices, (3) expression of the conducted experimental studies in order to assess blokage condition of a corridor unit, (4) proposing an sensor fusion approach, and (5) presentation of the performed case study as an implementation of the blockage assessment. The findings of this research can be made use of in future studies on sensor-based blockage assessment.

Keywords: Sensor Data, Sensor Fusion, Sensor Applications, Blockage Assessment

öz

DEPREM SIRASINDA BİNA YAPILARINDA GERÇEK ZAMANLI ALGILAYICI TABANLI BLOKAJ DEĞERLENDİRME YÖNTEMİ

Ergin, Tuluhan
M.Sc, Department of Civil Engineering
Tez Yöneticisi : Assoc. Prof. Dr. M. Altuğ Erberik
Ortak Tez Yöneticisi : Assoc. Prof. Dr. Özgür Kurç
Ocak 2013, 104 sayfa

Deprem sırasında ve sonrasında, hasar görmüş binanın içinde bulunan kişilerin seri ve güvenli biçimde tahliyesi ile bina dışındaki ilgili ekiplerin (örneğin ilk yardım ekipleri) binanın mevcut durumunu bilmeleri gerekmektedir. Tahliyenin hızla gerçekleşmesi için bu bilgi olabildiğince doğru ve zamanında edinilmelidir. Tahliye ve acil müdehale sırasında bu bilginin eksikliği malesef kayıp sayısını arttırmaktadır. Bu nedenle, binalarda hasar ve blokaj değerlendirmesine seri biçimde imkan veren bir yaklaşıma ihtiyaç duyulmaktadır.

Bu çalışma, deprem sırasında, binaların gerçek zamanlı algılayıcı tabanlı blokaj değerlendirmesine odaklanmakta ve temelde binanın blokajlı birimlerinin (örneğin koridorlar) çeşitli algılayıcılarla değerlendirilmesi fikrine dayanmaktadır. Kullanılan algılayıcıların sayıları ve yerleşimleri, binanın mevcut durumunu yansıtacak biçimde ayarlanmıştır. Bu çalışmada değerlendirilen algılayıcılar; ivmeölçer, jiroskop algılayıcı, kapalı devre kablo algılayıcısı ve video kameradır. Tez kapsamındaki araştırma adımları; (1) blokaja sebep olan hasar göstergelerinin incelenmesi, (2) görüntüleme cihazlarının değerlendirilmesi, (3) gerçek zamanlı blokaj durumunun değerlendirilmesine yönelik yürütülen deneylerin anlatılması, (4) algılayıcı verilerini birleştiren bir yaklaşımın önerilmesi ve (5) blokaj değerlendirme uygulaması olarak gerçekleştirilen vaka çalışmasının sunumudur. Bu araştırmanın bulguları, algılayıcı tabanlı blokaj değerlendirme konusunda gelecekte yapılacak çalışmalarda kullanılabilir niteliktedir.

Anahtar kelimeler: Algılayıcı Verisi, Algılayıcı Bilgilerinin Birleştirilmesi, Algılayıcı Uygulamaları, Blokaj Değerlendirme.

To my Family and Friends

ACKNOWLEDGEMENTS

This research is funded by a grant from the Scientific and Technological Research Council of Turkey (TUBITAK), Grant No. 109M263. TUBITAK's support is gratefully acknowledged.

I would like to thank my advisor Assoc. Prof. Dr. Murat Altuğ Erberik who has kindly accepted me as a student. I would not be able to complete my graduate studies without his supervising.

I would like to thank my co-advisor Assoc. Prof. Dr. Özgür Kurç for all his supports throughout my graduate studies.

I would like to thank Prof. Dr. Mustafa Talat Birgönül for his trust and support all throughout the project as a project coordinator.

I would like to thank Asst. Prof. Dr. Esin Ergen Pehlevan for her academic guidance and kind hospitality throughout my visits to İstanbul.

I would like to thank Asst. Prof. Dr. Sanem Sarıel Talay for her advices and supports on my studies.

I would like to thank my colleagues; Gürşans Güven Işın, Burak Özbaş and Tuna Sönmez for all their kind friendship, hospitality, help and support along my visits to İstanbul. I will never forget their contributions on this thesis.

I would like to thank my friend Murat Ayhan for his companionship along the project. His support always finds me at the darkest moments.

I would like to thank Hasan Metin who is an indispensable employee of the Structure Mechanics Laboratory of METU. It would be impossible for me to complete the experiments without his enormous support.

I would like to thank Gülsüm Sevde Baltaşı for all her support inside and outside of the laboratory. Her assiduity clear the way for this study.

I would like to thank Dr. Sinan Atay and his lovely family for all their academic and moral support to me. They convert difficulties into beauties.

I would like to thank my dearest friend, Hüseyin Yahya Baydar for all his support which is impossible to define by words. He always revives me at my most hopeless moments.

I would like to thank my dearest Iranian friends; Pourang Ezzatfar, his lovely wife Maryam Daneshvar and his roommate Mahdi Ghaffarinia for all the fun we had, all the support they gave, and all the good memories.

I would like to thank my friends Anıl Şeker, Bora Gündoğdu, Dr. Buğra Sezen Buğrahan Uğuz, Çağlar Fırat, Fırat Köseoğlu, Güneş Sözüdoğru, İrem Oğuzcan, Kaan Demirkazıksoy, Nazif Uğur Kaya, Özlem Yavuzyılmaz Gündoğdu, Recep Can

Okay and Tolga Nalbantoğlu. These are the greatest friends a man can ever have, even if the distances separate us.

I would like to thank my mother Gaye Ergin, my father Ertan Ergin, my sister Dirun Ergin and my brother Uluğhan Ergin for their full support no matter what happens.

Last but not least I would like to thank Hasan Tekin Kuşhan and his venerable wife Rukiye Kuşhan. It is always going to be an honour to know them. Their love is my most precious presence.

TABLE OF CONTENTS

LIST OF TABLES

TABLES

LIST OF FIGURES

FIGURES

LIST OF SYMBOLS AND ABBREVIATIONS

a	**:**	Lateral floor acceleration (m/s2)
$\mathbf{a_{overturn}}$	**:**	Critical floor acceleration for overturn (m/s^2)
$\mathbf{a_{slide}}$	**:**	Critical floor acceleration for slide (m/s^2)
A	**:**	Intersected area rate of the post-experiment stages
AREF	**:**	Analog Referance
B	**:**	Intersected area rate of the pre-experiment stages
C	**:**	Change of intersected area rate of the bands/ribbons between the pre-experiment and the post-experiment stages
csv	**:**	Comma seperated values
CB	**:**	Cupboard
CCC	**:**	Closed cable cicuit
CM	**:**	Center of mass
CR	**:**	Center of rigidty
$\mathbf{d_1}$	**:**	Measured distance at pre-experiment stages
$\mathbf{d_2}$	**:**	Measured distance at post-experiment stages
$\mathbf{d_h}$	**:**	Height of the camera sensor (mm)
$\mathbf{d_w}$	**:**	Width of the camera sensor (mm)
D	**:**	Distance
e	**:**	Distance between center of mass and the center of rigidity
Exp	**:**	Experiment
f	**:**	Lens focus distance (mm)
$\mathbf{f_{max}}$	**:**	Flexure capacity of the wall
F	**:**	Lateral force caused by earthquake acceleration (kN)
FTDI	**:**	Future technology devices international
Fx	**:**	Total lateral force that act on to the element
Fμ	**:**	Friction force
flv	**:**	Flash Video
g	**:**	Gravitational acceleration (is assumed to be 9.81 m/s^2 in this thesis)
GND	**:**	Grounding
H	**:**	Height of the element (m)
LBC	**:**	Left behind cord
LFC	**:**	Left front cord
m	**:**	Mass of the element (kg)
$\mathbf{M_{max}}$	**:**	Maximum moment
Mw	**:**	Moment magnitude scale
N	**:**	Normal force
PCB	**:**	Printed circuit board
Ph.	**:**	Phase
OSB	**:**	Oriented structural boards
$\mathbf{r_{AB}}$	:	Distance between point A and B
RBC	**:**	Right back cord
RFC	**:**	Right front cord
SC 1	**:**	Suspended ceiling 1
SC 2	**:**	Suspended ceiling 2
SC 3	**:**	Suspended ceiling 3
t	**:**	Thickness of the element (m)
tv	**:**	Threshold value for URF
URF	**:**	Ultrasonic range finder
USB	**:**	Universal serial bus
V	**:**	Voltage

$\mathbf{V_A}$	:	Absolute linear velocity of the column bottom end
$\mathbf{V_B}$	:	Absolute linear velocity of the column top end
$\mathbf{V_{B/A}}$	:	Velocity of the column top end with respect to the column bottom end
Vcc	:	Collector supply voltage
Vin	:	Input voltage
W	:	Weight of the element (kN)
$\mathbf{\alpha_h}$	:	Horizontal angle of the view (°)
$\mathbf{\alpha_v}$	:	Vertical angle of the view (°)
$\mathbf{\gamma}$	:	Density of the unit hallow brick
$\mathbf{\mu_f}$	:	Friction coefficient
$\mathbf{\sigma_{max}}$	:	Maximum normal stress
$\mathbf{\psi}$	:	Coefficient combines the in-plane and out-of-plane damage for infill walls
$\mathbf{\omega}$	:	angular velocity

CHAPTER 1

INTRODUCTION

During and after disasters, occupants inside a damaged building should be evacuated rapidly and safely while the first responders outside the building should be informed about the current condition of the building. Obviously, this information should be as accurate as possible and accessed timely in order to speed up the guidance of occupants to safe exits from a building under the effect of hazards. Unfortunately, the absence of such information during evacuation and emergency response operations, which is the common case, results in increased number of casualties. Hence, there arises a need for an approach to determine blocked passages in damaged building structures in order to guide the occupants to the exits safely and timely during evacuation by utilizing the sensor information.

This research mainly focuses on a real-time sensor-based blockage assessment for the passages of a building in the case of disaster. The sections below briefly summarize the motivating cases of this research, provide the literature review relevant to the subject and finally state the aims and objectives of the thesis with scope and limitations.

1.1 Motivating Cases

1.1.1 Motivating Cases 1: Explosions

The first motivating case is explosions. There are two fatal accidents that occurred in Ankara in 2011. These incidents happened on the same day and a total number of 20 people lost their lives. The reason for the two disasters is the same: the explosion of the LPG tank located at the buildings. The former explosion occurred in a facility producing generator at OSTİM in which 80 people work. The two of the four stories collapsed after the explosion and the victims got stuck under debris (Figure 1.1a). The latter one occurred at a workshop in İvedik Organized Industry Site. The fire got started after the explosion and the workers got trapped in the building (Figure 1.1b).

(a) (b)

Figure 1.1 The photos of the explosions that occured in Ankara; a) OSTİM, b) İvedik Organized Industry Site (Birgönül, et al., 2012)

1.1.2 Motivating Cases 2: Terrorist Attacks

The explosions caused by the terrorist attacks may give rise to heavy damage to the building. Moreover, the building can get collapsed totally or partially.

The most striking case is the terrorist attack to the World Trade Center in New York State of the United States of America. This terrorist attack happened in 2001. The Twin Towers with 110 stories collapsed and 2.752 people were found dead in it. A similar attack occurred in Turkey in 2003. A terrorist attack aimed at the headquarter building of a bank in Levent, İstanbul (Figure 1.2). People got stuck in it for hours with great panic.

Figure 1.2 A photo of the attacked bank at Levent, İstanbul (Birgönül, et al., 2012)

1.1.3 Motivating Cases 3: Earthquakes

The most hazardous and effective events that resulted in the loss of many lives and property are earthquake disasters. The majority of the population of Turkey lives around active faults; so, many fatal earthquakes happen in the region. Two recent examples of major earthquakes from Turkey are the 1999 Marmara Earthquake and the 2011 Van Earthquake. According to the official numbers, 96,796 residences and 15,939 commercial buildings got collapsed or heavily damaged and 17,480 people passed away in the destruction of the Marmara Earthquake. In Van Earthquake, 601 people died. 5,739 out of 10,621 buildings were stated to be heavily damaged and 2.262 of them were stated to be collapsed. The photos of the heavily damaged buildings in Van are shown in Figure 1.3. In both cases, thousands of people got trapped under debris.

(a) (b)

Figure 1.3 The photos of the heavily damaged buildings caused by Van Earthquake; a) a commercial building, b) a residental building[1]

[1]Photos taken by Murat Ayhan in Van at 26.10.2011

1.1.4 Summary of Outcomes from the Motivating Cases

These cases indicate that the causes such as explosion, terror attack or earthquake may result in loss of lives and properties. In order to mitigate these fatal consequences, the information about the damaged buildings should be gathered as fast and correct as possible. This can be achieved with sensors. Damage and blockage assessment is important not also for occupants to be evacuated but also for the first responders to rescue.

1.2 Literature Review

In this section, the studies related to damage estimation are examined. There are numerous studies related to the damage estimation of building structural elements under different load conditions (Beck et al., 1999; Porter et al., 2001; Beck et al., 2002; Krawinkler, 2002; Miranda and Aslani, 2003; CUREE, 2005; NEES, 2007). None of these studies aim at the estimation of structural damage. The objective of these studies is to estimate the structural behavior of a structural element or a structural system during a possible disaster.

Apart from that, there are studies related to real-time or instant damage evaluation but these are not for one building. In general these studies focus on regional damage or loss estimation for a building stock (Kircher et al., 1997a; Kircher et al., 1997b and Wu et al., 2002). Various methods are used in order to determine the real damage distribution of a building stock. Most important remote sensing methods are using satellite images (Kerle and Oppenheimer, 2002) and aerial photos (Steinle et al., 2001). However it should be noted that such applications are far from supplying the detailed damage information about a building to the researchers.

In addition, studies related to the determination of the real-time damage by monitoring the instantaneous change in the dynamic properties of a building are also available in the literature (Todorovska et al., 2004; Niousha and Motosaka, 2007). Damage generally affects the stiffness of the building. So, in these studies the change in the natural vibration frequency is examined after analyzing the recorded acceleration that has been measured by the help of accelerometers. But some researchers claim that damage does not affect the natural vibration frequency of a building (Şafak, 2005) while other state that the change in parameters such as rain, temperature change and wind affects the natural vibration frequency (Clinton et al., 2004). These studies show that using only acceleration data results in deceptive information about actual damage.

1.3 Aim, Scope and Limitations of the Thesis

The aim of this thesis study is to assess the blockage of a passage at the post-disaster stage. To achieve this, different types of sensors are examined. These sensors and video camera are mounted to a corridor model and some experiments are conducted. Image processing is performed with the videos recorded during the experiment. The information gathered through the sensors and image process is fused in order to assess the blockage of the passage by decision tree approach. Finally, the decision tree approach is tested on the simulation platform.

This study focuses on determining the blockage caused by only physical events like earthquakes. In other words, blockage caused by other events like fire, explosion, etc. are not taken into consideration. The results of this study are

obtained only with the limited type of building components with limited type of sensors. The proposed method is considered only for the buildings which have more than one entrance, exit and ladder with fewer stories, large floor areas and usually used by many occupants.

In order to achieve the aim of the study, damage indicators which could possibly cause a blockage in the passages of the building are examined in Chapter 2. In Chapter 3, sensors considered in this study, which can be listed as accelerometer, gyro sensor, closed cable circuit (CCC) and ultrasonic range finder (URF), and other monitoring devices (e.g. video camera, microcontroller) are assessed in detail according to the perspective given in Chapter 2. In Chapter 4, the conducted experiments on prototype models and the obtained results are given. The experimental studies are related to assess the dynamic interaction between the statuses of a damaged building by the help of the sensor data. The main purpose of these experiments is to receive data in order to generate and test a sensor fusion approach. Of the sensors mentioned in Chapter 3, only CCC and URF are used in the experiments. Video camera is also used in the experiments. After the presentation of the experiments, sensor fusion is given in Chapter 5. Sensor fusion is important estimate the current blockage condition of a passage unit. In this research, the decision tree approach was employed to gather the sensor data. In Chapter 6, this system is tested with a case study. The main goal of this chapter is to test the performance of the decision tree. In order to achieve this, pilot building which is located in Nevşehir, Turkey and used as a faculty building of Nevşehir University is selected. After modeling the structural system of the building on a structural analysis program, two different earthquake acceleration records which are moderate and severe levels, are applied to the model. Damage of the structural and non-structural components are estimated by using the acceleration and the drift results of the structural elements which are obtained from the analyses. Lastly, Chapter 7 summarizes major conclusions, findings and recommended future works.

CHAPTER 2

DAMAGE INDICATORS

2.1 Introduction

This chapter presents the damage indicators which could cause a possible blockage in the passages of the building. This information is important for selecting the location and number of the monitoring devices.

2.2 The Concepts Related to a Building Regarding to Damage Monitoring and Blockage Assessment

Figure 2.1 presents the building units and the relationships between these units that are used for local monitoring and blockage assessment system. Similar definitions have been made by different researchers (Schütz et al., 2008; Dibley et al., 2011).

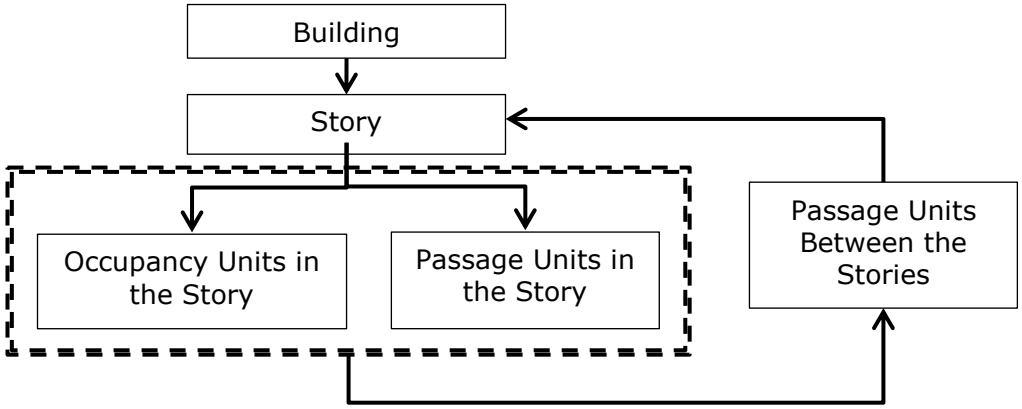

Figure 2.1 The structural units used for monitoring and blockage assessment

According to the flowchart in Figure 2.1, buildings consist of one or more stories, which can be regarded as a sub-unit. The units in the story are further divided into two sections: the occupancy units and the passage units. The occupancy units are the places where the occupants stay together. In other words, these places are the room units, which people occupy for different purposes. The number of the people that stay in a unit may vary depending on the intended purpose of the unit. For example, a room unit built for office usage generally contains one or two occupants, but a room unit built for meeting is likely to contain ten to fifteen occupants at the same time. In post-disaster cases, victims generally get trapped in a room unit. It is extremely essential to know the intended use of the room units in terms of estimating the location where people get trapped and guiding them to the available exits during evacuation.

The passage units in the story (or horizontal passage units) are the units that allow the movement of occupants in the story like corridors. It may not be possible to evacuate people from the blocked passage units in case of blockage, so; it is essential to monitor the passage units with sensors for the purpose of

determining as to whether the passages in question are blocked or not and to decide on which path to use during disaster.

The passage units between the stories are the units that enable the people to be transferred between two stories. These are generally elevators, stairs or ramps. In a post-disaster situation, the unblocked passage units between the stories are important for safe evacuation of occupants. These units should also be monitored with sensors for blockage.

The alternative ways to be followed to evacuate the occupants to a secure place outside the building in a post-disaster situation are given briefly in Figure 2.2. Specifying the valid alternatives available in the post-disaster situation is the fundamental function of the sensors and monitoring process; on the other hand, it is the fundamental function of the guiding model to determine the most efficient alternative (Ayhan, 2012).

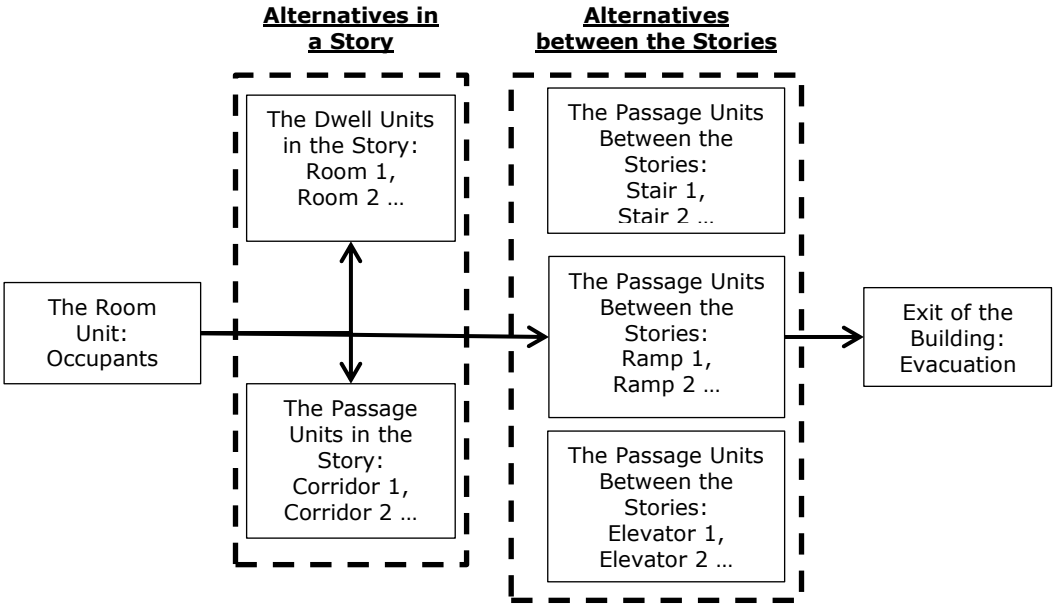

Figure 2.2 The schematic drawing, shows the usual alternative ways to be followed to evacuate the occupants to a secure place outside the building in a post-disaster situation

In addition, the structural and the non-structural elements to be monitored by sensors should be determined. Structural elements can be defined as the elements that transfer the lateral and the vertical loads to the foundation of the structure safely. Columns, beams, shear walls, load-bearing masonry walls and slabs are the examples of the structural elements. If the vertical load-bearing elements (e.g. the columns and the load-bearing masonry walls) are damaged, the structural safety of the building is accepted to be under risk. Partial or total collapse is likely to occur depending on the level of damage. Hence, the occupants should not be guided to the locations with moderately or severely damaged load-bearing elements. In the course of decision-making, the information about the structural condition of the structure by sensors will help the decision maker to select among different options.

Non-structural elements are the non-load-bearing elements. If non-structural elements are damaged, the structural safety of the building is not threatened, only economic loss may occur. The suspended ceilings, infill walls or partial walls

and various types of furniture (e.g. cupboard, table, etc.) are some of non-structural elements. The damage to non-structural elements can cause injuries (e.g. fall of a cupboard on a person) or can block the passage units (e.g. a corridor blocked by damaged infill wall).

2.3 The Concepts Related to Localization and the Type of the Sensors

To set up the localization rules of the sensors in a building, sensor types and construction types should be examined individually. Before examining the types and the specifications of the sensors, structural aspects should be discussed. These include the structural system of building, the occupancy class, and the architectural and structural properties that are fairly important for both localizing and choosing the type of sensors.

2.3.1 The Structural System of the Buildings

Building could be constructed with different kinds of construction techniques and materials. The most frequent structural system used in the building can be listed as followings:

- Reinforced concrete frame system (with or without beam)
- Reinforced concrete with shear walls
- Masonry
- Steel framework
- Wood frame
- Hybrid buildings (more than one type of material and/or technique are used)

2.3.1.1 Reinforced Concrete Frame Systems

These frame structures consist of reinforced concrete beams, columns and slabs (Figure 2.3). Columns must transfer both the vertical (dead loads, live loads, etc.) and the lateral loads (earthquake, wind etc.) to the foundations of the building safely. In these systems, columns are the most critical elements because if the columns are severely damaged so that, it cannot carry the loads, the vertical stability of the building becomes critical. Hence, the sensors that monitor the columns should give detailed information about the present condition of the building. On the other hand, reinforced concrete frame systems are generally regarded as flexible buildings. As a result, the probability of being damaged, overturning or failure of a non-structural element is rather high. In case of an explosion with in the building, some columns of the building might be affected; therefore, partial or complete collapse can occur.

In the framework systems, non-load bearing infill walls or partition walls are placed into frames for sectioning the units or the rooms. These walls generally are made up from masonry materials like brick, concrete briquette, or autoclaved aerated concrete. Due to high lateral deformation properties of the framework systems, the first elements to be damaged under impact are the infill walls. So it is important to take this type of behavior into account. Selecting and placing the sensors in the light of this information are unquestionably essential.

Figure 2.3 Example of reinforced concrete frame systems (Birgönül et al., 2012)

2.3.1.2 Reinforced Concrete Flat Slab Systems

Reinforced concrete systems with flat slabs or mushroom slabs are similar to frame systems with beams. The only difference is that the flat slabs do not involve any beam to transfer loads; that is, the columns are directly connected with slabs (Figure 2.4). A system without beam causes a more flexible framework. More flexible framework causes the building to be deflected more under lateral loads. It means that the buildings can sustain damage due to excessive deformations. In addition, the critical regions of flat slabs are column-slab joints. If the thickness of the slab is not adequate or if sufficient reinforcement is not placed at this critical region, a failure mode called "punching", which can trigger a sudden collapse, may occur. Briefly, flat slabs are more flexible with respect to the framework systems with beams and sensors must be chosen and placed taking these characteristics into consideration. Sensors may be placed in a way that monitors the behavior of the column-slab joints, too.

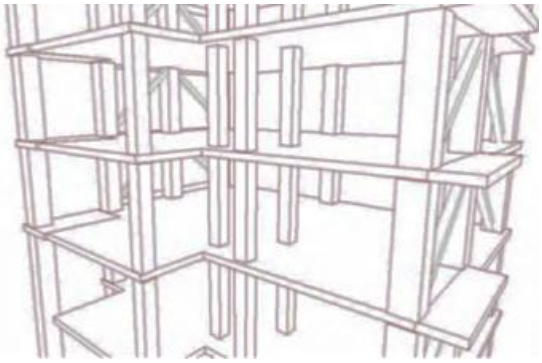

Figure 2.4 A general view of the reinforced concrete frame systems with flat slab (mushroom slabs) (Birgönül et al., 2012)

2.3.1.3 Reinforced Concrete Buildings with Shear Walls

Reinforced concrete buildings with shear walls consist of load-carrying reinforced concrete walls and slabs, and they are extremely rigid structures. It is possible to consider tunnel framework systems also in this group (Figure 2.5). These kinds of reinforced concrete structures possess better performance when compared with the framework structures. Because of their high rigidity, lateral deformations are less and shear walls, as vertical elements, have much more load bearing capacity than columns; so, the probability of damage to this type of structures is less. Hence it can be stated that, it is not necessary to monitor the load-bearing components of these structural systems with sensors. Monitoring only the non-structural components is sufficient.

Figure 2.5 A general view of a tunnel framework system (Birgönül et al., 2012)

2.3.1.4 Masonry Buildings

Masonry buildings are one of the common types of construction in Turkey (Figure 2.6). In this type of construction, generally brick, concrete briquette, stone or adobe is used as building wall material. Due to lack of lateral load-bearing capacity, they are vulnerable to seismic action. In masonry buildings, which consist of load-bearing walls placed parallel to the major axis of the building, it is possible to observe different types of failures. In other words, walls may be exposed to in-plane or out-of-plane damage. These different behavior modes can emerge depending on many factors (e.g. the locations of the walls, geometric properties, mechanic properties, the lateral and vertical loads etc.). In these types of buildings, the most important structural components are the load-bearing walls, so; it is proper to select and place the sensors to monitor the behavior of these walls.

Figure 2.6 An example of a masonry building (Birgönül et al., 2012)

2.3.1.5 Steel Framework

Steel buildings are generally constructed as industrial buildings in Turkey. They consist of steel beam and column members, which adjoin to each other (Figure 2.7). When compared with other structural systems such as reinforced concrete and masonry, steel structures are of high performance against earthquake. In these types of systems, it is not that necessary to monitor the load-bearing system with sensors. Monitoring only the non-structural elements would be more appropriate.

Figure 2.7 An example of a steel structure (Birgönül et al., 2012)

2.3.1.6 Wood-frame Structures

Wood-frame structures also have a framework system and in this type of buildings, horizontally and vertically placed wooden elements are supported by diagonal elements to increase the lateral capacity (Figure 2.8). Frames are generally filled with masonry material. These buildings are also substantially sturdy constructions against earthquake like steel structures. In these types of systems, it is not much necessary to monitor the load-bearing system with sensors. Monitoring only the non-structural elements is sufficient.

Figure 2.8 An example of a timber structure (Birgönül et al., 2012)

2.3.1.7 Hybrid Structures

Finally, hybrid structures are the ones that are made of more than one material and/or construction techniques (e.g. the structures with the reinforced concrete framework system and reinforced concrete shear walls). The behavior of these structures is controlled by the weakest material and/or the most disadvantageous construction technique that is used. In other words, the sensors

should be placed in the critical regions of the structure. For instance, in order to monitor the post-earthquake condition of reinforced concrete frame structures with shear walls, it is proper to locate the sensors to more flexible reinforced concrete framework system, which is most likely to be damaged.

2.3.2 Occupancy Class of the Building

Occupancy class of the building is another important parameter for choosing the type and localization of the sensors. The occupancy classes of buildings can be listed as follows:

- Residential buildings
- Governmental or public buildings (e.g. institution buildings, the buildings that belong to the emergency service units like police stations, fire stations etc.)
- Commercial buildings (e.g. shopping malls, office buildings, entertainment venues, etc.)
- Industrial buildings (e.g. factories, machine shops, etc.)
- Medical buildings (e.g. hospitals, polyclinics, laboratories, etc.)
- Educational buildings (e.g. schools, universities, etc.)
- Religious buildings (e.g. mosques, churches, etc.)

The passage zones in buildings where people are populated such as shopping malls, institution buildings, hospitals or educational buildings should be monitored precisely with more sensors taking the panic and the stampede atmosphere into consideration during the post-disaster situation.

To sum up, in buildings used for various purposes, specifying the critical zones and the issues which could occur in these zones is of great importance at the initial stage of choosing the type and the localization of the sensors.

2.3.3 Architectural and Structural Properties

The architectural and structural properties of the buildings have a prominent role for the localization of the sensors. The most important property is the irregularity of the building in plan and in elevation. These irregularities cause uneven distribution of loads and local damages during earthquake. For example, the effect of the torsion becomes critical for the buildings which have L or T shaped plan geometry as shown in Figure 2.9. In both type of structures, while the blocks vibrate with the earthquake impact, the circled regions are exposed to large stresses. In these types of buildings since the damage is concentrated in the connection regions, locating more sensors at these regions seems to be appropriate.

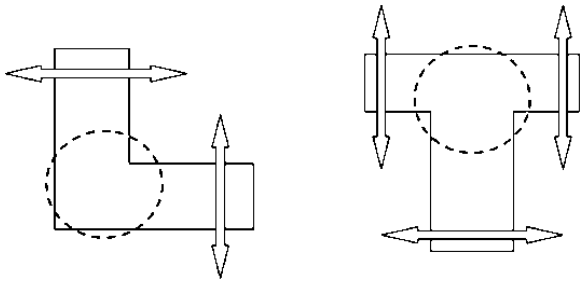

Figure 2.9 The most critical regions expected during an earthquake in buildings with L and T shaped plan geometry

The lateral forces that affect a building during an earthquake act on the center of mass (CM) of the structure. In most of the structures the CM is regarded as the geometric center of the structure. Besides, the center of rigidity (CR) of a building is the centroid of the rigidity of the vertical load bearing elements (column, shear wall, masonry wall, etc.). The eccentricity between these two centers (e) causes the lateral earthquake loads acting on the structure to rotate the building round a vertical axis passing through the CR (Figure 2.10).

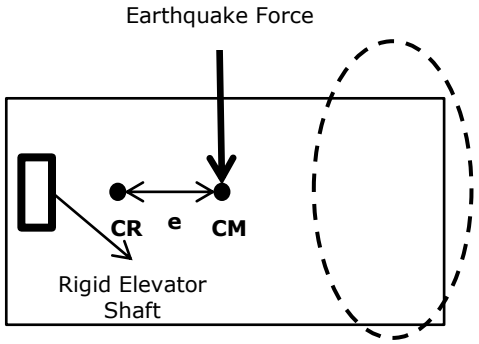

Figure 2.10 A building with irregularly distributed rigidity in plan and the expected region of damaged circle

The structural elements, normally designed for bearing loads with respect to their relative rigidities, are exposed to extra load in direct proportion to the distance from the center of rigidity. In this case, it is highly probable that the load-bearing elements showed in circle are in Figure 2.10 are likely to be damaged. As a result, at the stage of locating the sensors in a building with irregular distribution of rigidity, it would be appropriate to examine these critical regions.

Some issues regarding the structures with vertical irregularities should be kept in mind during the sensor location. For example, as shown in Figure 2.11, buildings can have more floor area at lower stories and less floor area at upper stories. These two regions show totally different dynamic properties during an earthquake. In this case, large stresses may occur in the regions of change in floor area. During the localization of the sensors in such buildings, it would be proper to pay attention to the stories where the floor area changes suddenly and to monitor this floor with more sensors.

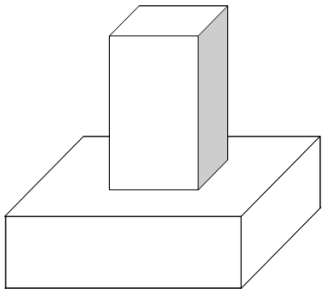

Figure 2.11 The buildings which have vertical irregularities

Even in the buildings which have vertical irregularities of mass and rigidity (Figure 2.11 and Figure 2.12), different dynamic properties could occur during an earthquake. It will be convenient to monitor the floors which have these irregularities with the sensors in detail.

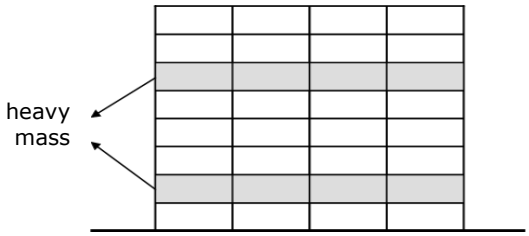

Figure 2.12 Buildings with vertical mass irregularity

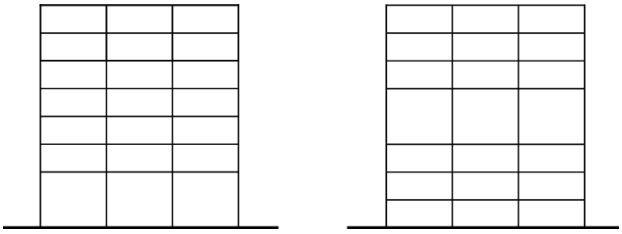

Figure 2.13 Buildings with vertical rigidity irregularity (soft or weak story)

CHAPTER 3

MONITORING DEVICES

3.1 Introduction

In this chapter, the considered monitoring devices are assessed in detail according to the perspective given in Chapter 2. The monitoring devices can be examined in two categories: sensing devices (e.g. sensors and video camera) and data acquisition devices (e.g. server computer and microcontroller). The sensors used in this study are CCC, URF, gyro sensor and accelerometer. Video camera is used with image processing. The software related to these devices is also examined.

3.2 Determining the Monitoring Devices

The first step to estimate the blockage is to estimate the damage induced by the structural and non-structural components in the monitored region. The most critical structural component of a building is vertical load bearing element, i.e. column. The failure of a column can cause the building to collapse partially or even entirely. So, in order to minimize the risk during evacuation, a region is considered to be blocked in case of monitoring even a single damaged column. In this study, gyro sensor is proposed to assess the damage of column members. This sensor measures the angular velocity of the mounted vertical load bearing element.

Besides damage to structural components, the impacts of an event to the non-structural components are also likely to cause blockage. The non-structural components that are examined in the scope of this study and susceptible to cause blockage are suspended ceilings, infill walls and non-structural objects. In this study, two sensors are proposed to estimate damage; CCC and URF. The CCC is a closed circuit which conducts electricity. If the cable is cut off, transmitted signal changes. The URF provides the required data, which is reflection time of the ultrasonic sound, to calculate the distance between the target and the sensor. The damage assessment of a non-structural component can be carried out by using this sensor.

In addition to the aforementioned sensors, accelerometer is also proposed in this study. Floor acceleration is measured with accelerometer to detect as to whether vibration of the building can cause any damage (or blockage) in terms of predefined performance limits or not.

The last monitoring device, proposed in this study is the video camera. This device is different from the sensors in terms of use. In other words, the sensors, except accelerometer, try to assess the damage status of a component to estimate the blockage. However the estimation of the blockage is enabled in a direct manner with a video camera through an image processing tool. As a result, the information is provided directly through video camera. Different image processing methods are performed and explained in Chapter 4.

The detailed measurement tests related to all of the aforementioned sensing devices are presented in Appendix A. Nevertheless, the localization implications of these devices are also presented in Section 3.5.2.

3.3 Setup of Sensors and Related Devices

In this section electronic setup of the data acquisition devices (microcontroller and server) and the sensing devices (CCC, URF, gyro sensor, accelerometer) are explained. Besides, the basic properties of the video camera are also introduced.

3.3.1 Electronic Setup of the Data Acquisition Devices

3.3.1.1 Connections between Monitoring Devices and Server

All of the sensors are connected to the microcontrollers named and modeled as Arduino Pro 168 and Arduino Mega 2560. The data gathered from the sensing devices is transferred to a server computer through these microcontrollers. The connection between microcontrollers and server computer is provided through universal serial bus (USB) port. The power to the microcontrollers and the sensors are supplied from the server computer. Video camera, unlike sensors, is connected to the server computer directly via IEEE 1394 port known as firewire port. Data can be transferred faster with this port from USB, which is essential for video camera. These connections are shown in Figure 3.1.

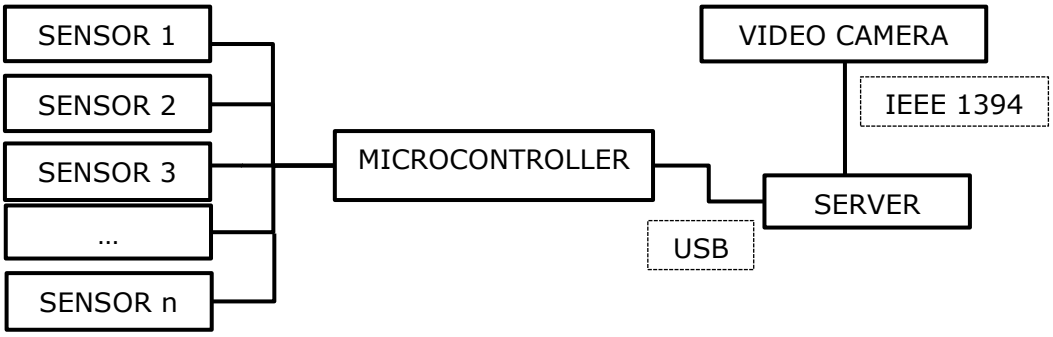

Figure 3.1 Connections between monitoring devices and server

3.3.1.2 Electronic Setup of the Microcontrollers

As mentioned above, two different microcontrollers are examined. One of them is Arduino 168 modeled microcontroller. The photo of this microcontroller with the inputs is shown in Figure 3.2. The main inputs of the Arduino 168 microcontroller are Future Technology Devices International (FTDI) breakout input, analog inputs, digital inputs, power inputs and outputs (collector supply voltage (Vcc), input voltage (Vin), grounding (GND), etc.), analog reference (AREF) output and reset. Detailed explanations of the inputs and outputs shown in Figure 3.2 are given below:

- AREF: Analog reference. The function of this input is to determine the reference voltage. The reference voltage is the voltage that runs the microcontroller. If this input is not connected, system works with 3.3 V.
- GND: Grounding. It completes the negative pole of the circuit.
- Vin: Input voltage. It completes the positive pole of the circuit.
- Vcc: Collector supply voltage. An input for regulated voltage.
- Reset: Works for restarting the microcontroller

- Digital Inputs (0-13): The digital data is transmitted from sensors to microcontroller through digital input. There are 14 inputs in Arduino Pro 168 and 54 inputs in Arduino Mega 2560.
- Analog Inputs (0-5): The analog data is transmitted from sensors to microcontroller through analog input. There are 6 inputs in Arduino Pro 168 and 16 inputs in Arduino Mega.

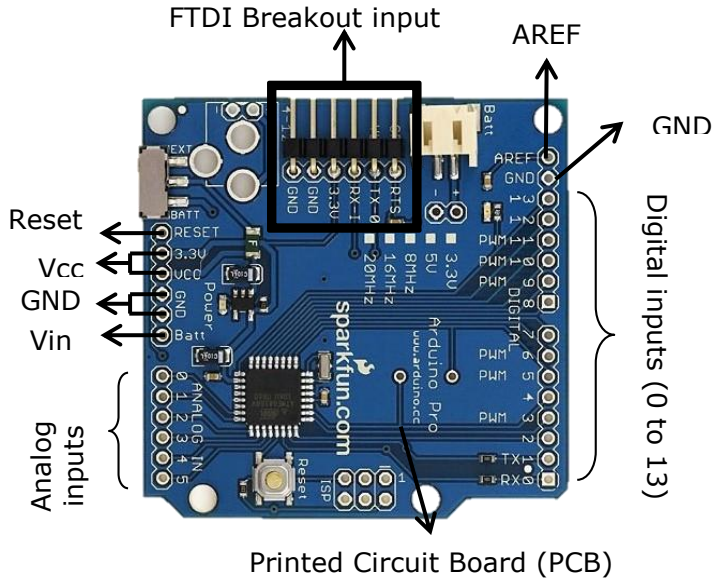

Figure 3.2 Microcontroller Arduino 168 with the inputs

In Figure 3.3 (a), the photo of Arduino Mega 2560 microcontroller, which has more analog/digital input than Arduino 168, is shown. In Figure 3.3 (b), a photo of FTDI basic breakout is shown.

(a) (b)

Figure 3.3 a) The front view of Arduino Mega 2560 microcontroller; b) FTDI basic breakout

A device named breadboard is used to wire the sensors to the microcontroller temporarily. The bread board is shown in Figure 3.4. The schematic display of the data transfer and the power transmission of the microcontroller, server computer, breadboard and sensors are visualized in Figure 3.5. The main advantage of using a breadboard is to multiply the VCC and GND of the microcontroller. Thus, the number of the sensors connected to a microcontroller is increased.

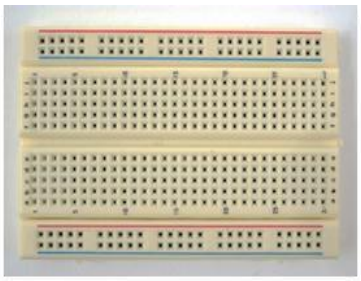

Figure 3.4 Photo of breadboard

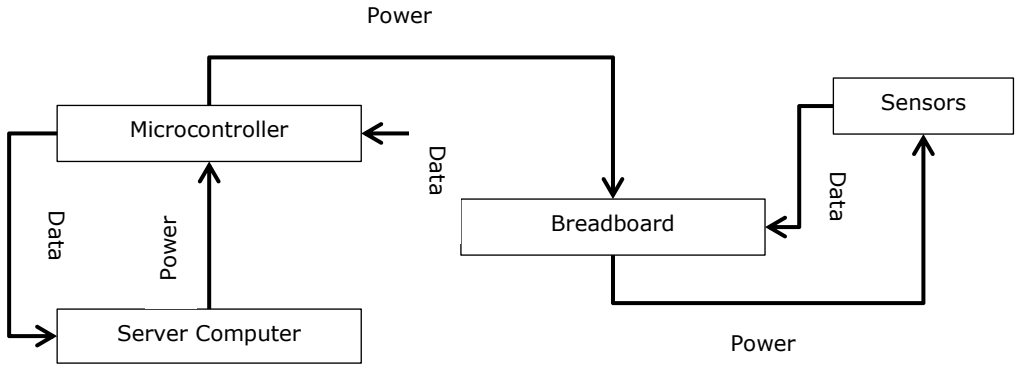

Figure 3.5 The schematic display of the data transfer and the power transmission of the microcontroller, server computer, breadboard and sensors

3.3.2 Electronic Setup of the Sensors

3.3.2.1 Setup of the Closed Cable Circuit (CCC)

The CCC is set up on a microcontroller with only wire and a resistance with 10,000 Ω. The resistance is used to prevent short-circuit. The wiring schema is shown in Figure 3.6. If the electricity is on the circuit, computer displays "1", otherwise "0".

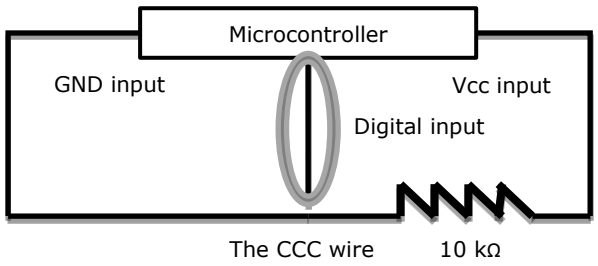

Figure 3.6 The wiring schema of the CCC

3.3.2.2 Setup of the Ultrasonic Range Finder (URF)

Maxbotix LV-MaxSonar-EZ1 Sonar Range Finder MB1010 and Ultrasonic Range Finder - Maxbotix LV-EZ4 modeled URF is used in this study. The difference between these two models is the detection patterns. Further information related to the detection pattern is provided in Appendix A. The front and the back view of the URF with input-output are shown in Figure 3.7.

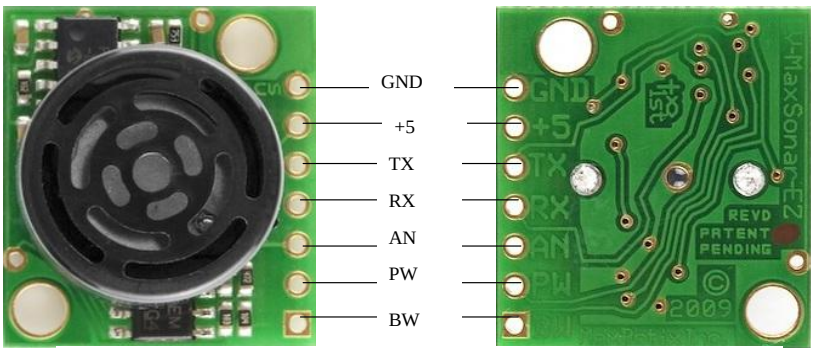

Figure 3.7 (a) The front and (b) the back view of the URF with input-output

The detailed explanations regarding the inputs and outputs of the URF are given below:

- GND: Grounding. Connected to the GND of the microcontroller. So, it completes the negative pole of the circuit.
- +5: Voltage input between 2.5 V – 5.0 V. It is connected to the VCC of the microcontroller. So, the positive pole of the circuit is completed.
- TX: Serial port communication pin. This pin is for communicating with serial port which is not used in this study.
- RX: This pin is for cutting the data transmitting which is also not used in this study.
- AN: Analog output. The measuring is transmitted to the microcontroller. It should be connected to one of the analog inputs of the microcontroller.
- PW: Pulse width output. If this pin is used with an oscilloscope, URF can check the pulse width and have more precise results at especially rough surfaces. This pin is also not used in this study.
- BW: This pin provides serial connection with other URFs. It is not used in this study.

The connection between the microcontroller and the URF is shown in Figure 3.8. As it is clearly seen in figure, the URF needs only one analog input pin of the microcontroller except for power pins.

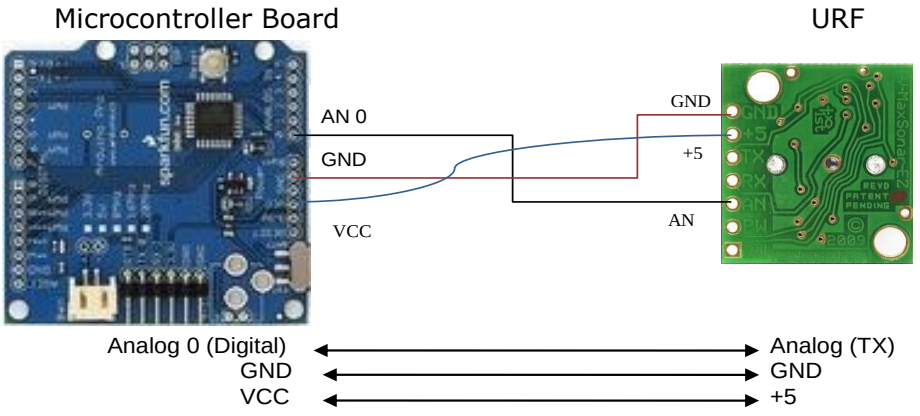

Figure 3.8 The connection between the URF and the microcontroller without breadboard

3.3.2.3 Setup of the Gyro Sensor

In this study, the sensor labeled as "IMU 5 Degrees of Freedom IDG500/ADXL335" is used as the gyro sensor. This sensor is actually the integration of two sensors. The first one is IDG500, which is a gyroscope with 2 axes. The second one is ADXL335, which is an accelerometer with 3 axes. Thus, "IMU 5 Degrees of Freedom IDG500/ADXL335" is an integrated sensor with 5 degrees of freedom. The accelerometer of the sensor has a measuring range ±3g in terms of acceleration. The gyroscope has a measuring range ±500º/s or ±110 º/s in terms of angular velocity with respect to the reference voltage. The output pins, operating range and the resolution[2] of the gyro sensor are given in Table 3.1.

Table 3.1 The output pins, operating range and the resolution of the gyro sensor

Axis	The Output Pin	Resolutions (mV/º/s)	Operating Ranges (±º/s)
X	X-OUT	2	500
	X4.5OUT	9.1	110
Y	Y-OUT	2	500
	Y4.5OUT	9.1	100

The front view of the sensor with input-output is shown in Figure 3.9, and the back view of the sensor with input-output is shown in Figure 3.10. The detailed explanations of the inputs and outputs are given below:

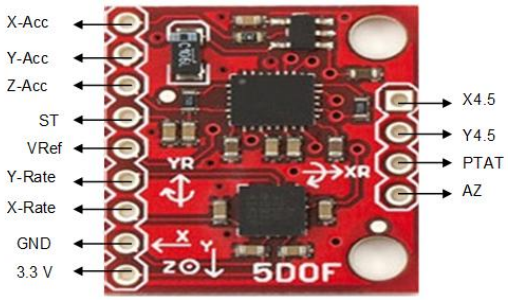

Figure 3.9 The front view of the IMU 5 DOF sensor with input and output pins

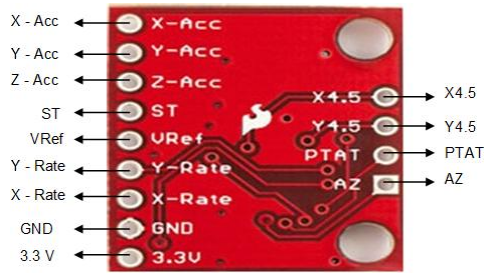

Figure 3.10 The back view of the IMU 5 DOF sensor with input and output pins

[2] The resolution of a sensor is the smallest change in measurand which produces

- GND: Grounding. Connected to the GND of the microcontroller. So, it completes the negative pole of the circuit.
- 3.3V: Voltage input (3.3 V). It is connected to the VCC of the microcontroller. So, it completes the positive pole of the circuit.
- X-Rate: Gyroscope X-axis (±500 º/s). The change of the angular velocity of the x-axis of the monitored object is transmitted to the microcontroller through this output. It should be connected to analog input pin of the microcontroller. The functioning range provided from this output is ±500 º/s with a precision of 2 mV/º/s. That much precision is not necessary to sense the structural damage of a column. So, in this study, this pin is not used.
- Y-Rate: Gyroscope Y-axis (±500 º/s). The change of the angular velocity of the y-axis of the monitored object is transmitted to the microcontroller through this output. It should be connected to analog input pin of the microcontroller. The functioning range provided from this output is ±500 º/s with a precision of 2 mV/º/s. That much precision is not necessary to sense the structural damage of a column. So, in this study, this pin is not used.
- X4.5: Gyroscope X-axis (±110 º/s). The change of the angular velocity of the x-axis of the monitored object is transmitted to the microcontroller through this output. It is connected to analog input pin of the microcontroller. The functioning range provided from this output is ±110 º/s with a precision of 9.1 mV/º/s. That much precision is enough for sensing the structural damage of a column. So, in this study, this pin is used.
- Y4.5: Gyroscope Y-axis (±110 º/s). The change of the angular velocity of the y-axis is transmitted to the microcontroller through this output. It is connected to analog input pin of the microcontroller. The functioning range provided from this output is ±110 º/s with a precision of 9.1 mV/º/s. That much precision is enough for sensing the structural damage of a column. So, in this study, this pin is used.
- X-Acc: Accelerometer X-axis. The acceleration on the x-axis of the monitored object is transmitted to the microcontroller through this output. It is connected to analog input pin of the microcontroller.
- Y-Acc: Accelerometer X-axis. The acceleration on the x-axis of the monitored object is transmitted to the microcontroller through this output. It is connected to analog input pin of the microcontroller.
- Z-Acc: Accelerometer X-axis. The acceleration on the x-axis of the monitored object is transmitted to the microcontroller through this output. It is connected to analog input pin of the microcontroller.
- PTAT: Proportional – To – Absolute – Temperature. The temperature information of the sensor is transmitted to the microcontroller through this output. It should be connected to the analog input of the microcontroller. It is the movement of mercury that enables this sensor to function. The volume of the mercury could change in different temperatures, which results in error. A temperature sensor is also integrated into this sensor in order to avoid this kind of errors. That type of precision is not necessary in this study; so, this pin is not used.
- AZ: Auto Zero. Sensor should be restarted in order to get rid of the accumulative error of the gyroscope. The necessary data is transmitted to the microcontroller in order to restart of the gyroscope itself automatically. It should be connected to analog pin of the microcontroller. This pin is not used in this thesis.
- VRef: Reference voltage. It should be connected to the VCC pin of the microcontroller. Thus, sensor can get the reference voltage. This pin is not used in this thesis.

- ST: Self - Test. This pin should be connected to the analog pin of the microcontroller. Necessary data that the accelerometer test itself is transmitted through this pin by the help of code compiled to the microcontroller. Self-test is not needed in this study; so, this pin was not used.

3.3.2.4 Setup of the Accelerometer

In this study, ADXL321 accelerometer is used. The acceleration data is provided from this device with 3 axes. The front view with input and output pins are shown in Figure 3.11. Range of this device is between ± 18 g. The detailed explanations of the inputs and outputs are given below:

- GND: Grounding. Connected to the GND of the microcontroller. So, it completes the negative pole of the circuit.
- VCC: Voltage input (-0.3V – +7.0V). It is connected to the VCC of the microcontroller. So, it completes the positive pole of the circuit.
- X-Acc: Accelerometer X-axis. The acceleration on the x-axis of the monitored object is transmitted to the microcontroller through this output. It is connected to analog input pin of the microcontroller.
- Y-Acc: Accelerometer X-axis. The acceleration on the x-axis of the monitored object is transmitted to the microcontroller through this output. It is connected to analog input pin of the microcontroller.
- Z-Acc: Accelerometer X-axis. The acceleration on the x-axis of the monitored object is transmitted to the microcontroller through this output. It is connected to analog input pin of the microcontroller.
- ST: Self - Test. This pin should be connected to the analog pin of the microcontroller. Necessary data that the accelerometer tests itself is transmitted through this pin by the help of code compiled to the microcontroller. Self-test is not needed in this study; so, this pin was not used.

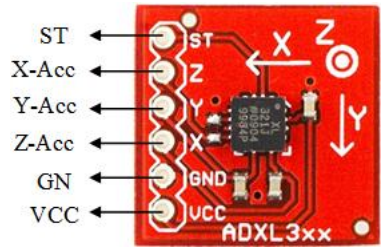

Figure 3.11 The front view of the ADXL321 accelerometer with input and output pins

3.3.2.5 The Video Camera

In order to monitor the blockage at the horizontal passage unit directly, "Canon LEGRIA HV40" modeled video camera is used. This video camera can capture the images with a resolution of 1920 x 1080. The recorded data can be transmitted to the server computer through firewire output of the video camera.

3.3.3 Software of the Devices

Two groups of software are used to monitor the blockage in the horizontal passage unit. These are:

- First Group: The software in the microcontroller to convert the voltage difference data gathered from sensors into meaningful data like distance, acceleration etc.
- Second Group: Software installed in the server computer to record the meaningful data transmitted from the microcontroller.

This process is shown in Figure 3.12 schematically.

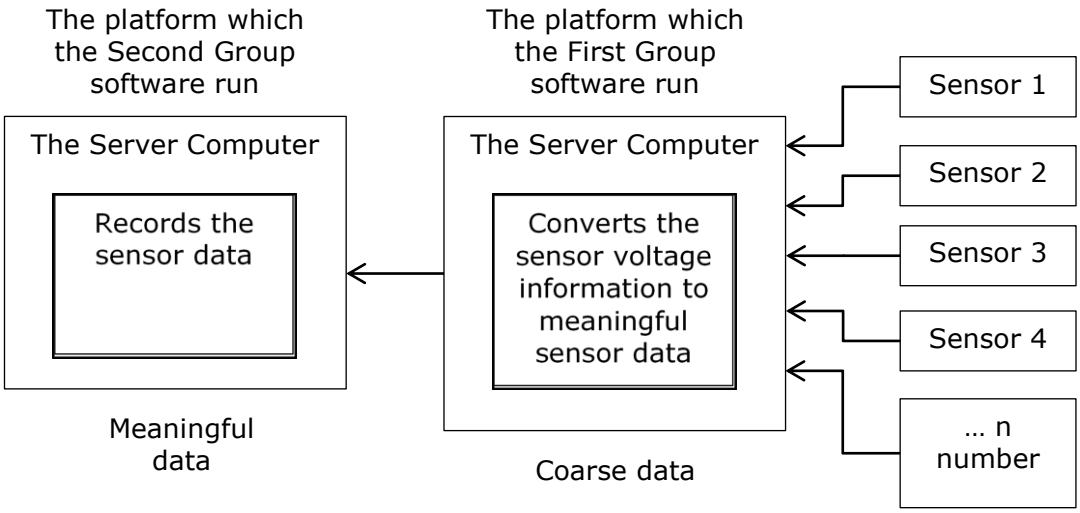

Figure 3.12 Schematic representation of the data transmission path and the steps in data processing

3.4 Characteristics of Sensors

3.4.1 Establishing the One-Spanned Experiment Model

In order to test the properties and the accuracy of the sensors, a single-span specimen was established. Only the CCC and the URF are tested on this model because these are the sensors that are used in the experiments explained in Chapter 4.

The single-span specimen was built in approximately 1/3 scale of an actual horizontal passage unit. The dimensions of the model with plan and side views are given in Figure 3.13.

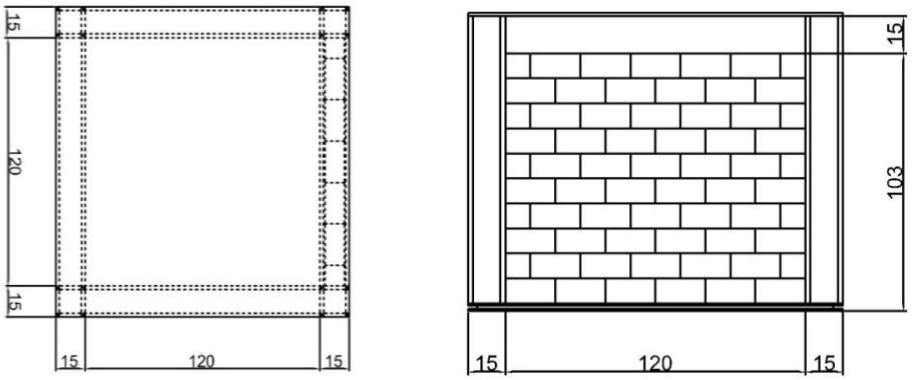

Figure 3.13 The dimensions of the model with plan and side view

The frame specimen is made up from wooden members with one span filled with infill wall. The infill wall of the model is built up from cardboard boxes (with the dimensions 100mm x 100mm x 200mm). In some experiments, cardboard panels were also used for the infill wall instead of cardboard boxes. Besides that in some experiments, cardboard panels were used for ceiling. A photo of the test specimen can be seen in Figure 3.14.

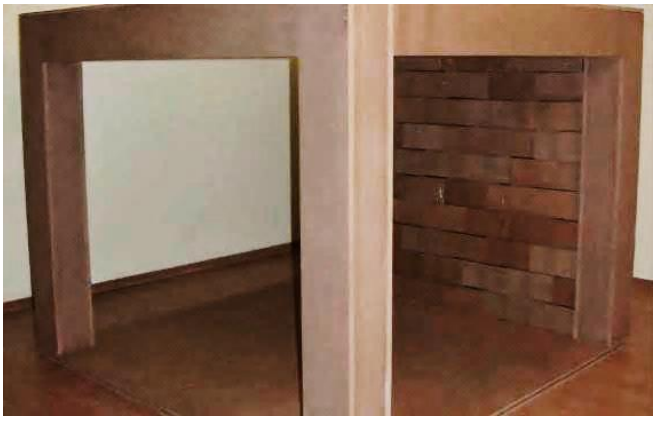

Figure 3.14 A photo of the one-spanned test specimen

3.4.2 The Experiments Conducted on the Single-Span Test Specimen

Totally 15 experiment were conducted on the single-span test specimen in order to understand the capability of the sensors. Eleven of the experiments are conducted for URF and 4 experiments are conducted for CCC. The details related to the these experiments are presented in Appendix A. Experiments results are combined with the information given in Chapter 2 in order to set the localization rules of the sensors.

3.4.2.1 The Results of the Experiments Conducted by the URF

- At the end of the experiments conducted by the URF, practical lower and upper limits are determined for the range of the URF as 300 mm and 6,000 mm respectively. These limits are within the conservative range of use for sensors. On the condition that this sensor is used within these limits, the collected data is supposed to be valid. The results beyond these limits should be evaluated diligently and the distances lower than 200 mm and upper than 6,600 mm should be ignored.
- The EZ-4 typed URF is more convenient for the purpose of this study.
- A virtual cylindrical volume with a diameter of 750 mm between the sensor and the target object must be clear to obtain accurate results.
- It is observed that location of this sensor is important. It should be across the target object, perpendicular to the ground.

3.4.2.2 The Results of the Experiments Conducted by the CCC

- Any number of CCC could be connected on the microcontroller.
- The length of the CCC wire is not important.

3.4.3 The Sensor Properties Obtained from the Results of the Experiments and Observations

3.4.3.1 The CCC

This sensor, which is proposed in this study, is based on whether the electricity is conducted or not. If electricity is conducted, the signal is transmitted as "1", otherwise "0".

Advantages: This sensor is a simple one. Many can be plugged on the microcontroller together. They can be mounted on both structural and non-structural elements.

Disadvantages: It may not be possible to understand what causes the malfunctioning of the sensor such as the damage of the element or the cable itself in case the electricity is not conducted.

3.4.3.2 The URF

Non-structural components are monitored by the URF in this study. This sensor is able to measure the distances between 300 mm and 6,000 mm. The URF has a changing beam width depending on the model. The beam width of the URF with respect to dowel radius is given in Appendix A.

The basic principle of the URF is that it senses the distance by measuring the change of the voltage. So it is important to determine the relationship between distance and voltage. The first experiment presented in Appendix A is conducted to determine this relationship. The empirical relationship obtained from experiment is given in Equation 3.1.

$$D=1.29\times V+4.02 \qquad 3.1$$

In Equation 3.1, D is the distance measured in cm and V is the voltage value read from the URF in mV. The distance can be calculated from URF voltage by using this expression.

3.4.3.3 Gyro Sensor

The angular velocity of the target object is provided by the gyro sensor in radian/second or degree/second. The present status of the target objects, especially structural components, could be assessed by using this information.

3.4.3.4 Accelerometer

The seismic action of the structures is monitored in terms of acceleration by these sensors. They usually have 3 degrees of freedom (two of them are horizontal and one of them is vertical). In general, the sensor is mounted on a floor slab and the time history of floor acceleration is monitored.

3.4.3.5 The Video Camera

The video camera is used as a sensor in this study. Determination of the view angle is important in order to locate the video camera properly. To achieve this, the following formulas are used:

$$\alpha_h = 2 \cdot \tan^{-1}(d_w/2/f) \quad 3.2$$

$$\alpha_v = 2 \cdot \tan^{-1}(d_h/2/f) \quad 3.3$$

In these equations; α_h is the horizontal view angle in degrees, d_w is the width of the video camera sensor in mm, f is the focus distance of the lens in mm, α_v is the vertical view angle in degrees, d_h is the height of the video camera sensor in mm. A sketch of the video camera view angles are shown in Figure 3.15.

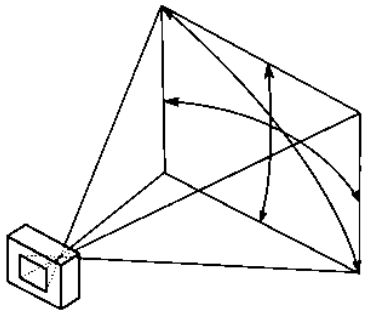

Figure 3.15 A sketch of the video camera view angles (Birgönül et al., 2012)

The video camera used is this study has a lens focus distance (f) that changes between 6.1 mm (maximum zoom out, view angle) and 61 mm (maximum zoom in, the narrowest view angle) with respect to the optical zoom used. The width of the video camera sensor (d_w) is 7.173 mm and the height of the video camera sensor (d_h) is 4.035 mm. The horizontal view angle (α_h) calculated from Equation 3.2 changes between 7° - 61°. Likewise, the vertical view angle (α_v) calculated from Equation 3.3 changes between 4° - 37°. These angles are calculated in view of 16:9 aspect ratio of the display used in this study.

As a result, in the light of the information given above, video camera should be located in a place that looks directly into the horizontal passage unit by considering α_h. The angle between video camera and ground should be adjusted with respect to the α_v

3.5 Principles and Rules about the Sensors Localization

The principles and rules about the number and locations of the sensors in a building are discussed in this section. First, the principles and the rules about the localization and the number of the sensors are given in general. Then, the detailed explanations for each sensor are provided.

3.5.1 General Principles and Rules

The principles and the rules regarding the number and the localization of the sensors are as follows:

- The number, the location and the type of the mounted sensors should be determined with respect to the structural system and the intended purpose of the building monitored.
- In addition to this, the architectural properties of the building can affect the localization of the sensors.
- Video cameras can monitor more than one span in a horizontal passage unit but all other sensors can transmit information from only one span.

- Each span of the horizontal passage units should be monitored with at least one sensor.
- The spans near the vertical passages and exits should be monitored in a more detailed manner because if a blockage occurs near exits or vertical passages, it would be impossible to guide occupants to the outside of the building.

3.5.2 Principles and Rules Based on Sensors

The placement and the number of sensors are given considering the properties of each sensor. In this study, only the building components that can cause blockage and that can be monitored by sensors are considered. For example, the data generated for infill walls by URF is appropriate. Besides, the physical placement of the sensors to an element is to be considered. For example, it is not possible to mount a gyro sensor to an infill wall practically.

3.5.2.1 Closed Cable Circuit (CCC)

The building components on which this sensor can be mounted are as follows:

Suspended ceiling: The fact that the suspended ceiling that is not connected well to slab or that contains freely moving covering plates may lead to blockage of the passages with the dislocated or ruptured pieces during an earthquake. There are also some secondary risks for the victims like electrical leakage (Figure 3.16). The CCC can be used to monitor this type of damage (Figure 3.17).

Figure 3.16 The damage caused by the collapse of the suspended ceiling

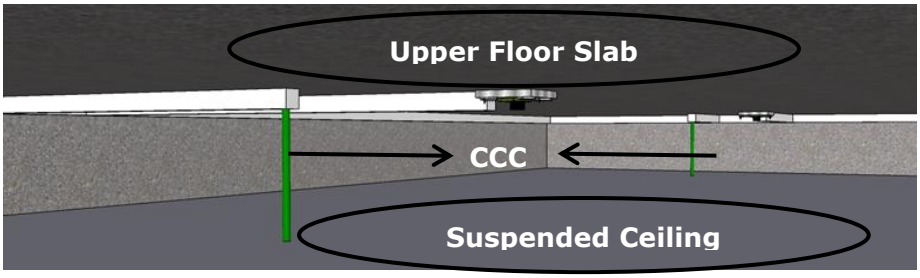

Figure 3.17 The CCC mounted to suspended ceiling

Non-load-bearing (infill) walls: The infill walls made up from materials like brick, concrete briquette, and autoclaved aerated concrete behave like shear walls during a low intensity ground shaking and restrict the horizontal movement of the building to some degree. On the contrary, the infill walls cracked and

damaged during a high intensity ground shaking could be damaged in the out-of-plane direction despite the overall structural system of the building has not been damaged severely yet. This can cause blockage at the passage units.

Figure 3.18 A building infill walls of which collapsed after the 1999 Marmara Earthquake

Under which conditions the infill walls will be damaged or collapse depends on the geometrical and material properties of both the infill wall and elements that are in touch with the infill wall. The most common failure modes are given in Figure 3.19 (Tomazevic, 1999). The infill wall is separated into a couple of blocks and can fail in the out-of-plane direction at each mode. It can be stated that mounting the CCC in the middle of the infill wall diagonally would be suitable after observing the failure modes mentioned above.

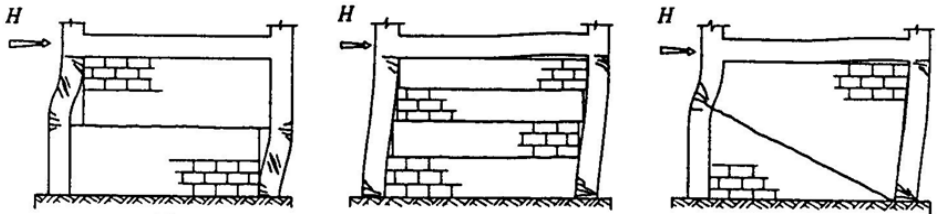

Figure 3.19 The most common failure modes of infill walls (Tomazevic, 1999)

Non-structural Units (e.g. furniture's, office equipment, cupboards…): The failure and collapse of the non-structural objects in the building can cause blockage (Figure 3.20). In this case, it is essential to monitor the objects having failure risk with the CCC (Figure 3.21). When the object which the CCC mounted fails, the wire of the CCC breaks off and that information is transmitted to the microcontroller. In some cases, despite the wire is broken, the object does not fail (only vibrates and returns to its stable state) or vice versa. In such cases, the data obtained from the other sensors (e.g. primarily the video camera) becomes important.

Figure 3.20 The failed office equipment and furniture during an earthquake

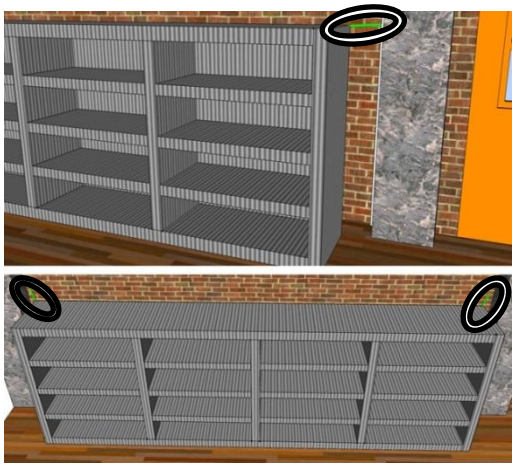

Figure 3.21 The mounted CCCs to monitor a non-structural object. The CCCs are circled

3.5.2.2 Ultrasonic Range Finder (URF)

The elements on which this sensor can be mounted are as follows:

Suspended ceiling: This sensor is mounted to the ceiling as in Figure 3.22 in order to determine any collapse. In this case, the threshold value of the URF is the distance between the upper floor slab and the suspended ceiling. More specific information about the threshold value is given in Chapter 4.

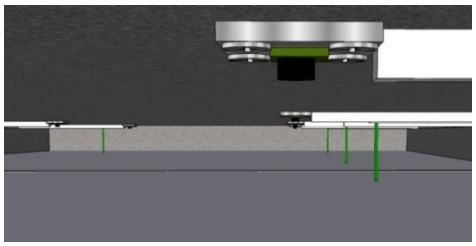

Figure 3.22 Placement of the URF in order to monitor the suspended ceiling

Non-load-bearing (infill) walls: The URF can be placed on an infill wall in order to monitor its current status. As mentioned before, while placing the sensors the most important parameter is the beam width of the URF. So the most practical solution to obtain reliable data is to mount the URF in the middle of the beam element across the infill wall in frame structures (Figure 3.23). The sensor should be projected toward the mid-region of the infill wall. The threshold value of the URF is the distance between the infill wall and the sensor itself. More specific information about the threshold value is given in Chapter 4.

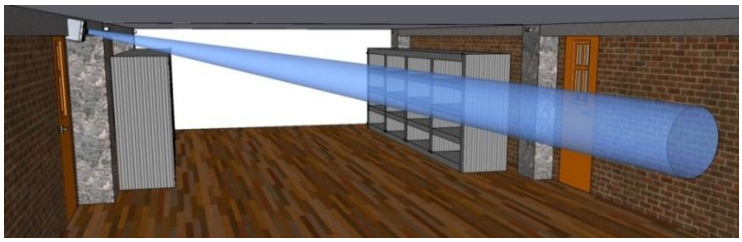

Figure 3.23 The placement of the URF to monitor a non-load-bearing infill wall

3.5.2.3 Gyro Sensor

The elements on which this sensor can be mounted are as follows:

Load-bearing units (columns): It is possible to monitor the lateral deformations which the columns are exposed of during an earthquake and the related probable damage by using the data obtained from the gyro sensor. A gyro sensor, which is placed to the upper section of the column, gives the angular velocity of the column with respect to the intensity of the earthquake during the movement (Figure 3.24). Considering the fact that a column is translated and rotated at the same time during an earthquake, the relationship of the linear velocities of the bottom and top column ends can be calculated based on basic dynamic engineering principles (Equation 3.4):

$$V_B=V_A+V_{B/A} \quad \textbf{3.4}$$

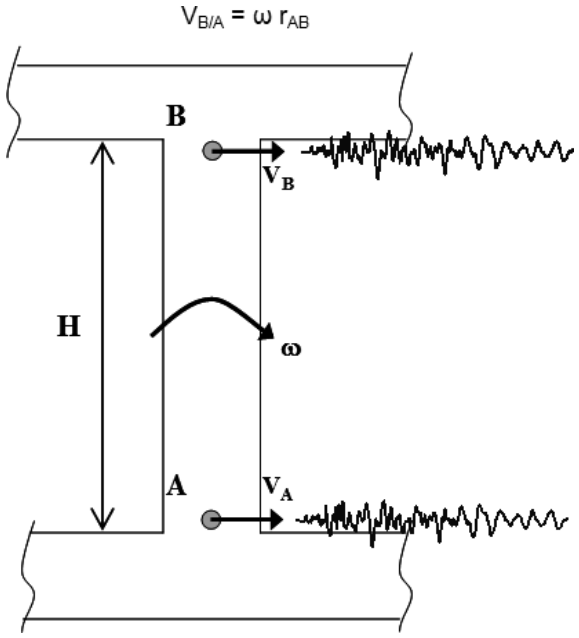

Figure 3.24 The movement parameters of a column which is exposed to the lateral earthquake impacts

The parameters V_A and V_B presented in Equation 3.4 are the absolute linear velocities of the column ends and $V_{B/A}$ is the linear velocity of point B with respect to point A. The relative velocity and the angular velocity can be related with the following equation (Equation 3.5):

$$V_{B/A}=\omega \cdot r_{AB} \quad \textbf{3.5}$$

In this equation, ω is the angular velocity and r_{AB} is the distance between points A and B, in other words, it is the height of the column (H). In the light of these equations, taking the integral of the recorded acceleration data of the bottom and the top column ends, the change of the linear velocity with respect to time is obtained. The angular velocity with respect to time can be found from Equation 3.6 by using these parameters.

$$\omega\ t = \frac{V_B\ t - V_A(t)}{H} \qquad \textbf{3.6}$$

The angular velocity of a typical column is calculated under the effects of two different earthquakes by using these equations. The first earthquake is a moderate earthquake (1995 Afyon-Dinar earthquake, Mw=6.4) and the second one is a large one (1999 Marmara Earthquake, Mw=7.2). The time histories of relative velocities obtained by the subtracting the calculated linear velocity of the top column end from the bottom column end is given in Figure 3.25.

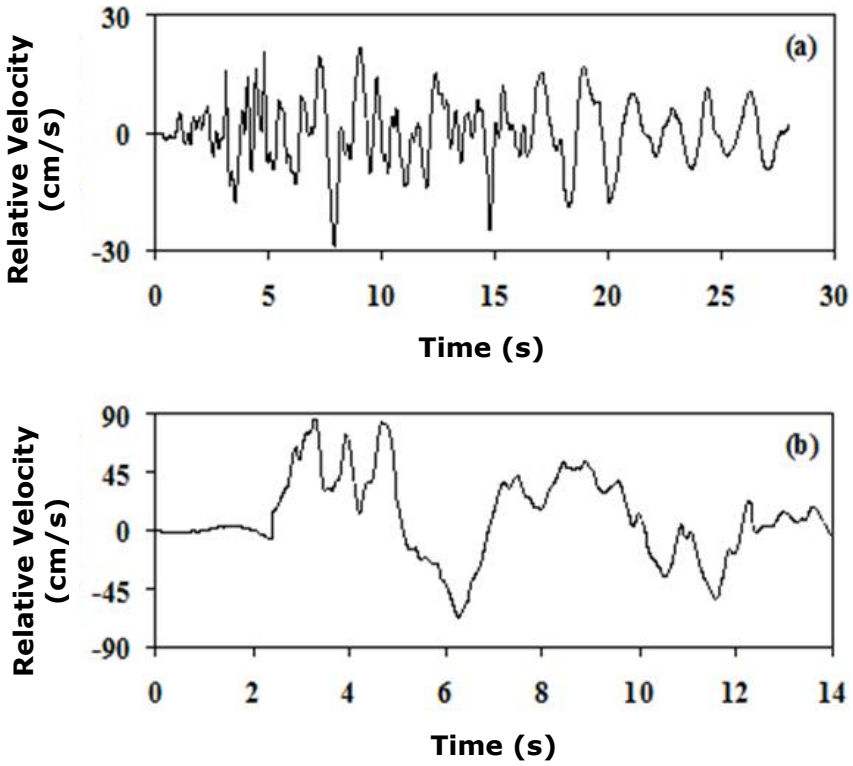

Figure 3.25 The relative linear velocity change of column from; (a) moderate earthquake, (b) heavy earthquake

As is seen, the moderate earthquake creates a maximum relative velocity of 30 cm/s. However, large earthquake creates a relative velocity of 90 cm/s, which means that the latter one is nearly 3 times more effective. The angular velocity variation of the same column, under the effect of the same earthquakes, is calculated by using Equation 3.6 and the time histories are presented in Figure 3.26.

As is seen in Figure 3.26, it is possible to observe the angular velocity with a magnitude of 5°/s for the moderate earthquake and 20°/s for the heavy earthquake respectively. This shows that if the data obtained from a gyro sensor mounted to a column is greater than 5 °/s, it is possible to observe that the column is severely damaged seriously. A severely damaged column may cause a partial failure of the building during a disaster. As a result, partial failure means blockage and gyro sensor could get that kind of information.

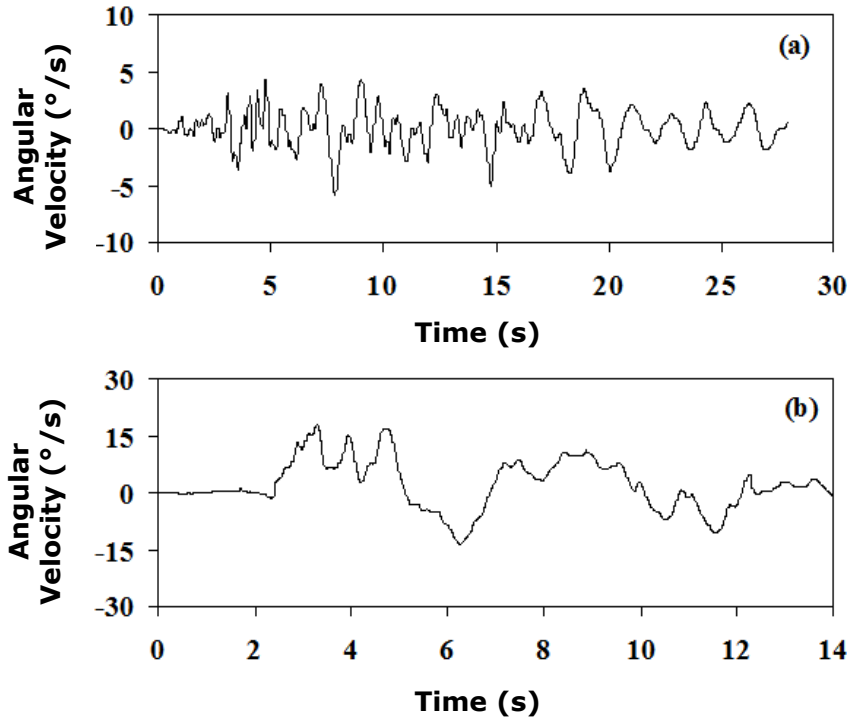

Figure 3.26 The relative change in angular velocity between the ends of columns (a) moderate earthquake, (b) heavy earthquake

3.5.2.4 Accelerometer

Many studies, related to the relationship between the measured floor acceleration during earthquake and the corresponding damage are available in the literature (Chaudhuri and Hutchinson, 2004; Mondal and Jain, 2005; Retamales et al., 2006; Sankaranarayanan, 2007; Lam and Gad, 2008). In these studies, the researchers stated that acceleration cannot be an indicator of damage by itself; some other different parameters must also be involved. Yet, some limits could be specified roughly. These limits could be a trigger for the system to start monitoring. As a result, at least an accelerometer should be mounted to each floor to obtain and record the building motion in terms of acceleration.

3.5.2.5 Video Camera (Image Processing)

Video camera used to realize whether the passage is free to pass by or not, rather detecting the blockage through the image processing software. The security cameras could also be used for this purpose. There are two image processing methods to be suggested for that purpose in this study. These approaches are suggested and explained in Chapter 4.

CHAPTER 4

EXPERIMENTAL STUDIES

4.1 Introduction

This chapter presents the experimental studies conducted in order to estimate real-time damage status of a horizontal passage unit (i.e. corridor unit) by the help of combined sensor data. The main purpose of these experiments is to receive data in order to generate and test a sensor fusion approach. Another purpose of these experiments is to develop and test different image processing approaches. In order to conduct these experiments, a 1/3 scaled horizontal passage unit with three spans is constructed. Twenty-nine experiments are carried out under five different experiment groups with sixty-four phases. In every experiment group, there is at least one experiment and in every experiment, there is at least one phase. Results of the experiments could be differed related to the aspect ratio of the horizontal passage unit cross-section. So, four of the experiment groups (1, 2, 3 and 4) are conducted on the same 1/3 scale model with an aspect ratio in terms of a height/width ratio of 12/17 is called in this thesis as "the wide corridor model". The other experiment group (5) is conducted by using a model with an aspect ratio in terms of a height/width ratio of 4/3 called in this thesis as "the narrow corridor model". All of the experiments are shown in Table 4.1.

Table 4.1 All experiment groups, experiments and phases

NAME OF THE GROUP	NAME OF THE EXP.	NUMBER OF PHASES
EXPERIMENT GROUP 1	EXPERIMENT 1	4
	EXPERIMENT 2	4
	EXPERIMENT 3	4
EXPERIMENT GROUP 2	EXPERIMENT 1	7
EXPERIMENT GROUP 3	EXPERIMENT 1	1
	EXPERIMENT 2	1
	EXPERIMENT 3	1
	EXPERIMENT 4	3
	EXPERIMENT 5	3
	EXPERIMENT 6	1
	EXPERIMENT 7	1
	EXPERIMENT 8	1
	EXPERIMENT 9	3
	EXPERIMENT 10	3
	EXPERIMENT 11	3
	EXPERIMENT 12	3
	EXPERIMENT 13	1
	EXPERIMENT 14	1
	EXPERIMENT 15	1
	EXPERIMENT 16	1
	EXPERIMENT 17	1
	EXPERIMENT 18	1

Table 4.1 (cont'd) All experiment groups, experiments and phases

NAME OF THE GROUP	NAME OF THE EXP.	NUMBER OF PHASES
EXPERIMENT GROUP 4	EXPERIMENT 1	7
EXPERIMENT GROUP 5	EXPERIMENT 1	1
	EXPERIMENT 2	1
	EXPERIMENT 3	1
	EXPERIMENT 4	1
	EXPERIMENT 5	1
	EXPERIMENT 6	3

Two of the experiments have missing data caused by technical difficulties. At all phases of the experiment group 1, experiment 1, the server is not be able to record the camera data and at experiment group 5 experiment 1, which has only one phase, server is not able to record the sensor data.

4.2 Construction of the Experimental Set-up

To conduct the experiments, a scaled model of a horizontal passage unit with three spans, which represents the horizontal passage unit of an actual public building, is constructed. The plan of the actual building and the selected horizontal passage unit are given in Figure 4.1. The sketch of the designed model is also shown in Figure 4.2. Construction of the experimental set-up consists of two phases: the construction of the model and the installation of the electronic equipment.

Figure 4.1 Plan of the actual building and the horizontal passage unit used for the experimental study

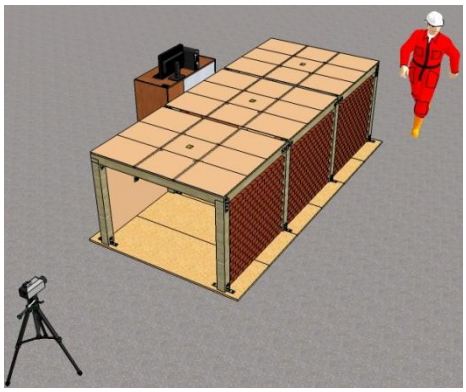

Figure 4.2 3-D view of the experiment model (wide corridor model)

4.2.1 Construction of the Model

Model is basically made up of two parts: the elements affected from an event and not during the experiments. The elements that are not affected from an event constitute the frame of the model (columns and beams) and ceilings. The elements that are affected from event during experiment and are rebuilt for the next experiment are walls suspended ceilings and cupboards which are prepared, representing the furniture in the building. The frame element and the actual ceiling are not affected by the event in the experiment. Any event to cause harm to these elements will cause damage to the essential instrumentation needed for the system. Besides, it is assumed that such an event is certain to cause blockage.

4.2.1.1 The Frame

The test frame stands on six fixed oriented structural boards (OSB). Dimensions of an OSB are 2,050 mm in length, 675 mm in width and 22 mm in thickness. Frame members (columns and beams) are made of wood. Cross-sectional dimensions of a frame element are 100 mm both in width and height. Length of a column is 1,200 mm which is also the length of a short beam. Length of a long beam is 1,500 mm for wide corridor model.

Columns are connected to OSB by L-shaped aluminum profiles. Beams are connected to columns with aluminum sheets. Aluminum sheets are screwed to both beams and columns.

Dimensions of the wide corridor model are 4,000 mm in length; 1,700 mm in width and 1,200 mm in height and the narrow corridor model are 4,000 mm in length; 900 mm in width and 1,200 mm in height as shown in the Figure 4.3. In addition to these sketches, photos of the wide corridor frame and the narrow corridor frame taken at the construction stage are shown in Figure 4.4.

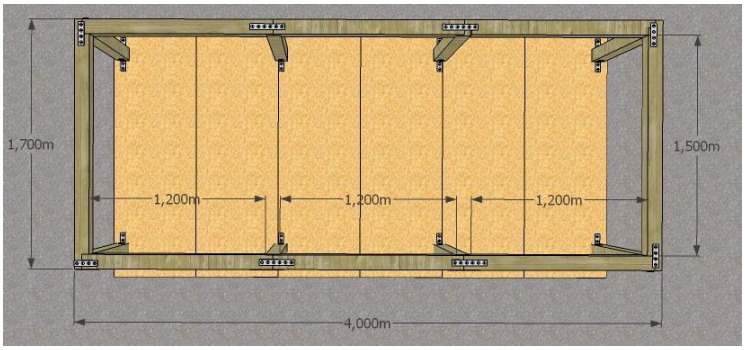

(a)

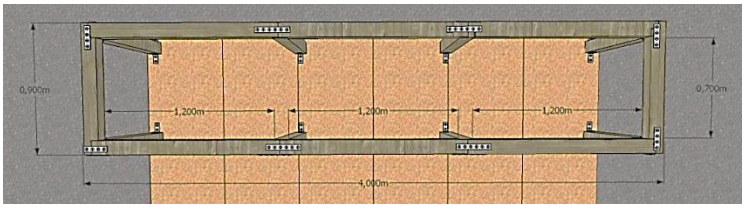

(b)

Figure 4.3 Plan view of the frame of (a) the wide corridor model (b) the narrow corridor model with dimensions

(a)

(b)

Figure 4.4 Photo of the frame of (a) the wide corridor model and (b) the narrow corridor model while construction carries on

4.2.1.2 The Ceiling

After the completion of the test frame, ceiling is constructed (one ceiling for each span). Ceilings are made from cardboards with 4 mm thickness and strengthened with thin wooden bars. Dimension of the ceiling is 1,300 mm in width and 1,700 mm in length. The ceilings are placed on the model without any connection element. A 3-D sketch of a ceiling with dimensions is presented in Figure 4.5 and also a sketch of the frame with ceilings is given in Figure 4.6.

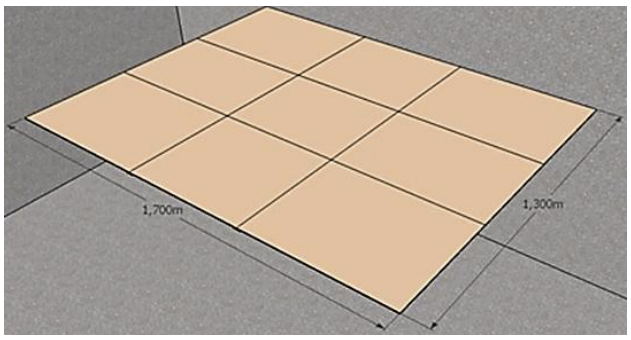

Figure 4.5 A 3-D sketch of a ceiling with dimensions

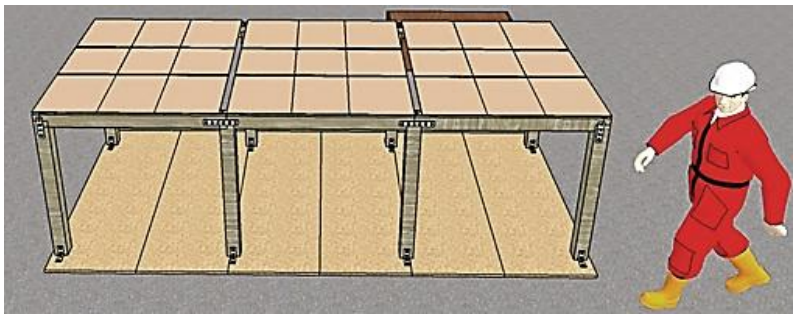

Figure 4.6 A 3-D sketch of the wide corridor model with ceiling

4.2.1.3 The Infill Walls

Walls are made from bricks with dimensions of 60 mm 80 mm 100 mm (Figure 4.7). During the experiments, four of the six spans are filled with walls. Labels and the locations of the walls are provided in Figure 4.8.

Figure 4.7 Photo of the bricks

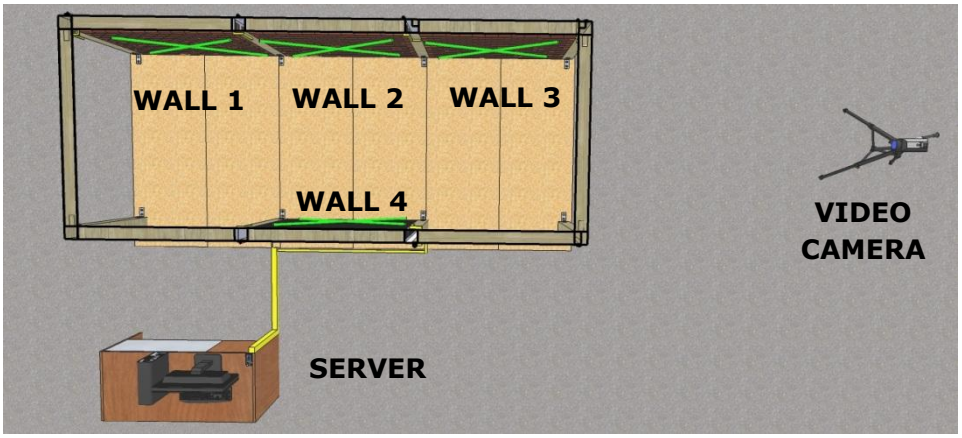

Figure 4.8 Plan of the wide corridor model and the name of the walls

The infill walls are expected to experience damage in out-of-plane direction easily by some means of external disturbance during the tests. It is also expected that the wooden frame would conceive no damage during the tests. Therefore three wall specimens with different layout of brick units and mortar characteristics are examined to see which one achieves this task (Figure 4.9).

(a)

(b)

(c)

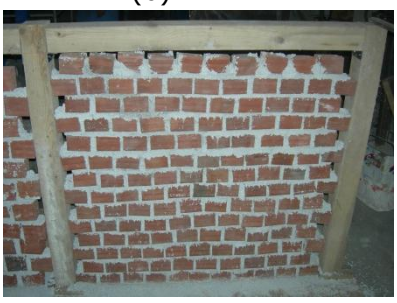

(d)

Figure 4.9 (a) General view of walls, (b) first wall, (c) second wall and (d) third wall

In the first and second wall specimens, lime mortar (lime:sand proportion is 1:6 by weight) has been used whereas in the third specimen, cement-lime mortar (lime:cement:sand proportion is 1:1:6 by weight) has been used. Amount of water is added by personal judgment according to the workability of the mix.

All the walls are constructed in running bond (i.e. the head joints align in alternate courses, and are aligned with the middle of the units in adjacent courses) with different unit orientations. In the first wall, the orientation is stretcher (height of unit is used in the stack) while the other two walls have shiner orientation (thickness of unit is used in the stack).

During the experiments, all three types of walls behaved in a satisfactory manner. They are demolished easily without any damage to the wooden test frame. However, there are slight differences in preparation of the test specimens, which affects the duration between any two consecutive experiments. It takes more time to construct the first wall specimen with stretcher bond and it takes more time to clean out the remains of the third wall specimen because of the cement used in the mortar. As a result, the second wall specimen is selected to simulate the infill wall in the horizontal passage unit during the tests. The wall specimens after the tests are shown in Figure 4.10.

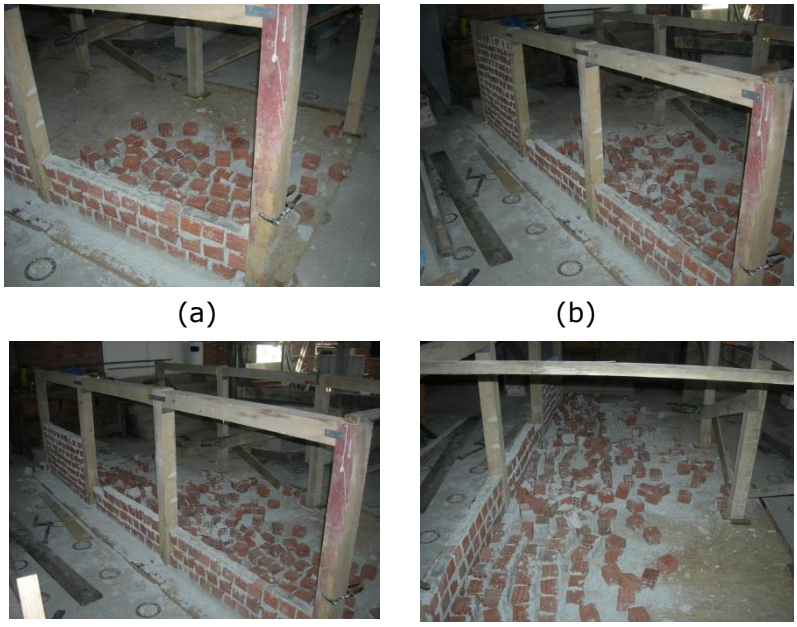

Figure 4.10 Photo of (a) failure of the third wall, (b) failure of the second and the third walls, (c) failure of all of the three walls and (d) horizontal passage unit after failure

4.2.1.4 The Suspended Ceilings (SC)

Another non-structural element of the tested frame, which is supposed to suffer some damage, is the suspended ceiling. The suspended ceilings are made from double layered corrugated cardboards. It is rectangular in shape. The length of the suspended ceiling is 500 mm whereas the width is 700 mm. The suspended ceilings are connected to the ceiling with a cord from each corner. The names of these cords are "left back cord" (LBC), "left front cord" (LFC), "right back cord" (RBC) and "right front cord" (RFC) (Figure 4.11).

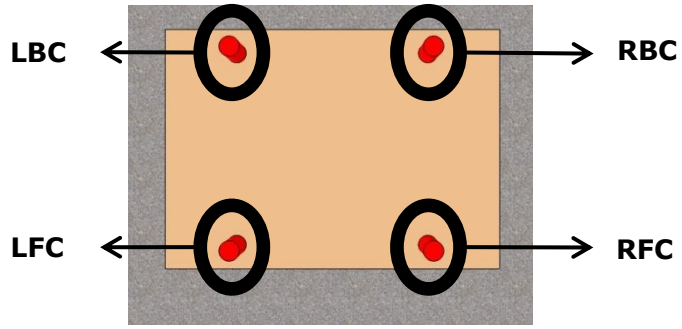

Figure 4.11 Locations and names of cords that connects suspended ceilings to the actual ceiling

A space of 100 mm is given between the suspended ceiling and the actual ceiling. A sketch with the dimensions of suspended ceiling can be seen in Figure 4.12. The suspended ceilings are used only in the wide corridor model experiments. In these experiments, damage is given to the suspended ceiling by unlacing the cord from the ceiling. So; it is assumed that a horizontal passage unit could be affected from suspended ceiling damage in 7 ways. The names and the descriptions of these damages are given in Table 4.2.

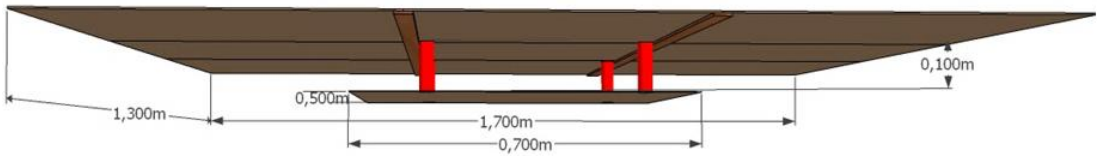

Figure 4.12 Side view sketch of the suspended ceiling and ceiling

Table 4.2 The names and the descriptions of the suspended ceiling damages

NAME	DESCRIPTION OF THE SUSPENDED CEILING DAMAGE
Type 0	No damage at suspended ceiling
Type 1	Unlacing one cord of the suspended ceiling
Type 2	Unlacing two cords presented diagonally at the suspended ceiling (e.g. LBC and RFC or LFC and RBC)
Type 3	Unlacing two cords presented parallel to the longitudinal direction of horizontal passage unit at the suspended ceiling (e.g. LBC and RBC or LFC and RFC in Figure 4.13)
Type 4	Unlacing two cords presented perpendicular to the longitudinal direction of horizontal passage unit at the suspended ceiling (e.g. LBC and RBC or LFC and RFC in Figure 4.13)
Type 5	Unlacing any three cords of the suspended ceiling
Type 6	Unlacing all of the cords of the suspended ceiling

There are three suspended ceilings on the test specimen for each span which are labeled as the suspended ceiling 1 (SC 1), suspended ceiling 2 (SC 2) and suspended ceiling 3 (SC 3). The sketch that shows the labels and the locations of the suspended ceilings is given in Figure 4.13.

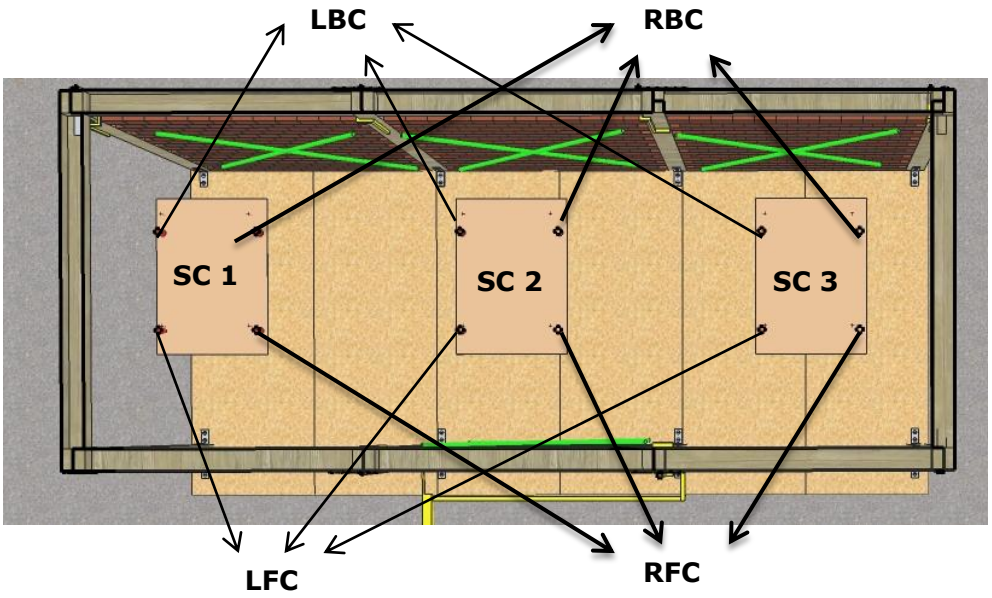

Figure 4.13 Locations and names of suspended ceilings and cords

4.2.1.5 The Non-structural Objects (The Cupboards)

To simulate the non-structural components that can block the horizontal passage unit after an event, cupboards (CB) made from wooden planks are used. Dimensions of the cupboards are 1,000 mm in height, 1,000 mm in width and 200 mm in thickness. The photo and the locations of the cupboards are presented in Figure 4.14.

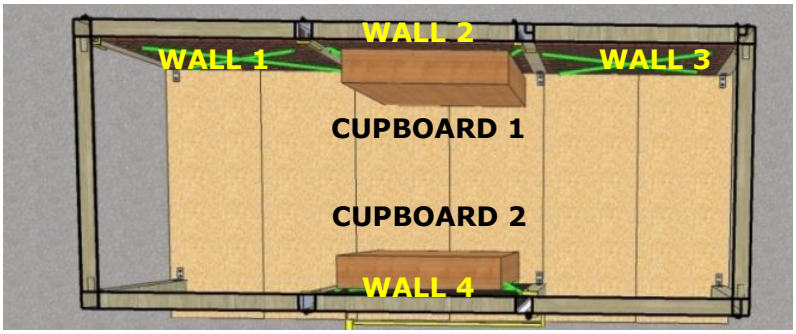

(a)

(b)

Figure 4.14 (a) Location and the labels of the cupboards on sketch and (b) photograph of the cupboard

4.2.2 The Instrumentation of the Test Specimen

Instrumentation of the test specimen consists of sensors, single-board microcontroller, video camera, server and the connection cables that transmit the necessary data and power between these devices. In the wide corridor model, 5 URF and 24 CCC are used. Besides that, number of the sensors in the narrow corridor model is different with respect to the condition of the experiment. However, a video camera is used in all the experiments. The locations of all this equipment is discussed in Section 4.3.

4.2.2.1 The Sensors

One of the main elements of instrumentation is the sensors. There are two kinds of sensors used in the horizontal passage unit models: CCC and URF. These sensors are connected to single-board microcontroller as explained in Chapter 3. Circuits of CCC are wired on a board instead of bread board. Apart from these, another circuit called as "trigger" is set up to mark the beginning and the end of the experiments in the collected data set.

The board is connected to single-board microcontroller whereas single-board microcontroller is connected to server via universal serial bus (USB). A photograph of the board and the single-board microcontroller can be seen in Figure 4.15. In addition, a computer code that is based on C++ language is written and installed to the single-board microcontroller to operate the sensors and the trigger.

4.2.2.2 The Video Camera

The properties and the image processing methods of the video camera are introduced in Section 4.5.3. Video is recorded to digital video cassette and to the server simultaneously. Video camera is connected to server via firewire port (IEEE 1394).

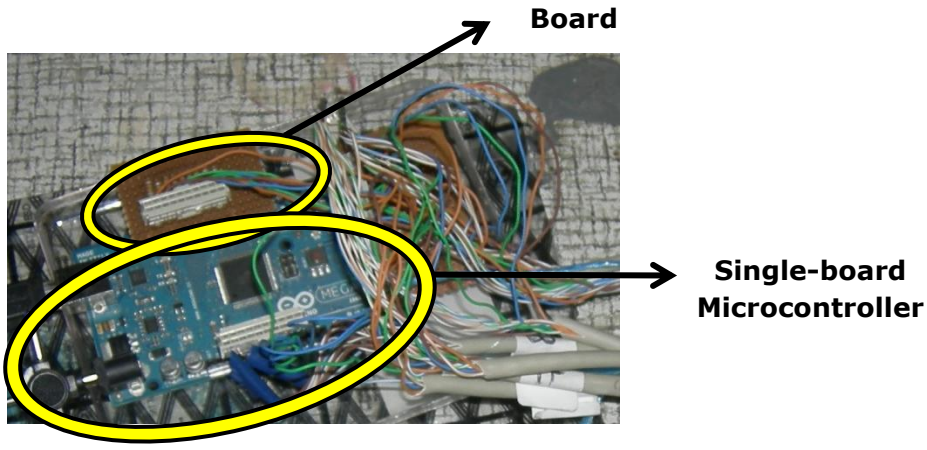

Figure 4.15 Photograph of the board and the single-board microcontroller

4.2.2.3 The Server

Sensors and the video camera are connected to a server as explained in previous sections. These devices transmitted the experiment data to the hard disk drive of

the server simultaneously by the help of a computer program while the experiments are conducted.

4.3 The Installation of the Devices to the Test Specimen

As mentioned in other sections; the walls, the suspended ceilings and the cupboards of the model are monitored by sensing devices. There are 4 walls, 3 suspended ceilings and 2 cupboards as explained in Section 4.2.1. Each cupboard is monitored by 2 CCC, whereas each suspended ceiling is monitored by 4 CCC (for each cord) and an URF at the middle of the ceiling. Two CCC are monitored on each wall. Besides CCC, URFs also monitored Wall 1 and Wall 3. The types and the numbers of the sensors monitoring the elements for wide corridor are given in Table 4.3.

Table 4.3 The types and the numbers of the sensors for monitoring the elements of the wide corridor specimen

MONITORED ELEMENT	CCC	URF
Cupboard 1	2	0
Cupboar1	2	0
SC 1	4	1
SC 2	4	1
SC 3	4	1
Wall 1	2	1
Wall 2	2	0
Wall 3	2	1
Wall 4	2	0
TOTAL	**24**	**5**

CCCs are mounted on the right and the left leg of the cupboards as showed in Figure 4.16. At the suspended ceilings, CCCs are installed near the cords, between the ceiling and the suspended ceiling. URF is placed to the center of the ceiling towards to the suspended ceiling. Sensors examining the suspended ceiling are shown in Figure 4.17. On the walls, CCCs are mounted from the up right corner to the left bottom one and the up left corner to the right bottom one in a diagonal manner (Figure 4.18). URFs are also placed to the center of the empty span across the wall as shown in Figure 4.19. Video camera is used for monitoring the condition of the horizontal passage unit and is placed as shown in Figure 4.20. The optimum distance between horizontal passage unit and the video camera is determined as 2,400 mm.

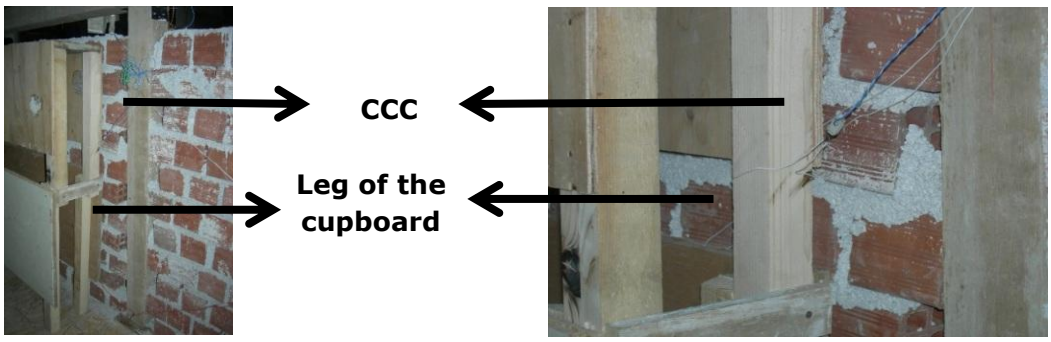

(a) (b)

Figure 4.16 (a) Overall view and (b) closed view of the CCC at the cupboard

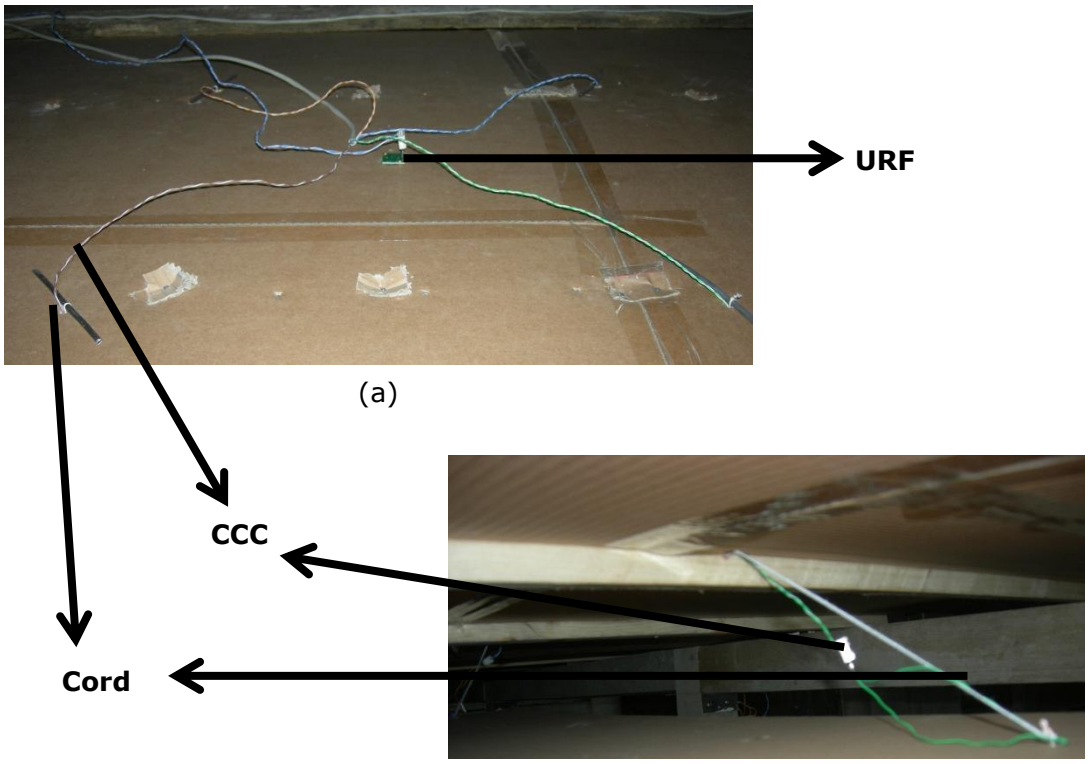

Figure 4.17 View of the cords and the devices (a) from outside of the model and (b) between ceiling and the suspended ceiling

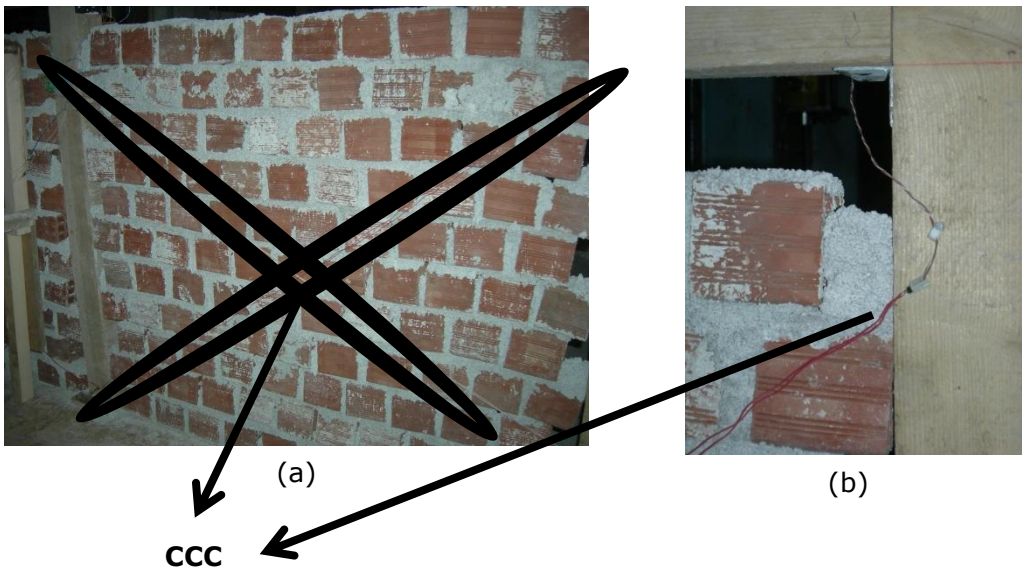

Figure 4.18 (a) General view and **(b)** close view of the CCC at the wall

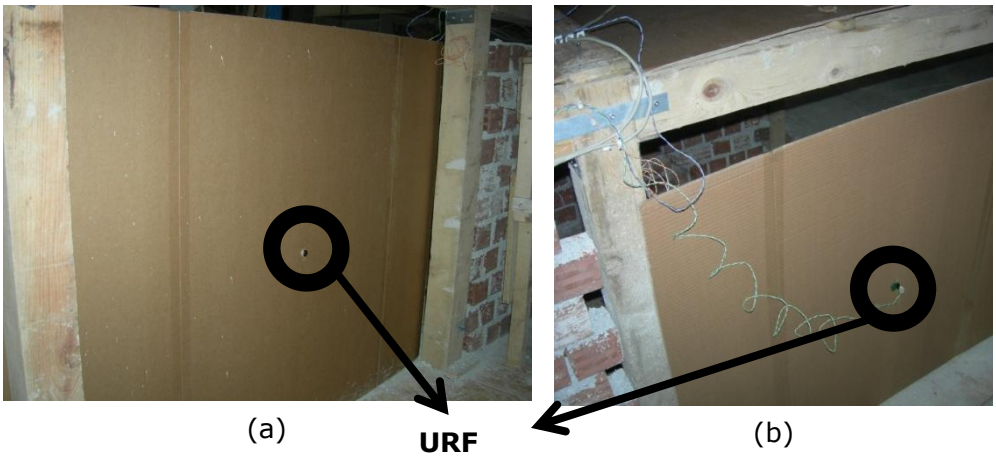

Figure 4.19 (a) View from the inside of the model and (b) view from the outside of the model of the URF at the wall

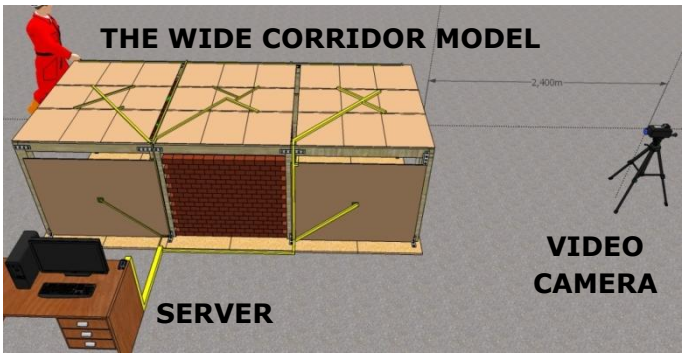

(a)

(b) (c)

Figure 4.20 (a) Sketch and (b, c) photographs of the video camera monitoring the wide corridor model

4.4 The Experiments and the Results

As mentioned before, four experiment series are conducted with wide corridor model and one experiment series is conducted with the narrow corridor model. Totally five experiment series are conducted with 3-spanned horizontal passage unit test specimen. Results of these experiments are evaluated for each span separately. In other words, blockage level of each span is assessed individually. As a result, 56 phases with 3-spanned wide corridor have 168 results and 8 phases with 3-spanned narrow corridor had 24 results, totally 192 results obtained from experiments. Due to technical difficulties, 3 of the 192

experiments have missing data; hence, 189 of them are taken into consideration. This is a huge amount of data, which can be used in sensor fusion studies in order to estimate the damage and blockage level of the horizontal passage unit specimen.

4.4.1 The Conducted Experiments

A standard procedure is followed while making experiments and gathering data. The process in a typical experiment series can be stated as follows:

1. The steps which have been followed during an experiment series are:
   a. First, all of the electronic equipment is checked whether it is working properly or not.
   b. Second, server is checked whether it records the data properly or not.
   c. Third, the trigger and the record mode of the video camera are turned on simultaneously and experiment is started afterwards.
   d. At the end of the experiment, the trigger and the record mode of the video camera are turned off and preparation for the next experiment takes place.
   e. After all the experiments are concluded in a series, the model is cleaned for the preparation of the next series of experiments.
2. Steps followed after an experiment series:
   a. Sensor and video data that have been obtained from the last experiment are collected and processed. The process is explained in Section 4.4.2.
   b. The specimen is prepared for the next experiment series.
   c. The results of the last experiment are assessed and further experiment series are planned after this assessment.

The experiments are summarized in Table 4.4 - Table 4.8. While cells containing "○" mark shows that the related element is not affected from event and the cells containing "●" mark shows that the related element is affected. However, the information of how the elements are affected is not given in those tables. All phases of the first group in the second experiment series from the whole experimental program are detailed in the next section as a sample.

Table 4.4 Experiments conducted within the first experiment series

EXP.	PH.	HORIZONTAL PASSAGE UNIT								
		SPAN 1		SPAN 2					SPAN 3	
		SC 1	Wall 1	CB 1	CB 2	SC 2	Wall 2	Wall 4	SC 3	Wall 3
1	1	○	○	●	●	○	○	○	○	○
	2	●	○	●	●	○	○	○	○	○
	3	●	○	●	●	●	○	○	○	○
	4	●	○	●	●	●	○	○	●	○
2	1	○	○	●	●	○	○	○	○	○
	2	●	○	●	●	○	○	○	○	○
	3	●	○	●	●	○	○	○	●	○
	4	●	○	●	●	●	○	○	●	○
3	1	○	○	●	●	○	○	○	○	○
	2	●	○	●	●	○	○	○	○	○
	3	●	○	●	●	●	○	○	○	○
	4	●	○	●	●	●	○	○	●	○

Table 4.5 Experiments conducted within the second experiment series

EXP.	PH.	HORIZONTAL PASSAGE UNIT								
		SPAN 1		SPAN 2					SPAN 3	
		SC 1	Wall 1	CB 1	CB 2	SC 2	Wall 2	Wall 4	SC 3	Wall 3
1	1	○	○	●	●	○	○	○	○	○
	2	○	○	●	●	○	●	●	○	○
	3	○	○	●	●	○	●	●	○	●
	4	○	●	●	●	○	●	●	○	●
	5	●	●	●	●	○	●	●	○	●
	6	●	●	●	●	●	●	●	○	●
	7	●	●	●	●	●	●	●	●	●

Table 4.6 Experiments conducted within the third experiment series

EXP.	PH.	HORIZONTAL PASSAGE UNIT								
		SPAN 1		SPAN 2					SPAN 3	
		SC 1	Wall 1	CB 1	CB 2	SC 2	Wall 2	Wall 4	SC 3	Wall 3
1	1	●	○	○	○	○	○	○	○	○
2	1	○	○	○	○	●	○	○	○	○
3	1	○	○	○	○	○	○	○	●	○
4	1	●	○	○	○	○	○	○	○	○
	2	●	○	○	○	●	○	○	○	○
	3	●	○	○	○	●	○	○	●	○
5	1	●	○	○	○	○	○	○	○	○
	2	●	○	○	○	●	○	○	○	○
	3	●	○	○	○	●	○	○	●	○
6	1	●	○	○	○	○	○	○	○	○
7	1	○	○	○	○	●	○	○	○	○
8	1	○	○	○	○	○	○	○	●	○
9	1	●	○	○	○	○	○	○	○	○
	2	●	○	○	○	●	○	○	○	○
	3	●	○	○	○	●	○	○	●	○
10	1	●	○	○	○	○	○	○	○	○
	2	●	○	○	○	●	○	○	○	○
	3	●	○	○	○	●	○	○	●	○
11	1	●	○	○	○	○	○	○	○	○
	2	●	○	○	○	●	○	○	○	○
	3	●	○	○	○	●	○	○	●	○
12	1	●	○	○	○	○	○	○	○	○
	2	●	○	○	○	●	○	○	○	○
	3	●	○	○	○	●	○	○	●	○
13	1	○	○	●	●	○	○	○	○	○
14	1	○	○	●	●	○	○	○	○	○
15	1	○	○	●	●	○	○	○	○	○
16	1	○	○	●	●	○	○	○	○	○
17	1	○	○	●	●	○	○	○	○	○
18	1	○	○	●	●	○	○	○	○	○

Table 4.7 Experiments conducted within the forth experiment series

EXP.	PH.	HORIZONTAL PASSAGE UNIT								
		SPAN 1		SPAN 2					SPAN 3	
		SC 1	Wall 1	CB 1	CB 2	SC 2	Wall 2	Wall 4	SC 3	Wall 3
1	1	○	○	●	●	○	○	○	○	○
	2	●	○	●	●	○	○	○	○	○
	3	●	○	●	●	●	○	○	○	○
	4	●	○	●	●	●	○	○	●	○
	5	●	●	●	●	●	○	●	●	○
	6	●	●	●	●	●	●	●	●	○
	7	●	●	●	●	●	●	●	●	●

Table 4.8 Experiments conducted within the fifth experiment series

EXP.	PH.	HORIZONTAL PASSAGE UNIT						
		SPAN 1		SPAN 2			SPAN 3	
		CB 1	Wall 1	CB 2	Wall 2	Wall 4	CB 3	Wall 3
1	1	●	○	○	○	○	○	○
2	1	○	○	○	○	○	●	○
3	1	●	○	○	○	○	○	○
4	1	●	○	●	○	○	○	○
5	1	○	○	●	○	○	●	○
6	1	○	○	●	●	●	●	○
	2	○	●	○	●	●	●	○
	3	○	●	○	●	●	●	●

4.4.1.1 The Sample Experiment

At the first phase of this experiment, Cupboard 1 and Cupboard 2 are tipped simultaneously. Cupboards are pushed with hand and they are overturned. At the second phase, Wall 2 and Wall 4 are collapsed at the same time and after that at phases 3 and 4; Wall 1 and Wall 3 are collapsed respectively. Walls are again collapsed by pushing manually. At phases 5, 6 and 7 suspended ceilings 1, 2 and 3 are affected from impact respectively. At phase 5, LBC and LFC of the suspended ceilings 1 are unlaced (Type 4). At phases 6 and 7, LBC and RBC of the suspended ceilings 2 and 3 are unlaced respectively (Type 3). Unlaced cords of the suspended ceiling (circled ones) and the label of the affected walls and suspended ceilings from impact are shown in Figure 4.21. The photographs of the model taken after the sample experiment are also shown in Figure 4.22.

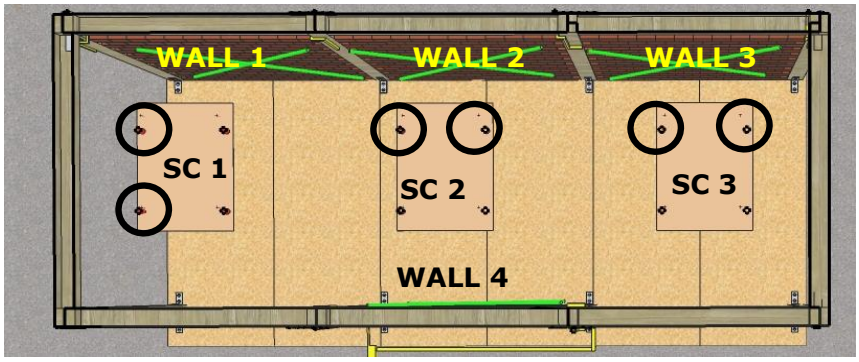

Figure 4.21 Sketch of the wide corridor model which shows the labels of the affected walls and suspended ceilings with ruptured cords of suspended ceilings

4.4.2 The Results of the Conducted Experiments

After an experiment is conducted, the related data can be accessed from the server. There are two types of data obtained from the server. First one is video file of the camera, gathered as Flash Video (flv) format. Video file is copied from the server to a local computer. Then image processing is carried out with the method mentioned in Section 4.5.3. The second one is the sensor data from the single-board microcontroller. This data is gathered from the server in Comma Separated Values (CSV) format. All sensors (24 CCC and 5 URF) transmit a value per second. A row is a data sub-set which consists of 29 different sensors and a time code; in other words, there are 30 elements in total. The duration of an experiment series changes between 15 minutes to 2 hours, which means that more than a set of 7,000 rows can be gathered from some of the experiment series. The set of data rows is then divided into experiments and phases, respectively. After separation, proper rows from these subsets as results of the phases.

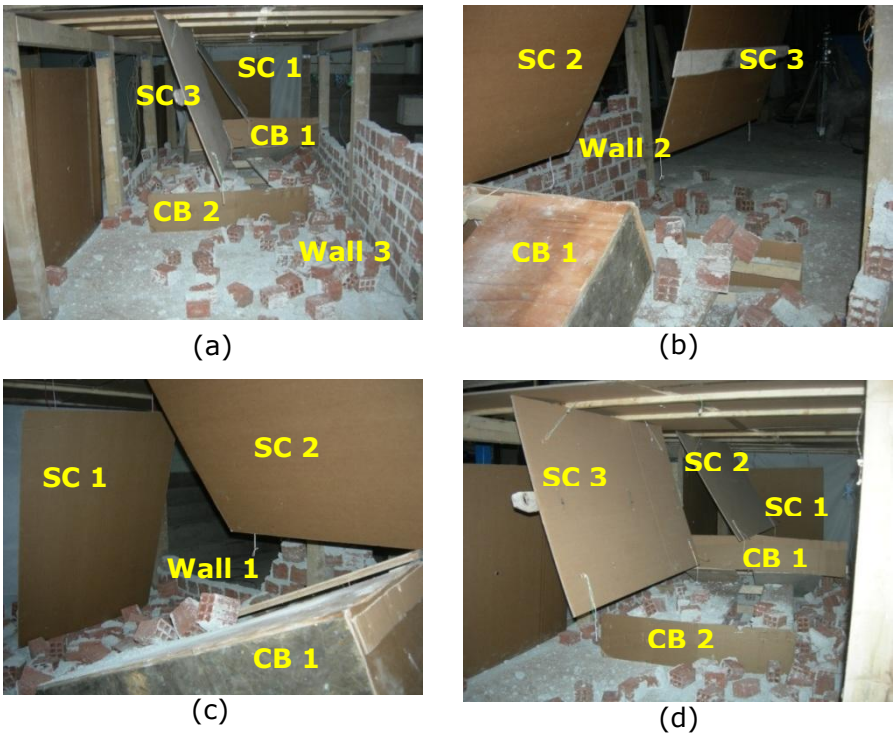

Figure 4.22 Photographs taken after the sample experiment (a) general view of the wide corridor model, (b) view of span 1, (c) view of span 2 and (d) view of span 3

Besides, two different kinds of signals are obtained from sensors: digital or analog. The output of the digital signal consists of binary data (either 0 or 1). The CCC gives digital signal. Unlike CCC, the URF gives analog signal. A value, which has a lower and upper limit, is collected through analog signal. Resolution, lower and upper limits of the URF is stated in Chapter 3. To evaluate two different types of data together, analog data is converted to digital.

This conversion is carried out by specifying a threshold value for different elements in different conditions. If the absolute value of the difference between the measured distances by URF at pre-experiment (d_1) and post-experiment (d_2) stages is greater than the threshold value for URF (tv) times the measured

distance at pre-experiment stages (d_1), a change is detected and the resulted as "1", otherwise it is "0". In other words, if the measures correspond to Equation 4.1, value "1" is gathered. If the measures correspond to Equation 4.2, value "0" is gathered. The threshold values specified by survival analysis (Birgönül, et al., 2012) are given in Table 4.9.

$$d_1 - d_2 > tv \times d_1 \quad \textbf{4.1}$$

$$d_1 - d_2 \leq tv \times d_1 \quad \textbf{4.2}$$

Table 4.9 Threshold values for URF

ELEMENT	THRESHOLD VALUE (tv)
Wall at Narrow Corridor	41%
Wall at Wide Corridor	115%
Suspended Ceiling	95%

4.4.2.1 The Results of the Sample Experiment

In this section, only the last phase of the sample experiment is examined. The sensor results of the sample experiment are tabulated in Table 4.10. According to these results, both CCCs of the cupboards are disconnected, which means that it worked well. The CCCs of the suspended ceiling yields accurate results as in the case of cupboards. The same condition is valid for the URF in the suspended ceiling. If the distance measured between the suspended ceiling and the actual ceiling changes more than 95%, the element is considered to be damaged. This situation refers to "1". All CCCs of the wall 1, 2 and 3 are disconnected as expected. Only CCCs on wall 4 are not disconnected, which means sensors are not able to sense the change. Like CCCs of wall 4, URFs of wall 1 and 3 are not able to sense the change. The rate of change in those URFs is under the threshold value, so the value is considered as "0".

Table 4.10 Sensor results of the phase 7 of the sample experiment

SPAN NO	NAME of the ELEMENT	TYPE of the SENSOR		BEFORE EXP. (X)	PHASE 7 (Y)	Result (X-Y)
1	SC 1	CCC	LFC	1	0	1
			LBC	1	0	1
			RBC	1	1	0
			RFC	1	1	0
		URF	-	415.0 mm	1,177.6 mm	1
	WALL 1	CCC	Left Cord	1	0	1
			Right Cord	1	0	1
		URF	-	1,642.9 mm	1,823.8 mm	0
2	SC 2	CCC	LFC	1	1	0
			LBC	1	0	1
			RBC	1	0	1
			RFC	1	1	0
		URF	-	415.0 mm	2,470.1 mm	1
	Wall 2	CCC	Left Cord	1	0	1
			Right Cord	1	0	1
	Wall 4	CCC	Left Cord	0	0	0
			Right Cord	1	1	0

Table 4.10 (cont'd) Sensor results of the phase 7 of the sample experiment

SPAN NO	NAME of the ELEMENT	TYPE of the SENSOR		BEFORE EXP. (X)	PHASE 7 (Y)	Result (X-Y)
2	CB 1	CCC	Left Cord	1	0	1
			Right Cord	1	0	1
	CB 2	CCC	Left Cord	1	0	1
			Right Cord	1	0	1
3	SC 3	CCC	LFC	1	1	0
			LBC	1	0	1
			RBC	1	0	1
			RFC	1	1	0
		URF	-	311.6 mm	1,229.3 mm	1
	Wall 3	CCC	Left Cord	1	0	1
			Right Cord	1	0	1
		URF	-	1,617.0 mm	815.7 mm	0

4.5 The Assessment of the Blockage

This section is focused on the method proposed for assessing the blockage in the horizontal passage unit as it is one of the main goals of this study. First the definitions of the blockage classes are introduced and then the results of the experiments are interpreted according to these blockage classes.

4.5.1 The Classification of the Blockage

To classify the blockage, the letters are determined with respect to accessibility of the occupants inside a building. The blockage classes and the definitions of these classes are given in Table 4.11. In Figure 4.23, also an example is shown for each blockage classes.

Table 4.11 Blockage classes and the definitions

BLOCKAGE CLASSES	DEFINITIONS
A	No damage, horizontal passage unit is totally clear
B	May be some little damage but horizontal passage unit is clear for both handicapped & healthy people
C	Comfortable access is denied. Horizontal passage unit is clear for only healthy people
D	Horizontal passage unit is closed. Access is possible for only healthy person with some physical effort
E	Horizontal passage unit is totally closed

(a) (b)

(c) (d)

(e)

Figure 4.23 Sample photos for each blockage classes; (a) class A blockage, (b) class B blockage, (c) class C blockage, (d) class D blockage and (e) class E blockage

4.5.2 The Assessment of the Blockage in the Experiments

The blockage classes are used to assess the blockage at the spans of the frame specimen. The contribution of every single component of the frame to the blockage is considered. For suspended ceiling, there are 7 different damage cases mentioned in Section 4.2.1.4. The damage cases of the cupboards which affect the blockage of the horizontal passage unit are:

1. No damage at cupboards (not moved from their initial locations)
2. One cupboard dislocated or overturned
3. Two cupboards cupboard dislocated or overturned

For walls, there are 2 different damage cases affecting the blockage of the horizontal passage unit:

1. No out-of-plane damage in walls
2. Collapse of the wall(s) in out-of-plane direction

These cases and the combinations of these cases are considered for wide and narrow corridor differently. Each of them is classified in terms of blockage by

educated guess[3]. The blockage classifications for each case are shown in Table 4.12 and Table 4.13. Table 4.12 and Table 4.13 are for the narrow and wide corridor model respectively. For example, the suspended ceiling has Type 1 damage and other components are not affected from the impact in narrow corridor model. This represents class B blockage. But, besides damage at suspended ceiling, if one cupboard is overturned or the wall is collapsed, the blockage class shifts from class B to class D blockage. Another example can be given for the wide corridor model. The suspended ceiling has Type 1 damage and other components are not affected from the impact. This denotes class B blockage. If one cupboard is overturned, the blockage class is shifted from class B to class C blockage. In the experiments, a significant difference in terms of blockage level between overturning of one cupboard and two cupboards is observed. On the contrary, an important difference in terms of blockage level between collapse of one wall and two walls is not observed in the experiments.

Table 4.12 Blockage classes of the cases for the narrow corridor model

BLOCKAGE CLASS	SUSPENDED CEILING	CUPBOARD	WALL
A	Type 0	No damage	No damage
B	Type 1	No damage	No damage
	Type 2	No damage	No damage
D	Type 0	Only one cupboard tipped	No damage
	Type 1	Only one cupboard tipped	No damage
	Type 2	Only one cupboard tipped	No damage
	Type 0	No damage	Collapse of the wall(s)
	Type 1	No damage	Collapse of the wall(s)
	Type 2	No damage	Collapse of the wall(s)
E	Type 3	No damage	No damage
	Type 3	Only one cupboard tipped	No damage
	Type 3	Only one cupboard tipped	Collapse of the wall(s)
	Type 3	Both cupboards tipped	No damage
	Type 3	Both cupboards tipped	Collapse of the wall(s)
	Type 3	No damage	Collapse of the wall(s)
	Type 4	No damage	No damage
	Type 4	Only one cupboard tipped	No damage
	Type 4	Only one cupboard tipped	Collapse of the wall(s)
	Type 4	Both cupboards tipped	No damage
	Type 4	Both cupboards tipped	Collapse of the wall(s)
	Type 4	No damage	Collapse of the wall(s)
	Type 5	No damage	No damage
	Type 5	Only one cupboard tipped	No damage
	Type 5	Only one cupboard tipped	Collapse of the wall(s)
	Type 5	Both cupboards tipped	No damage
	Type 5	Both cupboards tipped	Collapse of the wall(s)
	Type 5	No damage	Collapse of the wall(s)

[3] An estimate, a guess value based on experience or theoretical knowledge.

Table 4.12 (cont'd) Blockage classes of the cases for the narrow corridor model

BLOCKAGE CLASS	SUSPENDED CEILING	CUPBOARD	WALL
E	Type 6	No damage	No damage
	Type 6	Only one cupboard tipped	No damage
	Type 6	Only one cupboard tipped	Collapse of the wall(s)
	Type 6	Both cupboards tipped	No damage
	Type 6	Both cupboards tipped	Collapse of the wall(s)
	Type 6	No damage	Collapse of the wall(s)
	Type 0	Only one cupboard tipped	Collapse of the wall(s)
	Type 1	Only one cupboard tipped	Collapse of the wall(s)
	Type 2	Only one cupboard tipped	Collapse of the wall(s)
	Type 0	Both cupboards tipped	No damage
	Type 1	Both cupboards tipped	No damage
	Type 2	Both cupboards tipped	No damage
	Type 0	Both cupboards tipped	Collapse of the wall(s)
	Type 1	Both cupboards tipped	Collapse of the wall(s)
	Type 2	Both cupboards tipped	Collapse of the wall(s)

Table 4.13 Blockage classes of the cases for the wide corridor model

BLOCKAGE CLASS	SUSPENDED CEILING	CUPBOARD	WALL
A	Type 0	No damage	No damage
B	Type 1	No damage	No damage
	Type 2	No damage	No damage
C	Type 0	Only one cupboard tipped	No damage
	Type 1	Only one cupboard tipped	No damage
	Type 2	Only one cupboard tipped	No damage
	Type 0	No damage	Collapse of the wall(s)
	Type 1	No damage	Collapse of the wall(s)
	Type 2	No damage	Collapse of the wall(s)
	Type 0	Only one cupboard tipped	Collapse of the wall(s)
	Type 1	Only one cupboard tipped	Collapse of the wall(s)
	Type 2	Only one cupboard tipped	Collapse of the wall(s)
D	Type 3	No damage	No damage
	Type 3	Only one cupboard tipped	No damage
	Type 4	No damage	No damage
	Type 4	Only one cupboard tipped	No damage
	Type 5	No damage	No damage
	Type 5	Only one cupboard tipped	No damage
	Type 6	No damage	No damage
	Type 6	Only one cupboard tipped	No damage
	Type 0	Both cupboards tipped	No damage
	Type 1	Both cupboards tipped	No damage
	Type 2	Both cupboards tipped	No damage
	Type 0	Both cupboards tipped	Collapse of the wall(s)
	Type 1	Both cupboards tipped	Collapse of the wall(s)
	Type 2	Both cupboards tipped	Collapse of the wall(s)

Table 4.13 (cont'd) Blockage classes of the cases for the wide corridor model

BLOCKAGE CLASS	SUSPENDED CEILING	CUPBOARD	WALL
E	Type 3	No damage	Collapse of the wall(s)
	Type 3	Only one cupboard tipped	Collapse of the wall(s)
	Type 3	Both cupboards tipped	No damage
	Type 3	Both cupboards tipped	Collapse of the wall(s)
	Type 4	No damage	Collapse of the wall(s)
	Type 4	Only one cupboard tipped	Collapse of the wall(s)
	Type 4	Both cupboards tipped	No damage
	Type 4	Both cupboards tipped	Collapse of the wall(s)
	Type 5	No damage	Collapse of the wall(s)
	Type 5	Only one cupboard tipped	Collapse of the wall(s)
	Type 5	Both cupboards tipped	No damage
	Type 5	Both cupboards tipped	Collapse of the wall(s)
	Type 6	No damage	Collapse of the wall(s)
	Type 6	Only one cupboard tipped	Collapse of the wall(s)
	Type 6	Both cupboards tipped	No damage
	Type 6	Both cupboards tipped	Collapse of the wall(s)

A striking extraction that can be obtained from Table 4.12 is that there is no class C blockage at the narrow corridor model. The reason is that narrow corridor model can be blocked easily with respect to the wide corridor model; so, a case which brings class C blockage for the wide corridor model corresponds to class D blockage for the narrow corridor model.

4.5.3 The Assessment of the Blockage with the Image Processing Methods for the Video Camera

Different image processing approaches are developed and assessed to predict the blockage in the horizontal passage unit with the video camera. The suggested methods are: (1) the method that scans the open space through the horizontal passage unit (Ellipsis Method) and (2) the method that scans each span individually (Ideal Method)

4.5.3.1 The method that scans the open space through the horizontal passage unit (Ellipsis Method)

This method is based on comparing the red, blue and green values of the neighbor pixels with reference pixels. In this way an ellipse that includes set of similar colored pixels is drawn. Pre-experiment and post-experiment images obtained with this method are presented in Figure 4.24 and Figure 4.25, respectively. The rectangle that represents the open space through the horizontal passage unit specimen and the ellipses are shown in Figure 4.26.

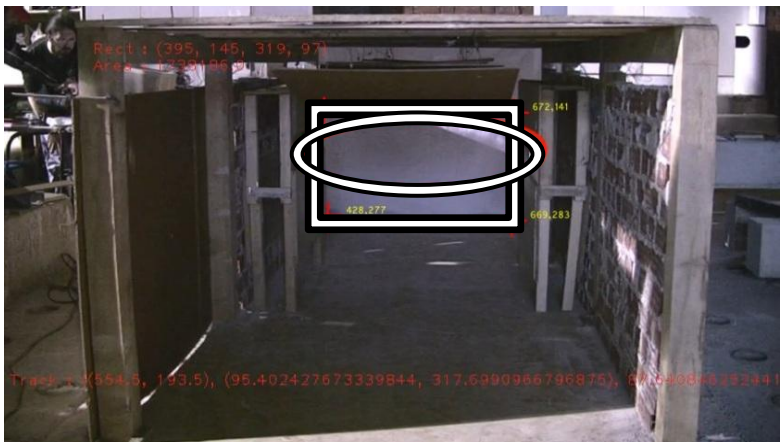

Figure 4.24 The rectangle that represents the open space and the ellipse that is drawn at the pre-experiment stage

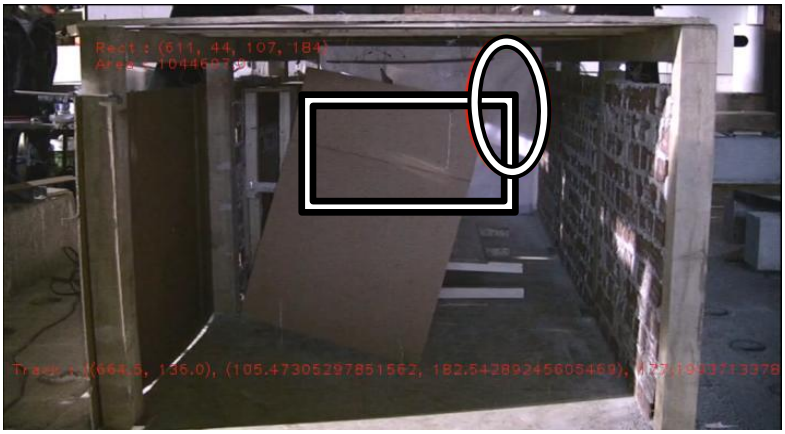

Figure 4.25 The rectangle that represents the open space and the ellipse that is drawn at the post-experiment stage

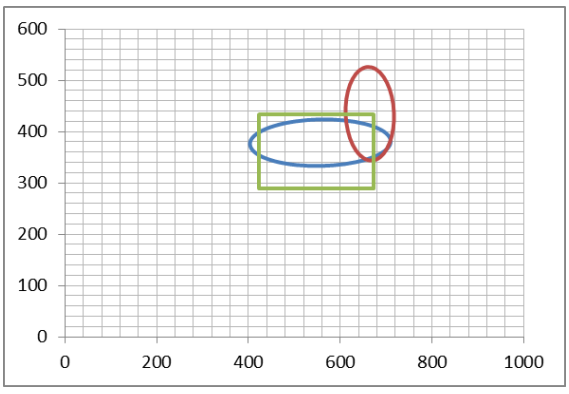

Figure 4.26 The rectangle that represents the open space and the ellipses

A matrix with 80 units in width and 45 units in height is placed into the rectangle as shown in Figure 4.26. The rectangle is divided into 5 vertical strips. The actual width of the wide corridor is 4,500 mm and an average door has a width of 900

mm; so, it is assumed that the wide corridor has a width of 5 doors which means that 5 people can pass through it simultaneously. The number of strips can be changed depending on the width of the horizontal passage unit.

So; the intersection cells of the pre-experiment or the post-experiment ellipses with the rectangle are filled with the value of "1". The non-intersecting cells are filled with the value of "0". These intersections are showed in Figure 4.27 and Figure 4.28. The intersected cells are colored in yellow and the non-intersecting ones are colored in black.

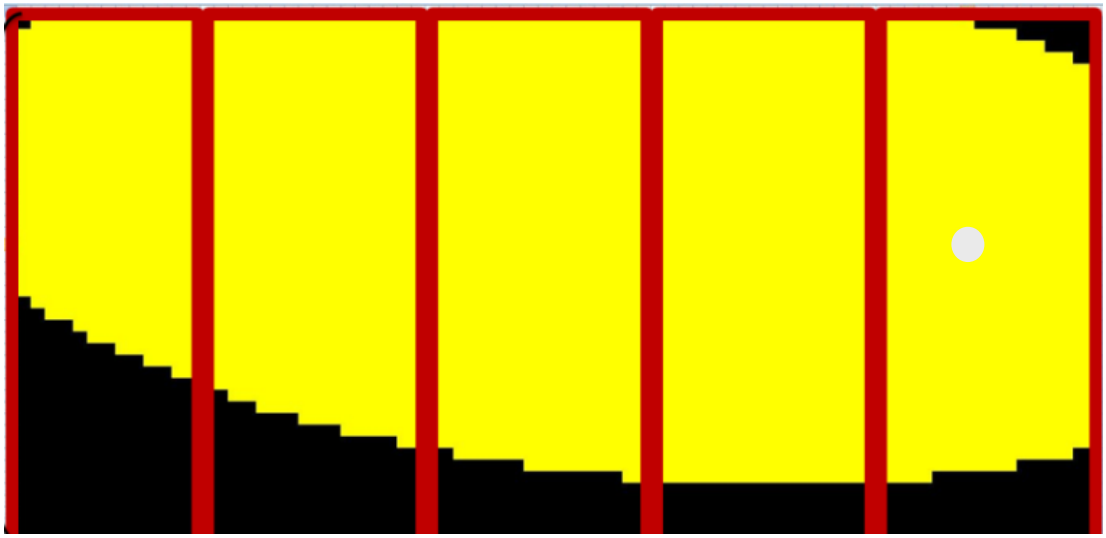

Figure 4.27 The intersection area of the ellipse drawn at pre-experiment stage in the rectangle with the strips

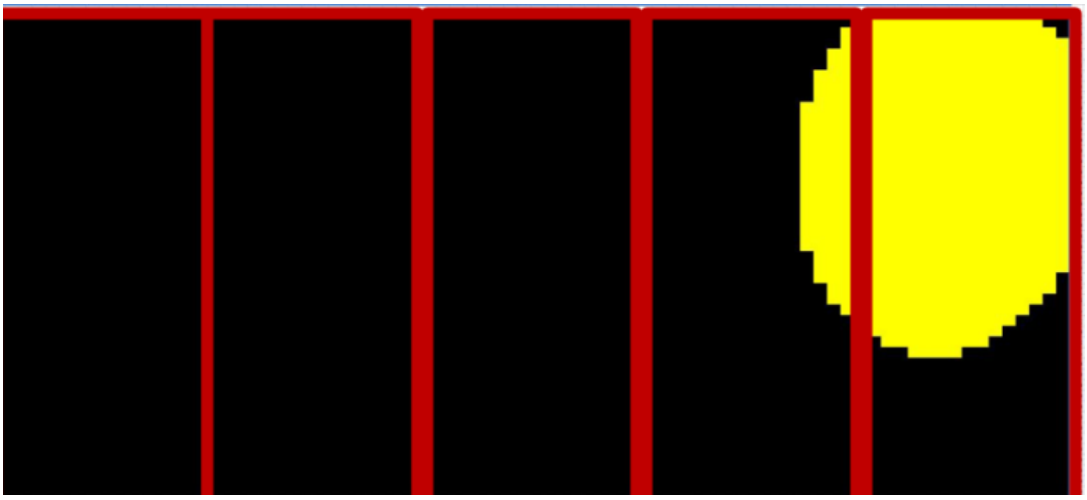

Figure 4.28 The intersection area of the ellipse drawn at pre-experiment stage in the rectangle with the strips

The strips shown in Figure 4.27 and Figure 4.28 have a width of 16 cells. Percent of intersected area is calculated for each strip. For example, the percent of intersected area of the first three strips from left in Figure 4.28 are 0%. Change in percent of intersected area for the strips between the pre-experiment and the post-experiment stages are calculated by using Equation 4.3.

$$C = \frac{B-A}{A} \qquad \textbf{4.3}$$

In this Equation, parameter A is the percent of intersected area of the post-experiment stages, parameter B is the percent of intersected area of the pre-experiment stages and parameter C is the change in percent of the intersected area for the strips between the pre-experiment and the post-experiment stages. The ranges of the change in percent of the intersected area for the strips between the pre-experiment and the post-experiment stages and the blockage status are given in Table 4.14.

Table 4.14 Blockage states with respect to the C value

C VALUE	BLOCKAGE STATE
Undefined	Blocked
Less than -10%	Blocked
Between -10% and 10%	Unblocked
Between 10% and 50%	Blocked
More than 50%	Unblocked

In general, the change between -10% and 10% is an undefined case. Hence the change is ignored and the strip is assumed to be unblocked. If the change is more than 50%, it means that the change in percent of the intersected area for the strip is switched from the blocked to the unblocked state. On the other hand, the changes that are less than -10% and more than 50% yield an unblocked state. If the ellipse does not pass from the strips at the pre-experiment stage, the result is regarded as undefined. In this case, the horizontal passage unit can be either clear or blocked; so, in order to be conservative, it is considered to be blocked. The blockage rate of horizontal passage unit is calculated from the blockage condition of the whole strips as 0/5, 1/5, 2/5, 3/5, 4/5 and 5/5 for the horizontal passage unit under consideration.

4.5.3.2 The method that scans each span individually (Ideal Method)

In this image processing method (Birgönül et al., 2012), each span is monitored and assessed individually. Instead of ellipse, polylines are used to determine the percent of the blocked area from the total area. Unlike Ellipsis Method, the matrix and the strip approach are not used. Another difference is the results gathered from this method. Instead of blockage rate, Ideal Method yields the v-blockage class[4] for result. The v-blockage classes corresponding to the blockage percentages are given in Table 4.15.

[4] The classification of the inaccessibility rate of a horizontal passage unit through ideal video image processing method

Table 4.15 The v-blockage classes corresponding to the blockage percentages (Birgönül et al., 2012)

RATE OF BLOCKED AREA FROM THE TOTAL AREA	THE V-BLOCKAGE CLASSES
0% - 20%	A
21% - 40%	B
41% - 60%	C
61% - 80%	D
81% - 100%	E

By using the information given in Chapter 4, an approach for sensor fusion is constituted. In this approach, image processing method labeled as the ideal method is used. Sensor fusion approach is going to be explained in detail in the next chapter.

CHAPTER 5

SENSOR FUSION

5.1 Introduction

This chapter presents an approach for sensor fusion. Sensor fusion is important for commenting sensor data for the purpose of understanding the blocked passage locations exactly. Generally, the research studies related to sensor fusion for buildings have focused on reducing the energy consumption of HVAC systems, which in turn activated the use of sensors for occupancy detection in office buildings (Dodier et al., 2006; Tachwali et al., 2007; Erickson et al., 2009; Lo and Novoselac, 2010; Benezeth et al., 2011). Some of the studies have performed sensor fusion using sophisticated analytical techniques (Hutchins et al., 2007; Lam et al., 2009; Meyn et al., 2009; Newsham and Birt, 2010; Hailemariam et al., 2011). In this study the decision tree approach is employed to estimate the blocked horizontal passage units in a building threatened by an earthquake.

5.2 The Decision Tree Approach

In order to combine all sensor information in a meaningful manner and to estimate the current blockage condition of a horizontal passage unit, the decision tree approach is used. The decision tree is a data mining method. The data mining is a path that reveals, decides and realizes the course of action from a data set which could contain various types of information. The data mining is used for gathering the invaluable information from large scaled data set; thus, it can present the relationships within the data in a successful manner (Han and Kamber, 2006). By using the decision tree method, fusing the sensor data and determining the critical sensors are possible.

There are also different data mining methods other than decision tree. These are anamoly detection (outliner detection) and artificial neural networks. Anamoly detection refers to detecting patterns in a given data set that do not conform to an established normal behavior (Chandola et al., 2009) so, this method is not proper for the goal of the study. Artificial neural networks require a large diversity of training for real-world operation and in this study there is not enough data to obtain a well trained neural network. Unlike these methods, decision tree helps to identify a strategy most likely to reach a goal. The output of decision tree is easy to understand and it is possible to train a decision tree with a small data set.

An open source Java implementation of the C4.5 algorithm in the Weka Data Mining tool called J48 is used to generate the decision tree. The C4.5 algorithm is an inductive learning algorithm (Quinlan, 1993). Results obtained by inductive learning algorithm are either definite or approximate decision trees or rule sets. Nowadays, C4.5 is the most popular and widely used algorithm to generate decision trees.

In order to achieve this task, a data set called training set is essential. In this study, the results of the experiments conducted with the wide corridor model (see Chapter 4) are used as the training set of the C4.5 algorithm. Hence, the training set has a size of 168 rows of data. The reason for which the wide corridor experiments are preferred instead of the narrow corridor experiments is the lack of sufficient and varied experiment conducted with narrow corridor to build up decision tree. This makes the decision tree case sensitive, means it works for only the horizontal passage units that the height is less than the width (wide passage unit). In order to involve the effect of the aspect ratio, shifting approach is proposed for the horizontal passage units that the height is greater than the width (narrow passage unit). According to this approach, if the decision tree is resulted class A, B and E blockages for a narrow passage unit, blockage class is not changed. However, if the decision tree is resulted class C and D blockages for a narrow passage unit, unlike wide corridor, the blockage classes shifts one class upper. In other words, class C blockage becomes class D blockage and class D blockage becomes class E blockage. This approach is deduced from experiments carried out to the narrow corridor model.

A holdout method is also necessary to create a decision tree. The holdout method is, sometimes called test sample estimation, partitions the data into two mutually exclusive subsets called a training set and a test set or holdout set. It is common to designate 2/3 of the data as the training set and the remaining 1/3 as the test set (Kovahi, 1995). K-fold cross-validation is used as the holdout method. The training set is given to the inducer, and the induced classifier is tested on the test set. The data set is divided into k subsets and the holdout method is repeated k times. Each time, one of the k subsets is used as the test set and the other (k–1) subsets are put together to form a training set. Then the average error across all k trials is computed (Polat and Güneş, 2007). In this study, the number of subsets has been chosen as 10.

5.2.1 The Attributes Used for the Decision Tree

As mentioned above, training set is composed of experiments conducted with the wide corridor model; thus, the input attributes of the training set involve all the sensors. Besides the input attributes obtained from sensors (direct input attributes), some other input attributes are obtained by fusing more than one sensor (indirect input attributes). These input attributes are given in Table 5.1. Abbreviations "SC" and "CB" used in Table 5.1 stand for suspended ceiling and cupboard, respectively. The input attributes obtained by fusing more than one sensor are constituted to obtain the relationships among the sensors for the decision tree. For example, if all the sensors related to suspended ceiling (CCC 1 to CCC 4 and URF) yield the value of 0 (which means that there is no damage or sensor in the monitored horizontal passage unit), "Type 0 at SC" attribute also yields the result as 0.

Table 5.1 The input attributes used in training set

DIRECT INPUT ATTRIBUTES	INDIRECT INPUT ATTRIBUTES
CCC 1 at Wall 1	Type 0 at SC-
CCC 2 at Wall 1	Type 1 at SC
URF at Wall 1	Type 2 at SC
CCC 1 at Wall 2	Type 3 at SC
CCC 2 at Wall 2	Type 4 at SC
URF at Wall 2	Type 5 at SC
CCC 1 at CB 1	Type 6 at SC

Table 5.1 (cont'd) The input attributes used in training set

DIRECT INPUT ATTRIBUTES	INDIRECT INPUT ATTRIBUTES
CCC 2 at CB 1	Situation of CB
CCC 1 at CB 2	
CCC 2 at CB 2	
CCC 1 at SC	
CCC2 at SC	
CCC3 at SC	
CCC4 at SC	
URF at SC	
Camera	

Overall, 24 attributes are chosen as input attributes and an output attribute (the experiment results) is also used. The results of the experiments are explained in Chapter 4. By using these attributes and the 10-fold cross-validation method, the decision tree is generated.

5.2.2 Generation of the Decision Tree

The acquired decision tree is shown in Figure 5.1. In the figure, attributes are denoted as ellipses and decisions are presented as rectangles. The possible decisions of the attributes and the corresponding meanings of these decisions are provided in Table 5.2.

Table 5.2 Answers to the attributes and their interpretations

ATTRIBUTE	ANSWER	INTERPRETATION
CCC 1 at Wall 1	1 or 0	1: Damage 0: No Damage
CCC 2 at Wall 1	1 or 0	1: Damage 0: No Damage
URF at Wall 1	1 or 0	1: Damage 0: No Damage
CCC 1 at Wall 2	1 or 0	1: Damage 0: No Damage
CCC 2 at Wall 2	1 or 0	1: Damage 0: No Damage
URF at Wall 2	1 or 0	1: Damage 0: No Damage
CCC 1 at CB 1	1 or 0	1: Damage 0: No Damage
CCC 2 at CB 1	1 or 0	1: Damage 0: No Damage
CCC 1 at CB 2	1 or 0	1: Damage 0: No Damage

Table 5.2 (cont'd) Answers to the attributes and their interpretations

ATTRIBUTE	ANSWER	INTERPRETATION
CCC 2 at CB 2	1 or 0	1: Damage 0: No Damage
CCC 1 at SC	1 or 0	1: Damage 0: No Damage
CCC2 at SC	1 or 0	1: Damage 0: No Damage
CCC3 at SC	1 or 0	1: Damage 0: No Damage
CCC4 at SC	1 or 0	1: Damage 0: No Damage
URF at SC	1 or 0	1: Damage 0: No Damage
Type 0 at SC	1 or 0	1: SC is not affected 0: SC is affected
Type 1 at SC	1 or 0	1: Type 1 Damage at SC 0: Not Type 1 Damage at SC (Type 0, 2, 3, 4, 5 or 6)
Type 2 at SC	1 or 0	1: Type 2 Damage at SC 0: Not Type 2 Damage at SC (Type 0, 1, 3, 4, 5 or 6)
Type 3 at SC	1 or 0	1: Type 3 Damage at SC 0: Not Type 1 Damage at SC (Type 0, 1, 2, 4, 5 or 6)
Type 4 at SC	1 or 0	1: Type 4 Damage at SC 0: Not Type 1 Damage at SC (Type 0, 1, 2, 3, 5 or 6)
Type 5 at SC	1 or 0	1: Type 5 Damage at SC 0: Not Type 1 Damage at SC (Type 0, 1, 2, 3, 4 or 6)
Type 6 at SC	1, 0 or 2	1: Type 6 Damage at SC 0: Not Type 6 Damage at SC (Type 0, 1, 2, 3, 4 or 5)
Situation of CB	1 or 0	0: None of the CBs are affected 1: One of the CB is affected 2: Both CBs are affected
Camera	A, B, C, D, E or 0	0: No camera used at horizontal passage unit A, B, C, D or E: The v-blockage class by the evaluation of the camera

It is clear from Figure 5.1 that only some of the attributes in Table 5.1 have been used. The reason for this is that the C4.5 algorithm does not consider the attributes which do not have a major effect on the result. The result (number or letter) of the former attribute is provided on the links between the attributes. There are also some values in the decision tree like (51/0) and (51/9). The values 51 and 0 correspond to the number of training set elements in the decision tree and the number of training set elements not consistent with the results of the decision tree, respectively. Performance results of the decision tree are presented in the next section.

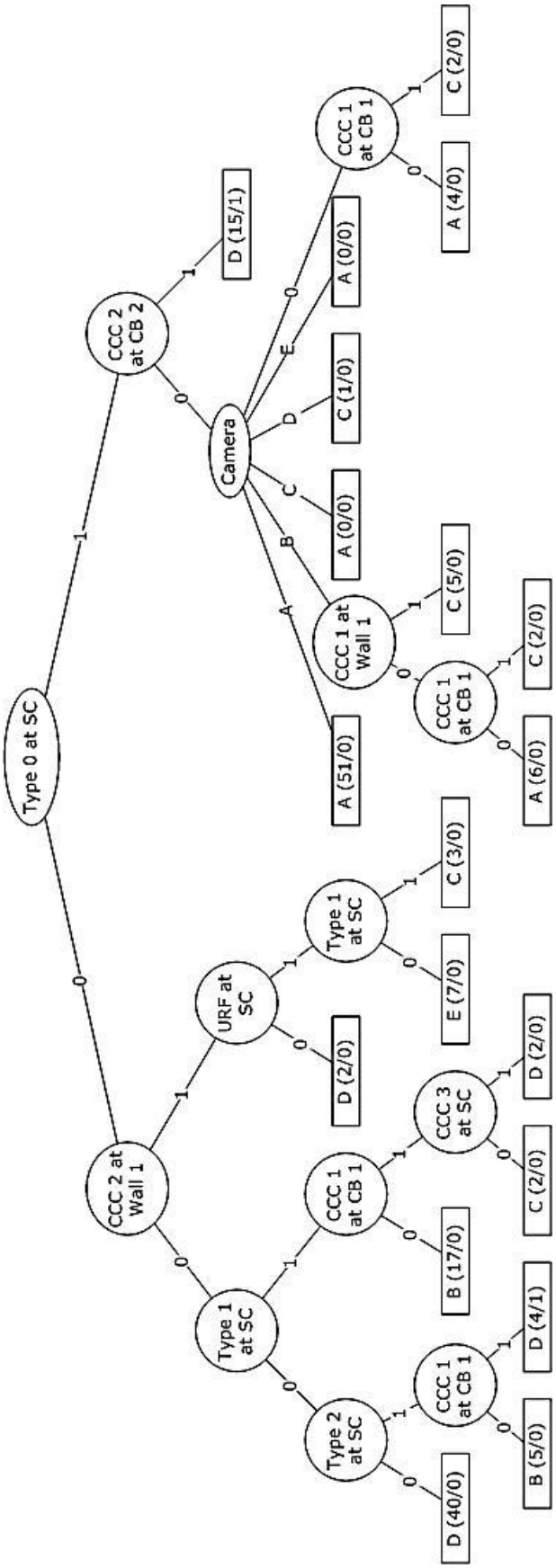

Figure 5.1 The decision tree obtained by the C4.5 algorithm

5.3 Results of the Decision Tree

The results of the decision tree are evaluated under two headings. These are the attribute evaluation and the confusion matrix.

5.3.1 The Attribute Evaluation

"InfoGainAttributeEval", which is an attribute class in Weka program, is used to sort the attributes in Table 5.3 by its effects on decision tree. Hence, it becomes possible to find out which attributes have significant effect on the response of the decision tree. Base algorithm is used to get an ordered feature set based on information gain which is evaluated using Weka attribute selection InfoGainAttributeEval filter (Witten and Frank, 2000). The evaluation given in Table 5.3 is performed only between input attributes, not the output.

Table 5.3 The ranking given by the attribute evaluation class

RANK	SCORE	THE INPUT ATTRIBUTE
1	0.623	Type 0 at SC
2	0.552	Type 1 at SC
3	0.505	CCC 2 at Wall 1
4	0.486	CCC 1 at Wall 1
5	0.452	Situation of CB
6	0.451	URF at SC
7	0.384	CCC 1 at SC
8	0.379	URF at Wall 1
9	0.346	Type 3 at SC
10	0.317	CCC 2 at SC
11	0.314	CCC 2 at CB 2
12	0.313	CCC 1 at CB 1
13	0.311	Type 4 at SC
14	0.309	CCC 4 at SC
15	0.308	CCC 2 at CB 1
16	0.298	CCC 3 at SC
17	0.289	CCC 1 at CB 2
18	0.263	Camera
19	0.242	Type 5 at SC
20	0.242	Type 6 at SC
21	0.205	CCC 2 at Wall 2
22	0.190	Type 2 at SC
23	0	URF at Wall 2
24	0	CCC 1 at Wall 2

According to this evaluation, it can be stated that the attributes "URF at Wall 2" and "CCC 1 at Wall 2" have no effect on the result so these are scored as 0 (Table 5.3). The reason for the "URF at Wall 2" is inoperative is that Wall 2 is not monitored by URF at the experiments. The reason for "CCC 1 at Wall 2" does not have effect on the result is that CCC 2 of the Wall 4 is not working properly and the output sent from that sensor is, eventually, inconsistent. So, algorithm is not able to find a connection between the result and these attributes ("URF at Wall 2" and "CCC 1 at Wall 2").

The attribute named as "Type 0 at SC" is the most important input attribute among all the input attributes. It is ranked as 1 with a score of 0.623 (Table 5.3). This attribute is also at the first step in the decision tree (Figure 5.1).

There is an interesting outcome for the attribute "Type 1 at SC". Despite the fact that this input attribute is the second most important one with respect to Table 5.3, it is at the third step in the decision tree (Figure 5.1). Likewise, the input attributes, "CCC 2 at Wall 1" and "CCC 2 at CB 2", are not the second most important input attributes with respect to Table 5.3 but they are at the second step in the decision tree (Figure 5.1).

Another interesting outcome is that functionally alternate sensors have not been used in the decision tree together (except CCC 2 at Wall 1 (ranking is 3 and score is 0.505) and CCC 1 at Wall 1 (ranking is 4 and score is 0.486)). These input attributes are:

1. **CCC 2 at CB 2 (ranking is 11 and score is 0.314)** and CCC 1 at CB 2 (ranking is 17 and score is 0.289)
2. **CCC 1 at CB 1 (ranking is 12 and score is 0.313)** and CCC 2 at CB 1 (ranking is 15 and score is 0.308)
3. **CCC 2 at Wall 2 (ranking is 21 and score is 0.205)** and CCC 1 at Wall 2 (ranking is 24 and score is 0)

Only the attributes written in bold are used in the decision tree. The ranks of the input attributes written in bold are also higher than the alternates. None of the input attributes related with the Wall 2 is used in the decision tree.

5.3.2 The Confusion Matrix

To visualize the performance of the decision tree, confusion matrix is constituted. A confusion matrix contains information about actual and predicted classifications done by a classification system (Devasena 2012). Confusion matrix shows the classification of the cases in the test dataset (for this study, test set is generated by 10-fold cross-validation method). In confusion matrix, the columns denote the actual cases and the rows denote the predicted ones (Parker 2001).

The confusion matrix of the generated decision tree is given in Table 5.4. The precision and the recall rates by blockage classes are given in Table 5.5. Recall is the proportion of positive cases that are correctly identified whereas precision is the proportion of the predicted positive cases that are correct. The results in Table 5.5 are deducted from Table 5.4.

Table 5.4 Confusion matrix of the decision tree

		PREDICTED					
	Σ	**A**	**B**	**C**	**D**	**E**	**Σ**
ACTUAL	**A**	61	0	0	0	0	**61**
	B	0	22	0	0	0	**22**
	C	2	0	11	4	0	**17**
	D	0	0	2	57	2	**61**
	E	0	0	1	0	6	**7**
	Σ	**63**	**22**	**14**	**61**	**8**	

Table 5.5 Precision and recall rates of the confusion matrix by blockage classes

BLOCKAGE CLASSES	PRECISION	RECALL
A	96.8%	100.0%
B	100.0%	100.0%
C	78.6%	64.7%
D	93.4%	93.4%
E	75.0%	85.7%
WEIGHTED AVERAGE	93.3%	93.5%

According to the results in Table 5.4, there are 61 cases of class A blockage, 22 cases of class B blockage, 17 cases of class C blockage, 61 cases of class D blockage and 7 cases of class E blockage in the experiments. All the cases in class A and B blockages are recalled by the decision tree; so, the recall rates of these two blockage classes are 100% (Table 5.5). These two blockage classes are the most successful blockage classes of the decision tree in terms of the recall rate. Six cases out of 17 from class C blockage are assessed faulty. Two of these cases confused with class A blockage and 4 of the cases confused with class D blockage. Thus, the recall rate of the class C blockage is 64.7%, which is the most unsuccessful blockage class in terms of recall rate. In class D blockage, the rate of the fault is determined to be 4 cases out of 61 which means 57 of them are correct (93.4%). Two cases are assessed to be class C blockage, and 2 cases are confused with class E blockage. Class E blockage is also considered to be one of successful blockage classes (85.7%). Only one experiment out of 7 is estimated to be in class C blockage.

If the confusion matrix is evaluated vertically, the precision rates can be obtained. The most successful blockage class in terms of prediction is class B blockage with a precision rate of 100%. None of the cases which resulted in blockage classes other than B are confused with class B blockage. Two cases of class C blockage are assessed as class A blockage. Despite the fact that there are 61 cases in class A blockage totally, it is assessed by decision tree that there are 63 cases in class A blockage (%96.8). Three cases of class C blockage are confused with class D blockage (2 cases) and class E blockage (1 case) (78.6%). Four cases of class D blockage are confused with class C blockage (93.4%). Class E blockage is the most unsuccessful blockage class in terms of prediction rates (75%). Two cases of class E blockage are assessed as class D blockage (75.0%).

5.4 Discussion of the Decision Tree

The decision tree is discussed under this heading. Looking at the decision tree in general, evaluation is carried out from general to specific and from the top to the bottom. For instance, at the first level of the decision tree, damage to suspended ceiling ("Type 0 at SC") is questioned as a general assessment. This attribute is also the top ranked one selected by the attribute evaluation algorithm as shown in Table 5.3.

5.4.1 Right Branch of the Decision Tree (Suspended Ceiling is affected)

According to the decision tree, the second CCC of the second cupboard (CCC 2 at CB 2) is evaluated in case there is no damage at the suspended ceiling (Type 0

at SC = 1). This attribute which is at the 11th rank according to the ranking given by the attribute evaluation class is evaluated at the second level of the decision tree. Although it seems a contradictory situation, the reason lying behind this is that C4.5 algorithm recognizes the relationship between indirect and direct attributes regarding the suspended ceiling (most of which are ranked higher than the "CCC 2 at CB 2" attribute). It gives priority to the second CCC of the second cupboard.

In cases when the second CCC of the second cupboard is disconnected (CCC 2 at CB 2 = 1), the outcome is evaluated as class D blockage directly. The reason for this is the lack of sufficient data in experiments for cupboards. In every experiment, it is expected that when the second cupboard tumbles down, first cupboard is already tipped. The decision tree considers that the tipping of the second cupboard is valid by assigning class D blockage. This situation shows itself in the attribute evaluation (Table 5.3) for the cupboard one. The first CCC of the first cupboard (CCC 1 at CB 1) is ranked at the 12th level and the second CCC of the first cupboard (CCC 2 at CB 1) is ranked at the 15th level and these attributes are not questioned at the right branch of the decision tree. Nevertheless, according to the decision tree, 15 out of 16 results are determined accurately.

In the cases that the second CCC of the second cupboard is not damaged (CCC 2 at CB 2 = 0); the decision tree considers the v-blockage class of the horizontal passage unit. The decision tree evaluates the class A, B, and D v-blockages according to the experiments. Class C and E v-blockages are not assessed valid to the experiments because there are no experiments for undamaged suspended ceiling and second cupboard with these v-blockage classes. As a result the decision tree gives random results (class A blockage) for both v-blockage classes. This situation affects the reliability of the decision tree. On the other hand, the activation of the camera at lower levels indicates that not only the camera data is unreliable, but also there is, at this stage, no any other reliable data to be evaluated in the decision tree. Besides, attribute evaluation algorithm (Table 5.3) considered camera data at the 18th rank and did not credit this attribute on decision making. It is anticipated that a better image processing approach could make this attribute more reliable and place camera attribute to a higher level at the decision tree.

5.4.2 Left Branch of the Decision Tree (Suspended Ceiling is not affected)

The first level of the left branch in the decision tree stands for a damaged suspended ceiling (Type 0 at SC = 1), and the next evaluation is observed to be located in the second CCC of the first wall (CCC 2 at Wall 1). It can also be examined that the effects of the wall attributes are more pronounced than the cupboard attributes on the result (Table 5.3).

After this level, if the second CCC of the first wall is disconnected (CCC 2 at Wall 1 = 1), the decision tree checks the suspended ceilings. Due to the fact that the suspended ceiling is known to be damaged from the very beginning, the important issue is to know the damage type of the suspended ceiling.

The decision tree considers the change of the URF (URF at SC) at this point. If there is no change at URF (URF at SC = 0), class D blockage is directly assigned by the decision tree. If there is a change at URF (URF at SC = 1) of the suspended ceiling, Type 1 damage at the suspended ceiling (Type 1 at SC) is questioned. The reason for this is that the URF at the suspended ceiling cannot

sense "Type 2" and "Type 1" at the suspended ceiling. As a result, if a CCC of the suspended ceiling is disconnected (Type 1 at SC = 1), the decision tree gives the class C blockage. If it is not Type 1 damage, more than one CCC are disconnected and resulted in class E blockage. The answer of the question why the decision tree does not consider the cupboard and class D blockage is simply the lack of experimental data. On the other hand, the decision tree yields a conservative result and gives the class E blockage.

At the second level of the left branch, if the status of the second CCC of the first wall is not changed (CCC 2 at Wall 1 = 0), the decision tree concludes that there is no damage at the first wall and focuses on the "Type 1" at the suspended ceiling. If a disconnected CCC is confirmed at the suspended ceiling (Type 1 at SC = 1), the first CCC of the first cupboard (CCC 1 at CB 1) is examined. If the first CCC of the first cupboard is not disconnected at the next level (CCC 1 at CB 1 = 0), decision tree assigns class B blockage. On the contrary, if the first CCC of the first cupboard is disconnected (CCC 1 at CB 1 = 1), the decision tree considers the third CCC of the suspended ceiling (CCC 3 at SC). This check is caused by the lack of experiment data for different combinations of the cupboard tipping and the situation of the cupboards is not questioned. Instead, the third CCC of the suspended ceiling is checked by the decision tree.

At the third level of the decision tree, if there is no Type 1 damage at the suspended ceiling (Type 1 at SC = 0), it means more than one CCC is disconnected and the decision tree checks the Type 2 damage at the suspended ceiling (Type 2 at SC). If there is no Type 2 damage at the suspended ceiling (Type 2 at SC = 0), this means that blockage probability is high due to the suspended ceiling damage, and the decision tree assigns class D blockage as 40 experiments yield the same results.

If there is Type 2 damage at the suspended ceiling (Type 2 at SC = 1), the decision tree considers the first CCC of the first cupboard (CCC 1 at CB 1). If cupboard 1 is affected from impact (CCC 1 at CB 1 = 1), decision tree decides assigns class D blockage, otherwise (CCC 1 at CB 1 = 0) decision tree assigns class B blockage.

It can be concluded that the decision tree does not use the URF data for walls. This is why URFs mounted for the walls do not give any different information from CCC at the walls. This can also be revealed from attribute evaluation algorithm (Table 5.3). The rank of the first and the second CCC of the first wall are at the forth and third rank respectively, the URF of the wall 1 is at the 8^{th} place.

CHAPTER 6

CASE STUDY

6.1 Introduction

This chapter presents the performed case study as an implementation of the blockage assessment with the sensor fusion which is provided by the decision tree approach. Main goal of this case study is to test the sensor fusion method. This is achieved on the simulation platform. After selecting the pilot building, the first step is to model the structural system of this building by using SAP 2000 analysis platform (version 15.0.0). Then the selected acceleration records taken from two different stations are applied to the building separately. By using assumptions, the damages sustained by the components of building are estimated. The next step is to generate the sensor data for two different damage levels with the assumption that the sensors worked flawlessly. Finally, the decision tree is employed for both of the seismic analyses and the results are discussed.

6.2 The Earthquake Records for Seismic Analysis

After modeling the structural system by SAP 2000 program, the building is analyzed by using the records of two different stations of the earthquake that happened on August 17th, 1999 in Northwest Region of Turkey, which is known as the 17 August 1999 (Kocaeli) Marmara Earthquake. These two stations are Düzce and Gebze Stations. The ground acceleration record of Düzce Station represents strong shaking intensity (Figure 6.1 and Figure 6.2) while the Gebze Station represents a moderate shaking intensity (Figure 6.3 and Figure 6.4).

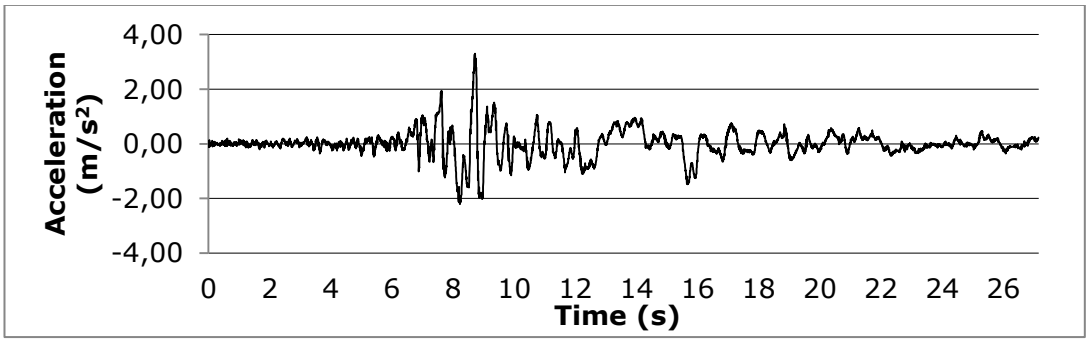

Figure 6.1 17 August 1999 Marmara (Kocaeli) Earthquake, North - South component of the ground acceleration record of Düzce Station

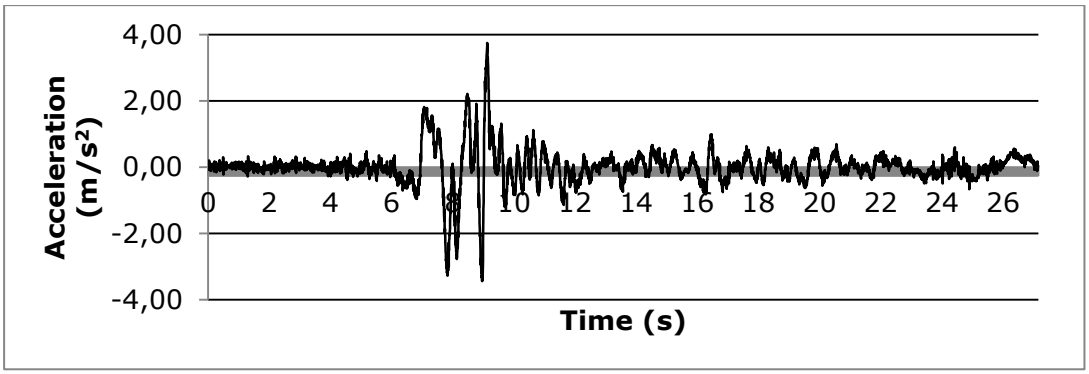

Figure 6.2 17 August 1999 Marmara (Kocaeli) Earthquake, East - West component of the ground acceleration record of Düzce Station

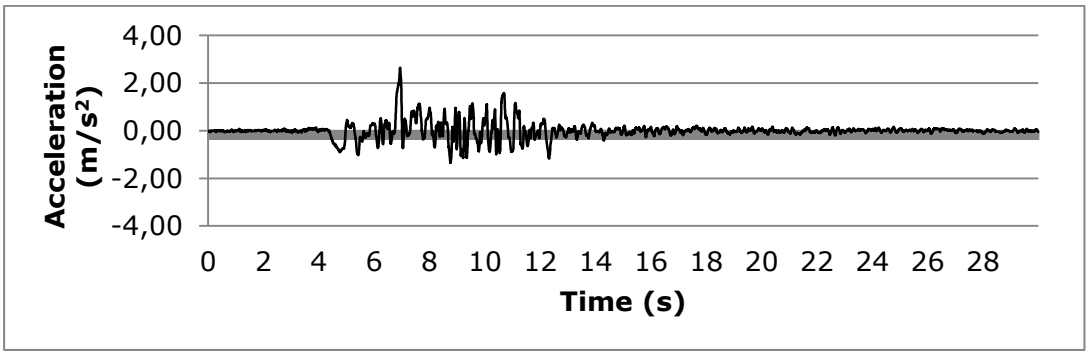

Figure 6.3 17 August 1999 Marmara (Kocaeli) Earthquake, North - South component of the ground acceleration record of Gebze Station

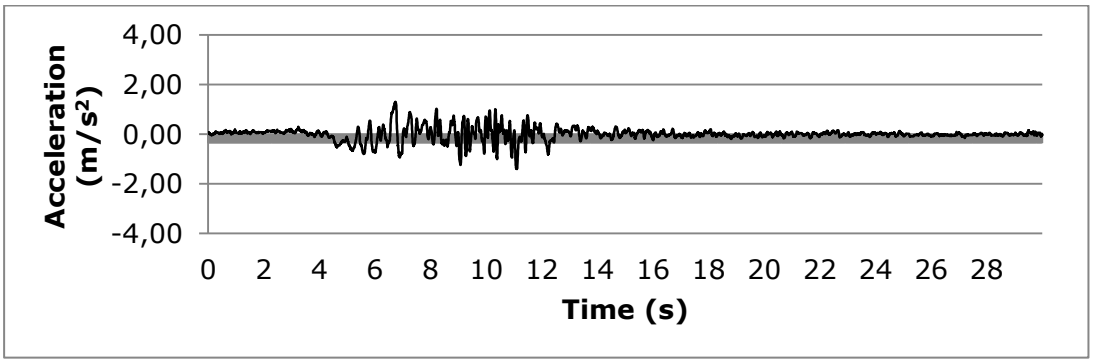

Figure 6.4 17 August 1999 Marmara (Kocaeli) Earthquake, East - West component of the ground acceleration record of Gebze Station

6.3 Modeling the Structural System of the Building

The structural system of the pilot building consists of two blocks separated by dilatation, A-Block and B-Block. Each block has been modeled separately. The structural system of both blocks is reinforced concrete with flat slab. 3-D image of the model is provided in Figure 6.5 and Figure 6.6.

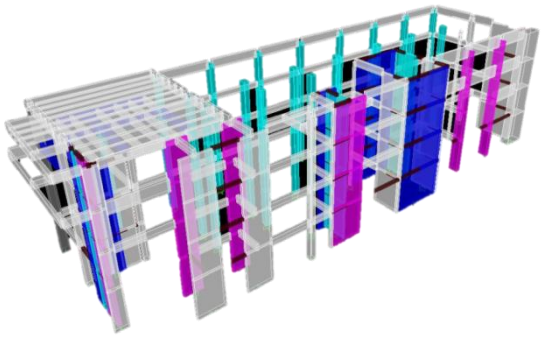

Figure 6.5 A 3-D image of the model of A-Block

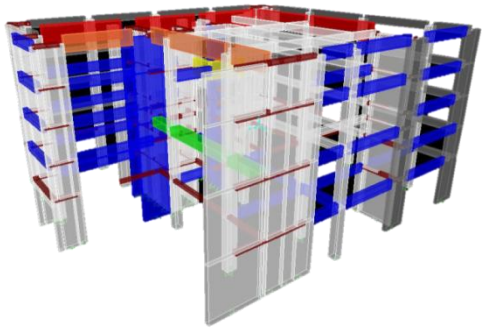

Figure 6.6 A 3-D image of the model of B-Block

The rigid diaphragm approach is used instead of shell elements for slabs and the structural loads are distributed by tributary area approach. The vibration periods of the first five modes are given in Table 6.1.

Table 6.1 Vibration periods of the modal for first five modes

MODES	PERIODS OF THE A-BLOCK (s)	PERIODS OF THE B-BLOCK (s)
1	0,44	0,69
2	0,29	0,58
3	0,25	0,42
4	0,12	0,18
5	0,10	0,15

After the modeling of the two blocks has been completed, Düzce and Gebze ground motion acceleration records of the 17 August 1999 Marmara (Kocaeli) Earthquake are applied to the model and non-linear time history analysis are conducted. As a result of these analyses, the local floor accelerations and inter-story drifts are obtained. The results are provided in Section 6.5.

There are four main components to be monitored in the case study building: infill walls, suspended ceilings and cupboards, which represent the non-structural objects, and columns. Infill walls and columns are placed in accordance with architectural drawings, but unlike these elements, the suspended ceilings and the cupboards are intentionally placed in the most proper locations. To test the proposed approach in a challenging way, the suspended ceilings and the cupboards are also located in some places different from architectural drawings.

6.4 The Localization of the Sensor

The localization of sensors, which are used to monitor the aforementioned components in the building, is carried out according to the principles mentioned in Chapter 3. Infill walls and cupboards in horizontal passage units are monitored with 2 CCCs. Some of the infill walls at the horizontal passage units are also monitored with 1 URF. All of the suspended ceilings at the horizontal passage units are monitored with 4 CCCs and 1 URF. Besides the damage in non-structural components, the damage in columns across the horizontal passage units is monitored with gyro sensor. In addition to these, the video cameras are located to the critical areas in specific locations in the horizontal passage unit.

The distribution of damage in the case study building is estimated by using floor accelerations and inter-story drift ratios of columns. The accelerations and the drift ratios have been extracted from the non-linear time history analyses of the pilot building under selected earthquakes. The damage estimation methods for the non-structural objects, the infill walls, the suspended ceilings and the columns are provided in the next sections.

6.4.1 The Non-structural Objects (The Cupboards)

A non-structural object could block a horizontal passage unit in two ways: overturning and/or sliding. These conditions are dependent on the acceleration of the component. In this study, the shape of the non-structural object is assumed to be a rectangular prism.

6.4.1.1 The Overturning Condition

The overturning of the non-structural object occurs if the floor acceleration unbalances the moment equilibrium of the non-structural object with respect to point O (Figure 6.7). Floor acceleration is assumed to be the average acceleration of the base and the ceiling of the floor.

$$F \times \frac{H}{2} = W \times \frac{t}{2} \quad (6.1)$$

where;

$$F = m \times a \quad (6.2)$$

and,

$$W = m \times g \quad (6.3)$$

so,

$$m \times a \times H = m \times g \times t \quad (6.4)$$

$$a \times H = g \times t \quad (6.5)$$

$$a = \frac{g \times t}{H} \quad (6.6)$$

The definitions of the abbreviations used in the equations from 6.1 - 6.6 are as follows:

$a_{overturn}$: critical floor acceleration for overturning (m/s^2)

F: lateral force caused by earthquake acceleration (kN)

g: the gravitational acceleration (is assumed to be 9.81 m/s^2 in this study)

H: height of the element (m)

m: mass of the element (kg)

t: thickness of the element (m)

W: weight of the element (kN)

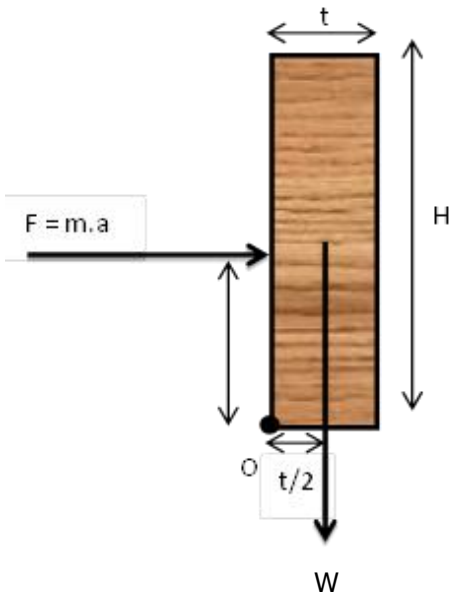

Figure 6.7 The explanations of the abbreviations used in equations 6.1 to 6.6 for checking the overturning condition of the cupboard

6.4.1.2 The Sliding Condition

The sliding of the non-structural object could occur if the lateral force caused by the floor acceleration (due to the earthquake) unbalances the friction force of the cupboard (Figure 6.7). The floor acceleration is assumed to be the average acceleration of the base and the ceiling of the floor.

$$F_x = 0 \quad (6.7)$$

$$m \times a_{sliding} = F_\mu = \mu_f \times N \quad (6.8)$$

due to the vertical equilibrium,

$$N = W \quad (6.9)$$

$$m \times a_{sliding} = \mu_f \times m \times g \quad (6.10)$$

$$a_{sliding} = \mu_f \times g \quad (6.11)$$

The definitions of the abbreviations used in equations 6.7 - 6.11 are as follows:

$a_{sliding}$: critical floor acceleration for sliding (m/s^2)

F_x: total lateral force that act on to the element

F_μ: friction force

N: normal force

μ_f: friction coefficient (to provide the randomness, it is considered as a random variable which has been chosen between 0.25 and 0.60 for each cupboard)

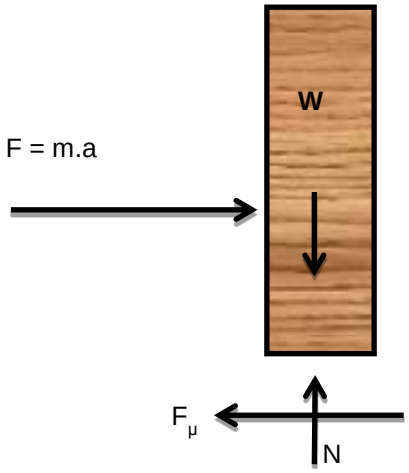

Figure 6.8 The explanations of the abbreviations used in equations 6.7 to 6.11 for checking the sliding condition of the cupboard

6.4.2 The Infill Walls

The damage to the infill walls has two types: in-plane damage and out-of-plane damage. The effect of these two types on the damage could be grasped substantially by evaluating these damage types separately or together. In this thesis, the damage is evaluated making use of both types of damage.

6.4.2.1 In-Plane Damage to Infill Walls

The assessment of in-plane damage in the walls can be estimated from the relative floor drift ratios. By considering the studies of Bayülke (1992), Kuran (2006), and Bal et al. (2008), the limits of the relative floor drift ratios with respect to the damage level are given in Table 6.2.

Table 6.2 The limits of the relative floor drift ratios with respect to the damage level

DAMAGE LEVEL	LOWER LIMIT	UPPER LIMIT
No Damage	0.0000	0.0025
Light Damage	0.0025	0.0050
Heavy Damage	0.0050	0.0100
Collapse	0.0100	1.0000

6.4.2.2 Out-of-Plane Damage to Infill Walls

The out-of-plane damage is caused by the earthquake acceleration. The floor acceleration is assumed to be the average acceleration of the base and the ceiling of the floor. The equations to determine the out-of-plane damage are as follow:

$$q = m \times a \quad (6.12)$$

$$m = \gamma \times t \times 1 \quad (6.13)$$

$$q = \gamma \times t \times a \quad (6.14)$$

The maximum moment occurs at mid-span;

$$M_{max} = \frac{q \times H^2}{8} \ (kNm) \quad (6.15)$$

$$M_{max} = \frac{\gamma \times t \times a \times H^2}{8} \ (kNm) \quad (6.16)$$

$$\sigma_{max} = \frac{M_{max} \times c}{I} \ (kN/m^2) \quad (6.17)$$

$$c = \frac{t}{2} \ (m) \quad (6.18)$$

$$\sigma_{max} = \frac{0.75 \times \gamma \times a \times H^2}{t} \ (kN\ m^2) \quad (6.19)$$

$$f_{max} < \sigma_{max} \quad (6.20)$$

The assumptions related to equations 6.12 - 6.20 and the definitions of the abbreviations related with the same equations are given below and in Figure 6.9.

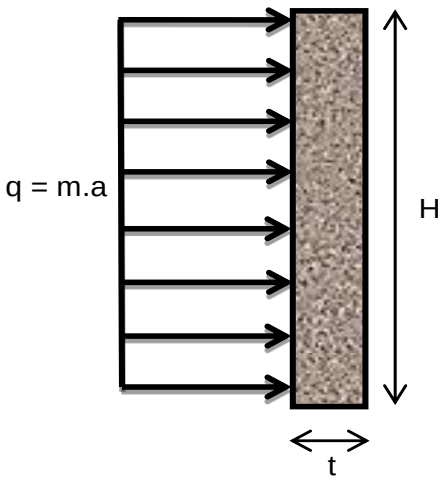

Figure 6.9 The explanations of the abbreviations used in equations 6.12 - 6.20

a: lateral floor acceleration (m/s^2)

γ: density of the unit hollow brick (to provide the randomness, a variable is chosen between 1.60 – 2.00 t/m^3 for each infill wall)

f_{max}: flexure capacity of the wall (to provide the randomness, a variable is chosen between 200 – 500 t/m^3 for each infill wall in accordance with BS5628-1 (1992) and Eurocode 6 (2003)).

t: thickness of the element (m) (for infill wall it is chosen as 0.20 m)

σ_{max}: maximum normal stress

M_{max}: maximum moment

To combine the effects of in-plane and out-of-plane damage together, a coefficient (Ψ) is proposed as shown in equation 6.21. This coefficient changes with respect to the relative drift ratios. The relative drift ratios with respect to the Ψ are provided in Table 6.3.

$$\Psi \times f_{max} < \sigma_{max} \quad 6.21$$

Table 6.3 The relative drift ratios limits are shown at with respect to the Ψ

LEVEL OF DAMAGE	Ψ	LOWER LIMIT	UPPER LIMIT
No Damage	1.00	0.0000	0.0025
Light Damage	0.75	0.0025	0.0050
Heavy Damage	0.50	0.0050	0.0100

6.4.3 The Suspended Ceiling

According to HAZUS MR4 (2009), the suspended ceiling is assumed to be damaged in case the floor acceleration is greater than 1g. In this thesis, in order to introduce the uncertainty in damage, 3 ranges are determined as limits for no damage, light damage and heavy damage (Table 6.4). Besides, the type of damage that suspended ceiling gets with respect to the acceleration limit is given in Table 6.5.

Table 6.4 The ranges determined for the damage level of the suspended ceilings

LEVEL OF DAMAGE	LOWER LIMIT	UPPER LIMIT
No Damage	0.0g	0.4g
Light Damage	0.4g	0.8g
Heavy Damage	0.8g	+∞

Table 6.5 The type of damage with respect to the acceleration limit

NORTH – SOUTH DIRECTION	EAST – WEST DIRECTION	TYPE OF THE DAMAGE
No Damage	No Damage	Type 0
No Damage	Light Damage	Type 1
Light Damage	No Damage	Type 1
Light Damage	Light Damage	Type 2
Heavy Damage	No Damage	Type 3 or 4 according to the direction of the destructive acceleration
No Damage	Heavy Damage	Type 3 or 4 according to the direction of the destructive acceleration
Heavy Damage	Light Damage	Type 5
Light Damage	Heavy Damage	Type 5
Heavy Damage	Heavy Damage	Type 6

6.4.4 The Columns

The results of the damage of the columns are based on the results of the SAP2000 analyses. If the results indicate that the performance criteria of a column are exceeded, the aforementioned column is accepted to have been damaged heavily and to have even collapsed thoroughly.

6.5 Results of Analyses and Location of Damage

After determining the damage estimation methods for each component, the locations of the damage are specified. The average floor accelerations analyzed using the Düzce Station records are given in Table 6.6 and the average floor accelerations analyzed using the Gebze Station records are given in Table 6.7.

Table 6.6 The average floor accelerations analyzed using the Düzce Station records

NAME OF THE FLOOR	A-BLOCK (NORTH – SOUTH)	A-BLOCK (EAST – WEST)	B-BLOCK (NORTH – SOUTH)	B-BLOCK (EAST – WEST)
Basement	0.00	0.00	0.00	0.00
Ground	1.82	2.12	2.21	1.87
+2.60	-	-	3.54	3.63
+4.20	3.04	3.57	3.77	4.55
+5.50	-	-	4.35	5.30
+8.40	4.24	5.72	5.94	7.08
Roof	6.93	8.72	7.76	9.72

Table 6.7 The average floor accelerations analyzed using the Gebze Station records

NAME OF THE FLOOR	A-BLOCK (NORTH – SOUTH)	A-BLOCK (EAST – WEST)	B-BLOCK (NORTH – SOUTH)	B-BLOCK (EAST – WEST)
Basement	0.00	0.00	0.00	0.00
Ground	1.25	1.20	1.37	1.15
+2.60	-	-	2.20	1.66
+4.20	2.05	1.58	2.72	1.64
+5.50	-	-	2.65	2.14
+8.40	3.40	2.06	3.69	2.97
Roof	5.07	3.13	4.67	3.94

The relative drift ratios analyzed using the Düzce Station records are given in Table 6.8 and the relative drift ratios analyzed using the Gebze Station records are given in Table 6.9. The relative drift ratios are different for each column; so, only one of them is given in Table 6.8 and Table 6.9.

Table 6.8 The relative drift ratios analyzed using the Düzce Station records

NAME OF THE FLOOR	A-BLOCK (NORTH – SOUTH)	A-BLOCK (EAST – WEST)	B-BLOCK (NORTH – SOUTH)	B-BLOCK (EAST – WEST)
Basement - Ground	0.0020	0.0043	0.0033	0.0041
Ground - +2.60	-	-	0.0055	0.0066
Ground - +4.20	0.0032	0.0077	0.0078	0.0061

Table 6.8 (cont'd) The relative drift ratios analyzed using the Düzce Station records

NAME OF THE FLOOR	A-BLOCK (NORTH – SOUTH)	A-BLOCK (EAST – WEST)	B-BLOCK (NORTH – SOUTH)	B-BLOCK (EAST – WEST)
+2.60 – +5.50	-	-	0.0057	0.0065
+4.20 – +8.40	0.0034	0.0082	0.0048	0.0053
+5.50 – +8.40	-	-	0.0056	0.0062
+8.40 – Roof	0.0036	0.0079	0.0050	0.0053

Table 6.9 The relative drift ratios analyzed using the Gebze Station records

NAME OF THE FLOOR	A-BLOCK (NORTH – SOUTH)	A-BLOCK (EAST – WEST)	B-BLOCK (NORTH – SOUTH)	B-BLOCK (EAST – WEST)
Basement - Ground	0.0018	0.0012	0.0024	0.0013
Ground - +2.60	-	-	0.0036	0.0025
Ground - +4.20	0.0028	0.0017	0.0052	0.0025
+2.60 – +5.50	-	-	0.0035	0.0026
+4.20 – +8.40	0.0030	0.0018	0.0033	0.0024
+5.50 – +8.40	-	-	0.0034	0.0025
+8.40 – Roof	0.0030	0.0016	0.0030	0.0022

By using acceleration and the relative drift ratio data, estimated damage distribution in the pilot building is determined. The summary of the damage calculated using the analysis results under both station records are given in Table 6.10 and Table 6.11.

Table 6.10 The summary of the damage calculated using the analysis results of the Düzce Station records

NAME OF THE FLOOR	SUSPENDED CEILING	INFILL WALLS	CUPBOARD	COLUMN
Basement	No Damage	No Damage	No Damage	No Damage
Ground	Partial Damaged	Partial Damaged	Partial Damaged	No Damage
+2.60	Partial Damaged	Partial Damaged	Partial Damaged	No Damage
+4.20	Partial Damaged	Partial Damaged	Partial Damaged	No Damage
+5.50	Totally Damaged	Totally Damaged	Totally Damaged	No Damage
+8.40	Totally Damaged	Totally Damaged	Totally Damaged	Partial Damaged

Table 6.11 The summary of the damage calculated using the analysis results of the Gebze Station records

NAME OF THE FLOOR	SUSPENDED CEILING	INFILL WALLS	CUPBOARD	COLUMN
Basement	No Damage	No Damage	No Damage	No Damage
Ground	No Damage	No Damage	Partial Damaged	No Damage

Table 6.11 (cont'd) The summary of the damage calculated using the analysis results of the Gebze Station records

NAME OF THE FLOOR	SUSPENDED CEILING	INFILL WALLS	CUPBOARD	COLUMN
+2.60	No Damage	No Damage	Partial Damaged	No Damage
+4.20	No Damage	No Damage	Partial Damaged	No Damage
+5.50	No Damage	No Damage	Partial Damaged	No Damage
+8.40	Partial Damaged	Partial Damaged	Totally Damaged	No Damage

6.6 Generating the Sensor Data

Sensor data is generated after the estimation of the damage distribution to the components of the pilot building. Ultrasonic range finder, closed cable circuit and gyro sensor data are generated with respect to the damage of the relevant component, assuming that all sensors work flawlessly. For the results of the video processing, the generalized camera results which have been discussed in Chapter 4 are used (Birgönül et al., 2012).

6.7 The Results of the Decision Tree

The estimated damage is calculated by using the analyses results and the sensor data is generated from the estimated damage. As a result, the sensor data is used as the input attributes for the decision tree to decide the blockage classes of the horizontal passage units. The effect of the gyro sensor data is considered in such a way that; if the gyro sensor yields the value "1" (i.e. means that column is damaged), the blockage class is shifted to class E blockage no matter what blockage class it is. The effect of the aspect ratio of the horizontal passage unit in terms of a height/width ratio is also considered such that; if the horizontal passage unit is narrow (which means that the height of the horizontal passage unit is greater than the width), class C and D blockages are shifted to one class up. In other words, class C blockage is shifted to class D blockage and class D blockage to class E blockage. Other blockage classes remain same.

6.7.1 The Results Obtained from the Düzce Station

The program Weka, which is explained in Chapter 5, employed in order to input sensor data as the test set to generate the confusion matrix, the recall and the precision rates. These outputs are given in Table 6.12 and Table 6.13.

Table 6.12 The confusion matrix of Düzce Station

		PREDICTED					
	Σ	**A**	**B**	**C**	**D**	**E**	**Σ**
ACTUAL	**A**	66	0	0	0	0	66
	B	0	12	0	0	0	12
	C	0	0	6	0	0	6
	D	3	0	0	24	0	27
	E	0	0	1	17	2	20
	Σ	**69**	**12**	**7**	**41**	**2**	

Table 6.13 The precision and the recall rates of Düzce Station

BLOCKAGE CLASS	PRECISION	RECALL
A	%95,65	%100,00
B	%100,00	%100,00
C	%85,71	%100,00
D	%58,54	%88,89
E	%100,00	%10,00
WEIGHTED AVERAGE	%88,61	%83,97

The results of Table 6.13 have been derived from Table 6.12. According to Table 6.12, there are 66 cases in class A blockage, 12 cases in class B blockage, 6 cases in class C blockage, 27 cases in class D blockage and 7 cases in class E blockage. All the cases in class A blockage have been detected by the decision tree. So, recall rate of class A blockage is 100%. Apart from class A blockage, all the cases in class B blockage has been exactly detected to be 12 out of 12. All the cases in class C blockage also detected to be 6 out of 6. These are the most successful blockage classes detected by the decision tree. In class D blockage, there are 2 erroneous data out of 27. This means 24 cases are correct, the rate of which is 88.89%. Class E blockage is the most problematic blockage class with a recall rate of 10%. Only 2 of the cases out of 20 have been obtained as correct. Seventeen of them are confused with class D blockage and one is confused with class C blockage. This is because of the lack of sufficient number of various experiments for this blockage class. The decision tree cannot fully comprehend this blockage class.

According to the precision rates, the most successful blockage classes seem to be class B and E blockages with rates of 100%. None of these blockage classes have been confused with others. Although this could be a good result especially for the determination of class B blockage, it is not valid for class E blockage since the major problem of class E blockage is the fact that the decision tree cannot detect class E blockage. Three cases from class A blockage are confused with class D blockage from 69 cases in class A blockage totally. The decision tree falls into error that there are 66 cases in class A blockage. This means a precision rate of 95.65%. One case in class D blockage is confused with class C blockage (85.71%). Seventeen data in class D blockage are confused with class E blockage (58.54%). The reason for why the precision rates are low for class D blockage is that the decision tree cannot detect class E blockage. This turns the class D blockage into a blockage class of totally blocked in respect to the precision rates.

6.7.2 The Results from the Gebze Station

The program Weka, which is explained in Chapter 5, employed in order to input sensor data as the test set to generate the confusion matrix, the recall and the precision rates. These outputs are given in Table 6.14 and Table 6.15.

Table 6.14 The confusion matrix of Gebze Station

		PREDICTED					
	Σ	**A**	**B**	**C**	**D**	**E**	**Σ**
ACTUAL	**A**	105	0	0	0	0	105
	B	0	1	0	0	0	1
	C	0	0	2	0	0	2
	D	7	0	0	8	0	15
	E	0	0	0	6	1	7
	Σ	112	1	2	14	1	

Table 6.15 The precision and the recall rates of Gebze Station

BLOCKAGE CLASS	PRECISION	RECALL
A	%93,75	%100,00
B	%100,00	%100,00
C	%100,00	%100,00
D	%57,14	%53,33
E	%100,00	%14,29
WEIGHTED AVERAGE	%90,01	%90,00

The results of Table 6.15 have been calculated from Table 6.14. According to Table 6.14, there are 105 cases in class A blockage, 1 case in class B blockage, 2 cases in blockage class C blockage, 15 cases in class D blockage and 7 cases in class E blockage. All the cases in class A blockage have been detected by the decision tree; so, the rate for recalling class A blockage is 100%. Except for class A blockage; class B blockage and class C blockage have been detected as 1 out of 1 and 2 out of 2, respectively. These 3 blockage classes are the most successful blockage classes detected by the decision tree. In class D blockage, there are 7 erroneous data and 8 correct data (53.33%) out of 15. Herein, 7 cases are considered as class A blockage. Class E blockage is the most problematic blockage class with a recall rate of 14.29%. Only 1 out of 7 cases are found out to be correct. Six of them are confused with class D blockage. This is because of the lack of sufficient number and type of experiments for this class. The decision tree cannot fully reflect this blockage class.

When examining the precision rates, the most successful blockage classes seem to be class B, C and E blockages with rates of 100%. None of these blockage classes have been confused with others. Although this could be a good result especially both for class B blockage and class C blockage, it is not valid for class E blockage because the major problem of class E blockage is that it cannot be detected by the decision tree. Seven cases in class A blockage are confused with class D blockage. Although there are 112 cases in class A blockage, the decision tree is able to determine 93.75% of these cases. Six cases in class D blockage are confused with class E blockage with a precision rate of 57.14%. The sensibility of class D blockage is low. It is due to the fact that class E blockage cannot be determined, but has been mistakenly determined as class D blockage instead. This made class D blockage the most problematic blockage class of all blockage classes.

Taking all these into consideration, it is clearly observed that there are, in general terms, no profound differences between the educated guess derived from the effect of gyro sensor and narrow corridor on the decision tree from outside, and the comparative results and also the results collected through cross validation method. Herein, only the results of class E blockage are dramatically

in a state of decline. The main reason for that is the lack of sufficient number and type of experiments for this blockage class. However, even this situation does not influence the overall results significantly. This is due to the fact that the cases in which class E blockage is involved have been considered as class D blockage (17 out of 20 for Düzce and 6 out of 7 for Gebze). Both of these blockage classes are configured to response to the shortest way algorithm as blocked passage (Birgönül et al., 2012). This indicates that the reliability of the shortest path algorithm would not be ineffective in terms of guiding the occupants to the safest path while evacuating the building in a safe and rapid manner.

CHAPTER 7

CONCLUSION

A methodology for real-time, sensor-based local monitoring of blockage in building structures is proposed in this thesis study. This methodology can provide blockage information of passage units by combining the sensor and image processing data. First, the damage indicators of buildings which can cause blockage are examined in order to achieve the aim. After that the sensors are selected and their capabilities are reviewed. Considering the sensor properties and damage indicators, the localization rules of the sensors are determined.

By using these localization rules, series of experiments are conducted on a test specimen, which is a 1/3 scaled corridor model. In these experiments, non-structural components (infill walls, suspended ceilings and cupboards) are monitored for blockage information by using the CCC and the URF. In addition, a video camera is used to view the corridor during experiments. Blockage classes are identified and employed in order to evaluate the final condition of the passage unit (i.e. the corridor) after each experiment. Image processing approaches are also taken into account to assess the blockage.

By using the results of the experiments, sensor fusion is carried out with the decision tree approach. In this approach, sensor data obtained from the experiments is considered as an input attribute to the C4.5 algorithm. The input attributes are also ranked to the influence on the decision tree by attribute class in Weka. The blockage condition of the experiment is also entered as an output attribute to the same algorithm. In the final stage, a decision tree is generated through the algorithm. It should be noted that the outcome of this decision tree is limited to the types, numbers and locations of the sensors and also the components used in the experiment.

An interesting result is the relative importance of the video camera. Although it is the only monitoring device that directly detects the blockage, it is ranked at 18^{th} place out of 24 attributes. This result leads to question the reliability of the method selected for the image processing. The results of the decision tree are tested with the 10-fold cross validation method and discussed with confusion matrix. According to the confusion matrix, the difference of the blocked and non-blocked corridor condition can be discriminated. In spite of that, the close blockage classes can be confused.

In order to test the decision tree, a case study is carried out as the last step of the study. First a pilot building is selected. This pilot building, which is a faculty building of a university, consists of two blocks with 4 and 5 floors. Case study is achieved through the pilot building, which is hypothetically exposed to the different levels of ground shaking: moderate and severe. The analytical model of the pilot building is constructed with a structural analysis software and time-history analysis are performed by using appropriate ground motion records that represent moderate and severe ground shaking. Then the damage to the non-structural components of the case study building are estimated by using the acceleration and drift information obtained from the time-history analysis. It is assumed that the sensors are located according to the previously determined

localization rules and they run flawlessly. In the next step, the simulated sensor data is used as an input for the decision tree approach. The results are discussed in accordance with the confusion matrix and are close to the results of the 10-fold cross validation. Hence it can be stated that the decision tree discriminates the distant blockage classes, but confuses the close ones.

It is perceived that the reason for the confusion of the blockage classes after running the decision tree is the lack of sufficient number of experiments. More detailed experiments should be carried out with more various types of components in future studies. This would increase the precision and recall rates provided from confusion matrix. Different approaches for sensor fusion like support vector machine and radial basis function neural network can also be used for future studies. Principle component analysis can be also applied to eliminate ineffective inputs. Using probabilistic assessment, instead of deterministic approaches, can also improve this study. In addition, a detailed image processing method with line detection algorithm should also be applied for better results.

This thesis, despite the discrepancies in some of the results, is a novel study in this research area and it can be a guideline for those who want to assess blockage with sensors. It is highly probable to improve the proposed methodology with the aim of mitigating the fatal consequences of disasters by making use of the outcomes of this study.

REFERENCES

Ayhan, M. (2012). "A model-based guidance and vulnerability assessment approach for facilities under the threat of multi-hazard emergencies". Unpublished master dissertation, Middle East Technical University, Ankara.

Bal, İ.E., Crowley. H., Pinho. R. (2008). "Development of a displacement-based earthquake loss assessment method for Turkish buildings". 14th World Conference on Earthquake Engineering. Beijing. China.

Bayülke, N. (1992). "Yığma yapılar". Bayındırlık ve İskan Bakanlığı Afet İşleri Genel Müdürlüğü Deprem Araştırma Dairesi. Ankara.

Beck, J.L., Kiremidjian, A.S., Wilkie, S., Mason, A., Salmon, T., Goltz, J., Olson, R., Workman, J., Irfanoglu, A. and Porter, K.A. (1999). Social, economic and system aspects of earthquake recovery and reconstruction, Consortium of Universities for Research in Earthquake Engineering, Richmond, California, United States of America.

Beck, J.L., Porter, K.A., Shaikhutdinov, R.V., Au, S.K., Moro, T., Tsukada Y. and Masuda M. (2002). Impact of seismic risk on lifetime property values, final report, Consortium of Universities for Research in Earthquake Engineering, Richmond, California, United States of America.

Benezeth, Y., Laurent, H., Emile, B. and Rosenberger, C. (2011). "Towards a sensor for detecting human presence and characterizing activity," Energy and Buildings, 43: 305-314.

Birgönül, M.T., Erberik, M.A., Kurç, Ö., Kiziltaş, S., Ergen, E., Dikmen İ., Akinci B., Ayhan M., Ergin T., Güven G., Baltaşi G.S., Özbaş B. and Gökdemir N. (2012). "A real-time damage assessment and a model-based evacuation and guidance approach in facilities for managing emergency response operations during multi-hazard emergencies", Final Report, TÜBİTAK 1010 EVRENA Project No 109M263, Middle East Technical University, Ankara, Turkey.

British Standard (1992). "BS5628-1: Code of practice for use of masonry; part 1: Structural use of unreinforced masonry". British Standards Institution. England.

Chandola, V., Banerjee A., and Kumar V. (2009). "Anomaly Detection: A Survey", ACM Computing Surveys, Vol. 41(3).

CEN (2003). "Eurocode 6: Design of masonry structures". prEN 1996 – 1. Brussels. Belgium.

Chaudhuri, S.R. and Hutchinson, T.C. (2004). "Distribution of peak horizontal floor acceleration for estimating nonstructural element vulnerability", 13th World Conference on Earthquake Engineering, Vancouver, B.C., Canada.

Clinton, J.F., Bradford, S.C., Heaton, T.H., Favela, J. (2004). The observed wander of the natural frequencies in a structure, Bulletin of the Seismological Society of America 96(1), 237-257.

CUREE (2005). Consortium of universities for research in earthquake engineering: Earthquake damage assessment and repair project, http://www.curee.org/projects/EDA/index.html.

Devasena, C.L. (2012). "Effectiveness prediction of memory based classifiers for the classification of multivariate data set", Computer Science & Information Technology, 07:413-424.

Dibley, M.J., Li, H., Miles J.C., and Rezgui, Y. (2011). "Towards intelligent agent based software for building related decision support", Advanced Engineering Informatics, 25(2), 311-329.

Dodier, R.H., Henze, G.P., Tiller, D.K. and Guo, X. (2006). "Building occupancy detection through sensor belief networks," Energy and Buildings, 38: 1033-1043.

Erickson, V.L., Kamthe, Y., Lin, A. and Brahme, R. (2009). Energy efficient building environment control strategies using real-time occupancy measurements. In: Proceedings of the First ACM Workshop on Embedded Sensing Systems for Energy-Efficiency in Buildings, 2009, Berkeley, United States.

Federal Emergency Management Agency. FEMA (2009). "HAZUS MR-4: Multi-hazard loss estimation methodology". Department of Homeland Security. USA.

Hailemariam, E., Goldstein, R., Attar R. and Khan, A. (2011). Real-time occupancy detection using decision trees with multiple sensor types. Symposium on Simulation for Architecture and Urban Design, 2011, Boston, United States.

Han, J. and Kamber M. (2006) "Data Mining: Concepts and Techniques", Morgan Kaufmann, San Francisco, CA, USA.

Homola, J. (2006). "Surface plasmon resonance based sensors"; Springer: Berlin, Germany.

Hutchins, J., Ihler A. and Smyth, P. (2007), "Modeling count data from multiple sensors: a building occupancy model," IEEE International Workshop on Computational Advances in Multi-Sensor Adaptive Processing, pp. 241-244.

Kerle, N. and Oppenheimer, C. (2002) Satellite remote sensing as a tool in lahar disaster management, Disasters, 26(2), 140-160.

Kircher, C.A., Nassar, A.A., Kustu, O. and Holmes, W.T. (1997a). Development of building damage functions for earthquake loss estimation, Earthquake Spectra, 13(4), 663-682.

Kircher, C.A., Reitherman, R.K., Whitman, R.V. and Arnold C. (1997b). Estimation of earthquake losses to buildings, Earthquake Spectra, 13(4), 703-720.

Kohavi R. (1995). "A Study of Cross Validation and Bootstrap for Accuracy Estimation and Model Selection", Proceedings of the International Joint Conference on Articial Intelligence, Montreal, Canada.

Krawinkler, H. (2002). A general approach to seismic performance objectives, International Conference on Advances and New Challenges in Earthquake Engineering Research, First Annual Meeting of ANCEER, Hong-Kong, China.

Kuran F. (2006). "Yığma yapıların çelik şeritlerle rehabilitasyonu". Yüksek Lisans Tezi. Gazi Üniversitesi Fen Bilimleri Enstitüsü İnşaat Mühendisliği Bölümü. Ankara.

Lam, K.H., Höynck, M., Dong, B., Andrews, B., Chiou, Y., Zhang, R., Benitez, D. and Choi, J. (2009). Occupancy detection through an extensive environmental sensor network in an open-plan office building. In: Eleventh International IBPSA Conference, 2009, Glasgow, Scotland.

Lam, N.T.K. and Gad, E.F. (2008). "Overturning of non-structural components in low-moderate seismicity regions", EJSE Special Issue: Earthquake Engineering in the low and moderate seismic regions of Southeast Asia and Australia, pg. 121-132.

Lo, L.J. and Novoselac, A. (2010). Localized air-conditioning with occupancy control in an open office. Energy and Buildings, issue 42, pp. 1120-1128.

MAXBOTIX INC. (2007), Ultrasonic Rangefinders Feature Custom Beam Width, Maxbotix Inc. Press Release.

Meyn, S., Surana, A., Lin, Y. and Oggianu, S. M. (2009). A sensor-utility-network method for estimation of occupancy in buildings. In: Joint 48th IEEE Conference on Decision and Control and 28th Chinese Control Conference, 2009, Shanghai, P.R. China.

Miranda, E. and Aslani, H. (2003). Probabilistic response assessment for building-specific loss estimation, Report No PEER-2003/03, Berkeley, CA: Pacific Earthquake Engineering Research Center, University of California, United States of America.

Mondal, G. and Jain, S.K., (2005) Design of Non-structural Elements for Buildings: A Review of Codal Provisions, The Indian Concrete Journal.

NEES, (2007). Network for earthquake engineering simulation nonstructural: simulation of the seismic performance of nonstructural systems, http://www.nees-nonstructural.org/index.html.

Newsham, G.R. and Birt, B.J. (2010). Building-level occupancy data to improve ARIMA-based electricity use forecasts. In: Proceedings of the 2nd ACM Workshop on Embedded Sensing Systems for Energy-Efficiency in Building, 2010, Zurich, Switzerland.

Niousha, A. and Motosaka, M. (2007). System identification and damage assessment of an existing building before and after retrofit, Journal of Structural Engineering, 53B.

Parker, J.R. (2001). "Rank and response combination from confusion matrix data", Information Fusion, Volume 2, Issue 2, Pages 113–120.

Polat, K. and Güneş, S. (2007). "An expert system approach based on principal component analysis and adaptive neuro-fuzzy inference system to diagnosis of diabetes disease," Digital Signal Processing, Volume 17, page 702-710.

Porter, K.A., Kiremidjian, A.S. and LeGrue, J.S. (2001). Assembly-based vulnerability of buildings and its use in performance evaluation, Earthquake Spectra, 17(2), 291-312.

Quinlan, J.R. (1993). "C4.5: Programs for Machine Learning", Morgan Kaufmann, San Mateo, CA, USA.

Retamales, R., Mosqueda, G., Filiatrault, A. and Reinhorn, A.M. (2006). "Experimental study on the seismic behavior of nonstructural components subjected to full-scale floor motions", 8th National Conference on Earthquake Engineering, San Francisco.

Şafak, E. (2005). Detection of seismic damage in structures from continuous vibration records, 9th International Conference on Structural Safety and Reliability (ICOSSAR), Rome, Italy.

Sankaranarayanan, R. (2007). "Seismic response of acceleration-sensitive nanostructural components mounted on moment-resisting frame structures", Ph. D., University of Maryland, College Park.

Schütz, R., Bernoulli, T., Wiessflecker, T., and Walder, U. (2008). "A context-adaptive building information model for real-time structural analysis in a disaster management system", CIB W78, 25th International Conference on Information Technology on Construction, Santiago, Chile.

Steinle, E., Kiema, J., Leebmann, J., Bahr, H. (2001). Laser scanning for analysis of damages caused by earthquake hazards, OEEPE Workshop on Airborne Laser Scanning and Interferometric SAR for Detailed Digital Elevation Models, Stockholm.

Tachwali, Y., Hazem, R. and Fagan, J.E. (2007). Minimizing HVAC energy consumption using a wireless sensor network. In: The 33rd Annual Conference of the IEEE Industrial Electronics Society (IECON), 2007, Taipei, Taiwan.

Todorovska, M.I., Hao, T.Y. and Trifunac, M.D. (2004). Building periods for use in earthquake resistant design codes – Earthquake response data compilation and analysis of time and amplitude variations, Report CE 04-02, University of Southern California, Department of Civil Engineering, Los Angeles, California, United States of America.

Tomazevic, M. (1999). "Earthquake-resistant design of masonry buildings, series on innovation in structures and construction", Vol. 1, Imperial College Press.

Witten, I.H. and Frank, E. (2000). Data Mining - Practical Machine Learning Tools and Techniques with Java Implementation. Morgan Kaufman San Francisco 2000.

Wu, Y. M., Hsiao, N.C., Teng, T.L. and Shin, T.C. (2002). Near real-time seismic damage assessment of the rapid reporting system, Terrestrial, Atmospheric and Oceanic (TAO) Sciences, 13(3), 313-324.

APPENDIX A

EXPERIMENTS CONDUCTED FOR SENSORS

A.1 Experiments Conducted for URF

The conducted experiments to assess the properties of URF are presented in the Table A.1 - Table A.17.

Table A.1 The presentation of the first experiment

Experiment No: 1
Purpose of the Experiment: Determining the voltage (mV) and the distance (mm) relationship of the URF
Sensor(s) Used in This Experiment: Maxbotix Range Finder EZ-1
Setup of the Experiment: In this experiment, the measurements are conducted in 30 different distances for the URF. These measurement points are selected referring to the URF resolution (25.4 mm).
Findings of This Experiment: The findings of this experiment are follows.

The results are given in Table A.2. The graph of the relationship between the voltage and the distance is given in Figure A.1. This empirical relationship shown in Equation **3.1** is almost linear[5].

$$D=1.29\times V+4.02 \qquad \textbf{A.1}$$

In Equation **3.1**, D is the distance measured in mm and V is the voltage value read from the URF in mV. The distance can be calculated from URF voltage by using this expression.

Table A.2 The findings of the first experiment

Reading No	Performed Measurement		Performed Measurement + The Thickness of the URF (mm)	The Voltage Read (mV)
	Inch	mm		
1	1	25.4	40.4	10
2	10	254.0	269.0	16
3	12	304.8	319.8	20
4	14	355.6	370.6	24
5	16	406.4	421.4	28
6	20	508.0	523.0	36

[5] R-square value of this relationship is 0.998

Table A.2 (cont'd) The findings of the first experiment

Reading No	Performed Measurement		Performed Measurement + The Thickness of the URF (mm)	The Voltage Read (mV)
	Inch	mm		
7	23	584.2	599.2	42
8	25	635.0	650.0	44
9	27	685.8	700.8	48
10	29	736.6	751.6	52
11	30	762.0	777.0	54
12	31	787.4	802.4	56
13	35	889.0	904.0	64
14	38	965.2	980.2	72
15	40	1,016.0	1,031.0	76
16	43	1,092.2	1,107.2	82
17	45	1,143.0	1,158.0	84
18	47	1,193.8	1,208.8	88
19	51	1,295.4	1,310.4	96
20	54	1,371.6	1,386.6	102
21	60	1,524.0	1,539.0	115
22	65	1,651.0	1,666.0	124
23	70	1,778.0	1,793.0	134
24	75	1,905.0	1,920.0	146
25	80	2,032.0	2,047.0	156
26	85	2,159.0	2,174.0	166
27	90	2,286.0	2,301.0	175
28	95	2,413.0	2,428.0	183
29	106	2,692.4	2,707.4	205
30	110	2,794.0	2,809.0	213

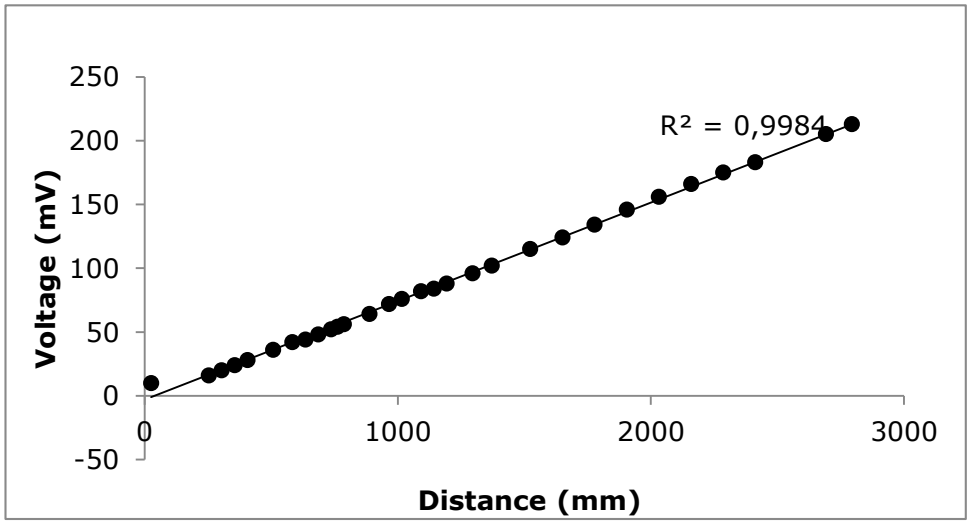

Figure A.1 The graph of the distance - mV relationship of the URF

Table A.3 The presentation of the second experiment

Experiment No: 2
Purpose of the Experiment: Determining the collapse of the wall with the URF
Sensor(s) Used at This Experiment: Maxbotix Range Finder EZ-1
Setup of the Experiment: In this experiment, the URF is placed opposite to the cardboard panel, at a height of 790 mm, in the middle of two columns and perpendicular to the floor. After that the cardboard panel is removed.
Prediction: Predicted measurement of the URF before removing: 1,422.4 mm – 1,447.8 mm Predicted measurement of the URF after removing: 2,463.8 mm – 2,489.2 mm

These predictions are determined after the measures have been verified with steel measuring tape. The distance between the sensor and the cardboard panel is measured at pre-experiment stage and the readout range is predicted with respect to the measured value and the resolution of the sensor. The distance between the sensor and the wall beyond the cardboard panel (Figure A.2 and Figure A.3) is measured at the post-experiment stage, and the readout range is predicted with respect to measured value and resolution of the sensor.

Table A.4 The findings of the second experiment

Findings of This Experiment: • Measured distance by the URF at the pre-experiment stage: 1,410 mm • Measured distance by the URF at the post-experiment stage: 1,500 mm – 1,514 mm

The URF measures the distance nearly 12.2 mm, which is lower than predicted for the pre-experiment stage. It also measures the distance between the column of the model and the sensor at the post-experiment stage, so; the result is nearly 1,000 mm lower than predicted.

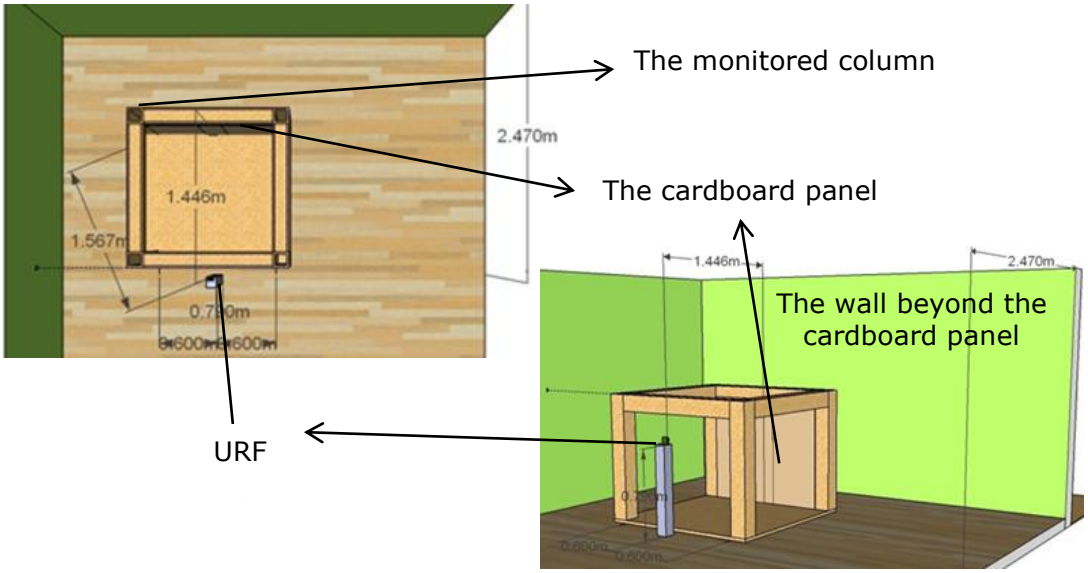

Figure A.2 The 3-D and plan view of the single-span model

Figure A.3 Photograph of the second experiment at the post-experiment stage

Table A.5 The presentation of the third experiment

Experiment No: 3
Purpose of the Experiment: It is observed from the results of the second experiment that the URF detects the nearest object in the beam width. As a result, the experiment no 3 is conducted in order to confirm this statement.
Sensor(s) Used at This Experiment: Maxbotix Range Finder EZ-1
Setup of the Experiment: The same setup is used for the experiment no 2. Only difference is that the cardboard panel is placed on the ceiling of the model instead of infill wall and a new readout is taken. Setup is shown in Figure A.4.
Prediction: • Predicted measurement of the URF: 1,480 mm • This is the distance between the URF and the cardboard panel.
Findings of This Experiment: • New measured distance by the URF: 1,487.8 mm

The cardboard panel is removed from span and fixed to the ceiling in this experiment. The URF is not able to measure the distance up to the wall behind the test specimen. It measures the distance up to the cardboard in the ceiling, which is within the beam width of the sensor. This indicates the necessity of calculating the beam width.

Figure A.4 A photograph of the experiment 3 and 5 setup

Table A.6 The presentation of the forth experiment

Experiment No: 4
Purpose of the Experiment: Questioning the difference between the Maxbotix Range Finder EZ-4 and Maxbotix Range Finder EZ-1.
Sensor(s) Used at This Experiment: Maxbotix Range Finder EZ-4
Setup of the Experiment: Same setup is used as for the second experiment

Table A.6 (cont'd) The presentation of the forth experiment

Prediction: • Predicted measurement of the URF before removing: 1,422.4 mm – 1,447.8 mm • Predicted measurement of the URF after removing: 2,463.8 mm – 2,489.2 mm

These predictions are made with respect to the measures verified with steel measuring tape. The distance between the sensor and the cardboard panel is measured at pre-experiment stage and the readout range is predicted with respect to measured value and resolution of the sensor. The distance between the sensor and the wall beyond the cardboard panel (Figure A.2) is measured in the post-experiment stage and the readout range is predicted with respect to measured value and resolution of the sensor.

Table A.7 The findings of the forth experiment

Findings of This Experiment: • The measured distance by the URF at the pre-experiment stage: 1,436.1 mm • The measured distance by the URF at the post-experiment stage: 2,508.8 mm – 2,521.8 mm

The distance is measured with a variation of 20-30 mm by the URF. The URF measures the distance up to the wall beyond the cardboard panel in the post-experiment stage. As a result, it can be concluded that EZ-4 typed URF is more suitable than EZ-1 for this study.

Table A.8 The presentation of the fifth experiment

Experiment No: 5
Purpose of the Experiment: Test if the beam width of the EZ-4 typed URF is sufficient to sense the wall without sensing the ceiling, also taking results of the experiment no 3 and 4 into consideration.
Sensor(s) Used at This Experiment: Maxbotix Range Finder EZ-4
Setup of the Experiment: Same with the third experiment
Prediction: Predicted measurement of the URF: 1,480 mm This was the distance between the URF and the cardboard panel.
Findings of This Experiment: New measured distance by the URF: 1,500.7 mm – 1,513.6 mm The findings of this experiment are supported with the findings of the experiments no 2, 3 and 4.

The URF is not able to measure the distance up to wall behind the cardboard; but it measures the distance up to the cardboard ceiling, which is within the beam width of the sensor instead. This reveals necessity of calculating the beam width.

Determining the Beam Width

Beam width can be defined as the diameter of the cross-section of the detection volume. The URF can sense an object if two conditions are met: the target object

must be in the detection volume and there is no other object between the URF and the target object. So, it is important to know the beam width of the URFs.

Illustration of the beam width, which is given in the technical specification sheet of the producer firm, is presented in Figure A.5. In addition to this, the approximate measures (in mm) of Figure A.5 (beam width– range) are presented in Table A.9. The relationship between diameter dowel and sensing distance is also given in Figure A.5 and Table A.9. The diameter dowel expression refers to the thickness of the object sensed. The objects sensed by the URF (the suspended ceilings and the infill walls) are thicker than the maximum diameter dowel (3.25 inch or 82.6 mm). So; the detection pattern of the URF is assumed as the detection pattern to a 3 ¼ diameter dowel.

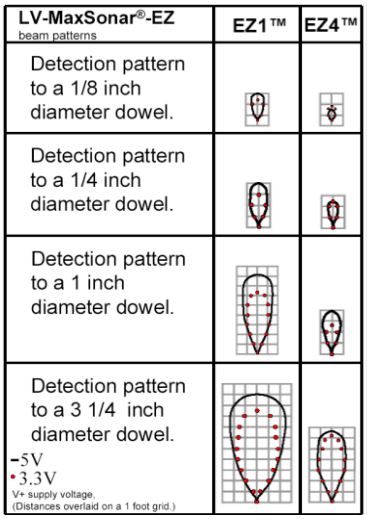

Figure A.5 Illustration of the beam width (horizontal axis) – range (vertical axis) relationship. The range shown on 1-foot grid to various diameter dowels (Beam plots are approximate) (MAXBOTIX INC., 2007)

Table A.9 The approximate values (in mm) of beam width - range values of Figure A.5

For EZ1 run at 5mV			**For EZ4 run at 5mV**	
Diameter dowel 0.125 inches = 3.1 mm			**Diameter dowel 0.125 inches = 3.1 mm**	
Range	**Beam Width**		**Range**	**Beam Width**
152.4	182.9		00.0	00.0
457.2	304.8		304.8	198.1
609.0	304.8		457.2	00.0
731.5	00.0		-	-
For EZ1 run at 5mV			**For EZ4 run at 5mV**	
Diameter dowel 0.25 inches = 6.4 mm			**Diameter dowel 0.25 inches = 6.4 mm**	
Range	**Beam Width**		**Range**	**Beam Width**
304.8	304.8		00.0	00.0
609.0	457.2		304.8	198.1
914.4	457.2		609.6	243.8
1,219.2	00.0		762.0	00.0

Table A.9 (cont'd) The approximate values (in mm) of beam width - range values of Figure A.5

Diameter dowel 1.00 inches = 25.4 mm		**Diameter dowel 1.00 inches = 25.4 mm**	
Range	**Beam Width**	**Range**	**Beam Width**
304.8	228.6	00.0	00.0
609.6	487.7	304.8	271.3
914.4	609.6	609.6	396.2
1,219.2	731.5	914.4	457.2
1,524.0	762.0	1,219.2	00.0
1,828.8	792.5	-	-
2,133.6	774.2	-	-
2,438.4	00.0	-	-
Diameter dowel 3.25 inches = 82.6 mm		**Diameter dowel 3.25 inches = 82.6 mm**	
Range	**Beam Width**	**Range**	**Beam Width**
304.8	335.3	00.0	0.00
609.6	1,005.8	304.8	253.0
914.4	1,188.7	609.6	469.4
1,219.2	1,322.8	914.4	694.9
1,524.0	1,402.1	219.2	737.6
1,828.8	**1,524.0**	1,524.0	**749.8**
2,133.6	1,493.5	1,828.8	554.7
2,438.4	1,219.2	1,981.2	00.0
2,743.2	00.0	-	-

The schematic view of the detection volume of the EZ-1 is presented in Figure A.6. As it can be clearly seen in Figure A.6; frame elements like beam and column which do not affect the presence of the wall, are within the detection volume. Because of this, EZ-1 failed to sense the presence of the wall at the experiments.

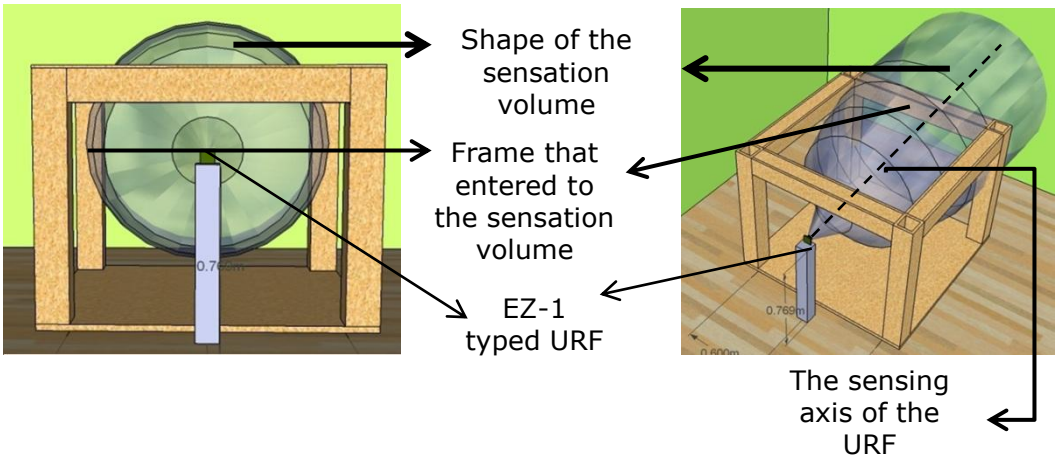

Figure A.6 The schematic view of the EZ-1 detection volume model

The schematic view of the detection volume of the EZ-4 is presented in Figure A.7. As it can be clearly seen in Figure A.7; frame elements like beam and column which do not affect the presence of the wall, are not within the detection volume. Because of this, EZ-4 has more accurate results than EZ-1 at the experiments.

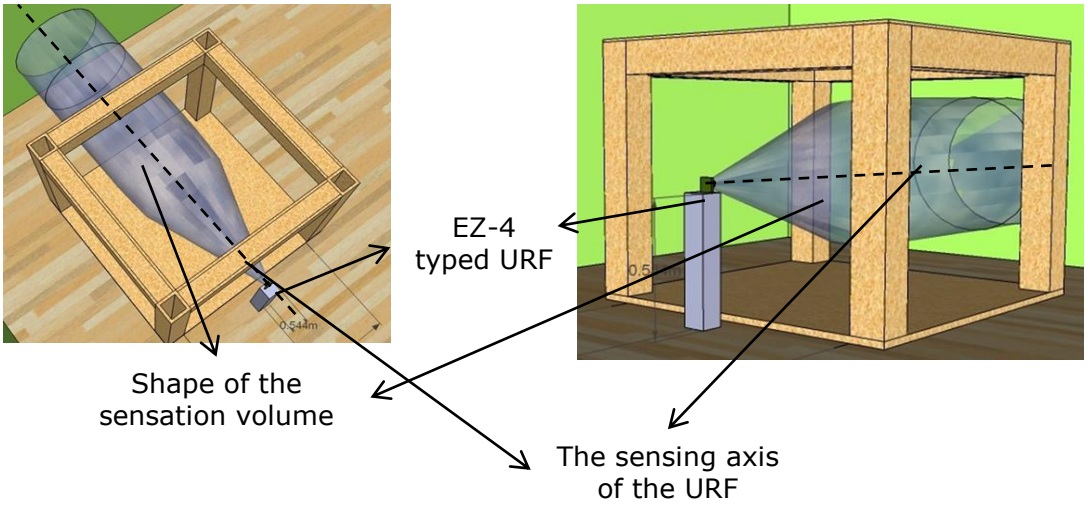

Figure A.7 The schematic view of the EZ-4 detection volume model

The shape of the URF detection volume is actually conic shaped (Figure A.6 and Figure A.7). In order to be conservative, shape of the URF beam width is assumed to be cylindrical with a diameter of the maximum beam width in this study. In other words, the beam width is assumed to be constant whatever the distance is. So, the beam width of the EZ-1 and EZ-4 are 1,524.0 mm and 749.8 mm, respectively. These values are the maximum values and written in bold in Table A.9 with the diameter dowel of 82.6 mm (3.25 inches). In this case EZ-4 is more convenient than EZ-1 because EZ-4 has a narrower beam width. So, the response of the target object to an event can be sensed incisively. Thus, sensing an object different than the target one is unlikely.

Table A.10 The presentation of the sixth experiment

Experiment No: 6
Purpose of the Experiment: Questioning the importance of the sensor positioning with respect to the target element (the infill wall) in terms of the angle between the URF sensing axis and the ground.
Sensor(s) Used at This Experiment: Maxbotix Range Finder EZ-4
Setup of the Experiment: The URF located in the middle of two columns at a height of 750 mm is placed facing downward to the first and the second rows of bricks of the cardboard wall (See the placement of the URF in Figure A.8 and Figure A.9). Then the infill wall knocked-down in the out-of-plane direction.
Prediction: • Predicted measurement of the URF before removing: 1,570 mm • Predicted measurement of the URF after removing: 2,050 mm – 2,070 mm

These predictions are made with respect to the measurements verified by steel measuring tape. The distance between the sensor and the first and the second lines of the infill wall from bottom is measured. The readout range is predicted with respect to measured value. The distance between the sensor and the

ground beyond the infill wall made from cardboard boxes is measured at the post-experiment stage and the readout range is predicted with respect to measured value and resolution of the sensor.

Table A.11 The findings of the sixth experiment

Findings of This Experiment:
• Measured distance by the URF at the pre-experiment stage: 1,500.7 mm – 1,513.6 mm • Measured distance by the URF at the post-experiment stage: 1,022.5, 1,048.3, 1,061.2, 1,074.2 mm

The distance measured by the URF, is nearly 60-70 mm less than the prediction made at the pre-experiment stage. The URF measures 1,000 mm less than the prediction made at the post-experiment stage. It is concluded that the URF measures the distance up to the strewed cardboard boxes at the post-experiment stage instead of the ground. The findings and the prediction made at the post-experiment stage has a difference approximately 1,000 mm. This proves that locating the URF as in the Figure A.8 or Figure A.9 is ineffective.

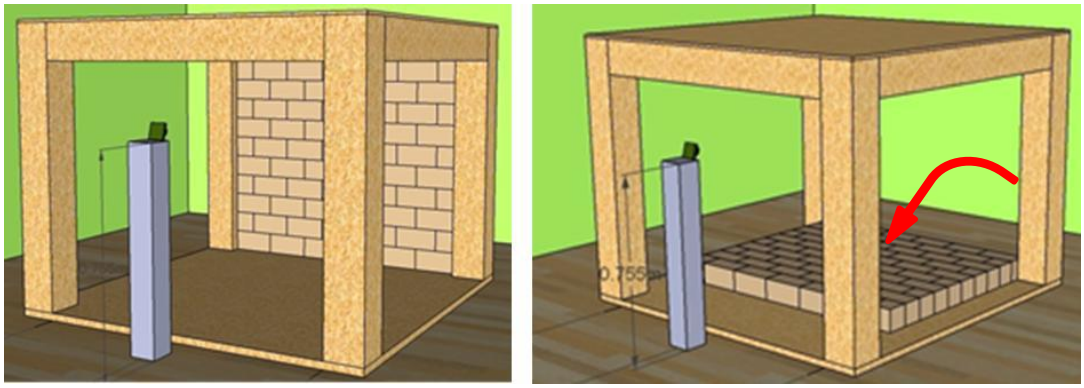

Figure A.8 Sketch of the specimen used in experiments 6 and 7 models. The pre-experiment stage on the left and the post-experiment stage on the right

Figure A.9 A photograph of the post-experiment stage of experiment 6 and 7

Table A.12 The presentation of the seventh experiment

Experiment No: 7
Purpose of the Experiment: Questioning the importance of the sensor location with respect to target element (the infill wall) in terms of the angle between the URF sensing axis and ground. The aim of this experiment is also to present the differences between EZ-1 and EZ-4.
Sensor(s) Used at This Experiment: Maxbotix Range Finder EZ-1
Setup of the Experiment: The same setup as the sixth experiment.
Prediction: • Predicted measurement of the URF before removing: 1,550 mm • Predicted measurement of the URF after removing: 2,050 mm – 2,070 mm
Findings of This Experiment: • Measured distances by the URF at the pre-experiment stage: 1,474.8 – 1,487.8 mm • Measured distances by the URF at the post-experiment stage: 983.7, 996.6, 1,009.5 and 1,022.5 mm • The distances measured by the URF are nearly 60-70 mm less than prediction made at the pre-experiment stage. • The distances measured by the URF are nearly 1,000 mm less than prediction made at the post-experiment stage. • Closer cardboard boxes are sensed by EZ-1 when compared with EZ-4

The URF measures the distance up to the strewed cardboard boxes at the post-experiment stage instead of the ground. The findings and the prediction made at the post-experiment stage has a difference of approximately 1,000 mm. This proves that locating the URF as in the Figure A.8 or Figure A.9 is ineffective. In addition to this, the placement of the URF does not matter significantly when EZ-1 is compared with EZ-4.

Table A.13 The presentation of the eighth experiment

Experiment No: 8
Purpose of the Experiment: Questioning the importance of the sensor location with respect to the target element (the infill wall) in terms of the angle between the URF sensing axis and the ground.
Sensor(s) Used at This Experiment: Maxbotix Range Finder EZ-1
Setup of the Experiment: The URF fixed in the intersection point of the top right column and the beam at a height of 1,000 mm is located facing the first and the second rows of the wall on the bottom (see the placement of the URF and see the Figure A.10 and Figure A.11). Then the infill wall was knocked down in the out-of-plane direction.
Prediction: • Predicted measurement by the URF before removing: 2,000 mm • Predicted measurement by the URF after removing: 2,050 mm

These predictions are made with respect to the measurements verified by steel measuring tape. The distance between the sensor and the first and the second lines of the infill wall from bottom is measured. The readout range is predicted with respect to measured value. The distance between the sensor and the

ground beyond the infill wall made from cardboard boxes is measured at the post-experiment stage and the readout range is predicted with respect to measured value and resolution of the sensor.

Table A.14 The findings of the eighth experiment

Findings of This Experiment:
• Measured distances by the URF at the pre-experiment stage: 1,526.5 – 1,539.5 mm • Measured distance by the URF at the post-experiment stage: 1,823.8 mm • The distance between the URF and the ground is measured instead of infill wall made up from cardboard boxes at the pre-experiment stage by the URF. • The distance between the URF and the column instead of the ground is measured at the post-experiment stage, so; erroneous results were obtained by the URF.

It is revealed that at the post-experiment stage the location of the URF (See the Figure A.10 and Figure A.11) causes erroneous readings like the results of the experiment 6 and 7.

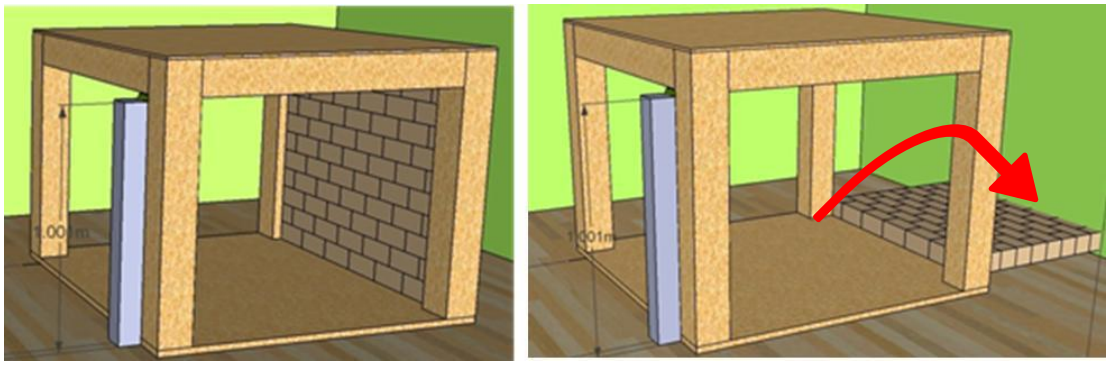

Figure A.10 Sketch of the specimen used in experiments 8 and 9 models. Pre-experiment stage on the left and the post-experiment stage on the right

Figure A.11 A photograph of the post-experiment stage of experiment 8 and 9

Table A.15 The presentation of the ninth experiment

Experiment No: 9
Purpose of the Experiment: Questioning the importance of the sensor positioning with respect to the angle between the URF sensing axis and ground. The aim of this experiment is also present the differences between EZ-1 and EZ-4.
Sensor(s) Used at This Experiment: Maxbotix Range Finder EZ-4
Setup of the Experiment: Same with the eighth experiment
Prediction: • Predicted measurement of the URF before removing: 2,000 mm • Predicted measurement of the URF after removing: 2,050 mm
Findings of This Experiment: • Measured distance by the URF at pre-experiment stage: 1,823.8 mm • Measured distance by the URF at post-experiment stage: 1,927.2 mm • The distance between the URF and the ground instead of infill wall made up from cardboard boxes is measured by the URF at the pre-experiment stage. • The distance between the URF and the column instead of the ground is measured by the URF at the post-experiment stage, so; unhealthy results were obtained.

It is revealed that at the post-experiment stage the location of the URF (See the Figure A.10 and Figure A.11) causes erroneous readings like the results of the experiment 6, 7 and 8. In addition to this, the placement of the URF does not matter significantly when EZ-1 is compared with EZ-4.

Table A.16 The presentation of the tenth experiment

Experiment No: 10
Purpose of the Experiment: Questioning the maximum distance that the URF can measure.
Sensor(s) Used at This Experiment: Maxbotix Range Finder EZ-4
Setup of the Experiment: The URF is taken to open air and aimed to the sky. The environment of the sensor is cleared from the disturbance of any object, so; the URF was provided with infinite space for the measurement.
Prediction: There is no prediction made for this experiment.
Findings of This Experiment: • Measured distance by the URF at the post-experiment stage: 6,580.5 mm and 6,593.4 mm • This is the maximum distance that the URF can measure.

Table A.17 The presentation of the eleventh experiment

Experiment No: 11
Purpose of the Experiment: Questioning the minimum distance that the URF can measure.
Sensor(s) Used at This Experiment: Maxbotix Range Finder EZ-4
Setup of the Experiment: An object is put at the zero point of the URF. Then the object is moved away gradually and the data is read.
Prediction: There is no prediction made for this experiment.

Table A.17 (cont'd) The presentation of the eleventh experiment

Findings of This Experiment: • Measured distance of the URF between 0 mm – 200 mm: 169.4 and 182.3 mm • Erroneous readings are obtained between 0 mm and 200 mm. The URF should not to be used within this range.

A.2 Experiments Conducted for CCC

Experiment No: 12

The circuit of the CCC is wired on the microcontroller (Figure A.12) and tested. It is observed that the CCC works properly. It yields the value of "1" when the electricity is on in the circuit, otherwise "0".

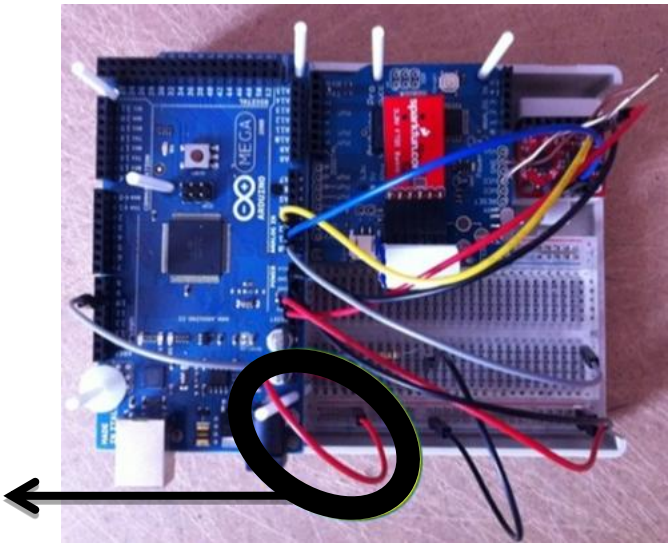

Figure A.12 The circuit of experiment 12. The circled cable belongs to the tested CCC.

Experiment No: 13

Three CCCs are wired on the microcontroller (Figure A.12) and tested. It was observed that all of the CCCs work properly. The value of "1" is obtained when electricity is on at the circuit; otherwise "0". As a result, the possibility of connecting more than one CCC on a microcontroller is verified.

Experiment No: 14

The CCC is wired with a 25,000 mm long cable. The resistivity of a cable increases in direct proportion to its length. The circuit is supplied with constant voltage; so, the current is decreased in inverse proportion to resistance. There is a risk that length of the cable could affect the working of CCC. As a result, in practice the circuit can be wired with any length of cable.

Table A.18 The presentation of the fifteenth experiment

Experiment No: 15
Purpose of the Experiment: Testing the CCC on the model
Sensor(s) Used at This Experiment: Ethernet wire
Setup of the Experiment: Ethernet cable connected to the CCC is located in front of the cardboard panel (Figure A.13) in this experiment. Then, the cardboard panel is overturned in order to examine the reaction of the CCC.
Prediction: • It is predicted that the cable is cut off; thus, the electronic signal of the computer is "0".
Findings of This Experiment: • Prediction is realized. Computer displayed "1" at the pre-experiment and "0" at the post-experiment stage (Figure A.13 and Figure A.14).

As a result, it is concluded that the CCC could be used in practice.

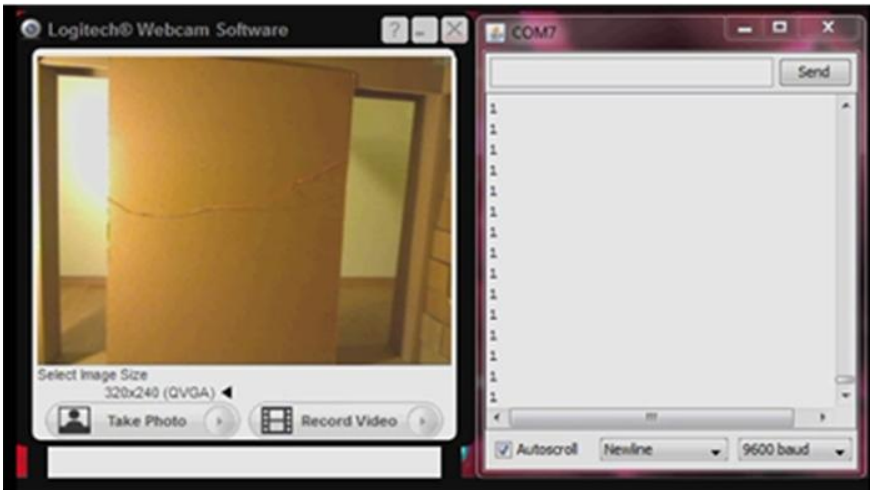

Figure A.13 The setup of the experiment no 15 (on the left side) and the data transmitted to the computer at the pre-experiment stage (on the right side).

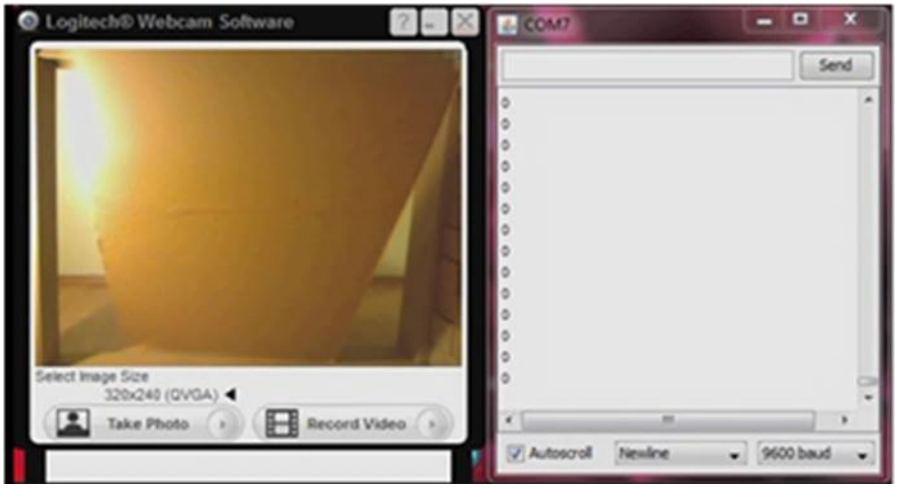

Figure A.14 The setup of the experiment no 15 (on the left side) and the data transmitted to the computer at the post-experiment stage (on the right side).